THE UNIVERSITY OF CALGARY

AN OPTIMAL ADAPTIVE POWER SYSTEM STABILIZER

by

ANTAL SOOS

A THESIS

SUBMITTED TO THE FACULTY OF GRADUATE STUDIES

IN PARTIAL FULFILLMENT OF THE REQUIREMENTS FOR THE

DEGREE OF MASTER OF SCIENCE

DEPARTMENT OF ELECTRICAL AND COMPUTER

ENGINEERING

CALGARY, ALBERTA

OCTOBER,1997

THE UNIVERSITY OF CALGARY

FACULTY OF GRADUATE STUDIES

The undersigned certify that they have read, and recommend to the Faculty of Graduate Studies for acceptance, a thesis entitled “An Optimal Adaptive Power System Stabilizer” submitted by Antal Soos in partial fulfillment of the requirements for the degree of Masters of Science

_____

Supervisor and Chairman, Dr. O. P. Malik

Department of Electrical and Computer Engineering

_____

Dr. S. A. Norman

Department of Electrical and Computer Engineering

_____

Dr. W. Y. Svrcek

Department of Chemical and Petroleum Engineering

October 10, 1997

Abstract

Power system operation is characterized by the random variation of load conditions, continuous change in generation schedule and network interconnections. Also, power systems are subject to different exogenous disturbances. An adaptive optimal controller is highly desirable to enhance the performance and guarantee stability under such complicated conditions.

An adaptive optimal controller, which will improve a power system's overall stability in the face of system non-linearity and external disturbances, is described in this thesis. The transfer function of the plant is estimated in real time by the Recursive Least-Squares (RLS) algorithm, and converted into its state equation. The plant states are estimated by Kalman filter. Control output is calculated by solving the Riccati algebraic equation. The applied structure enables improvement in performance from a linear controller.

A TMS320C30 Digital Signal Processor (DSP) and an ABB PHSC2 Programmable Logic Controller (PLC) were employed to develop a prototype real time digital control environment and to implement the optimal adaptive power system stabilizer.

Experimental results, which demonstrate the benefits of adapting the stabilizer parameters as the system dynamics change, are presented in this thesis.

Acknowledgments

It is a pleasure to express my sincere gratitude to my supervisor, Dr. O. P. Malik, for his advice, encouragement and support throughout the program. My enthusiasm in this subject is inspired by his profound knowledge in this area and his elegant research style.

I am especially indebted to Mr. Garvin C. Hancock for his help with the experimental tests. I also wish to thank the professors and support staff in the Department of Electrical and Computer Engineering, The University of Calgary, for their help during my study there.

I would like to thank Mr. D. Cameron Taylor, Dr. E. Barbara Olasz and Dr. Ken E. Scott, who reviewed the manuscript and provided valuable feedback.

The understanding and support of the management at Harris Inc. - Harris Wireless Access Division was greatly appreciated. The part-time position at this company during my academic years, provided financial security for my family.

Finally thanks are due to all of my friends, fellow students and all other people around me for their valuable advice.

Table of Contents

List of Tables

List of Figures

List of Symbols

TABLE 0-1 List of Symbols

A	Ammeter
ABB	Asea Brown Boveri Ltd., Zurich (Switzerland)
AC	Alternating Current
ANF PSS	Adaptive-Network-based Fuzzy Power System Stabilizer
ARMA	autoregressive moving average process
ARMAX	ARMA process with an exogenous signal
AVR	Automatic Voltage Regulator
A/D	Analog to Digital conversion
A_1, A_2	conventional power system stabilizer filter constants
$A(nT)$	state transition matrix
$B(nT)$	input gain matrix
C	capacitance
CPSS	Conventional Power System Stabilizer
$C(nT)$	measurement matrix
DC	Direct Current
D/A	Digital to Analog conversion
D_i	damping coefficient
$G(nT)$	process noise gain vector
H	generator inertia value
$H(t)$	Hamiltonian
IIR	infinite impulse response filter
ISA	Industry Standard Architecture bus
I_a	rotor winding current

TABLE 0-1 List of Symbols

I_c	field winding current
I_f	shunt winding current
J_N, J	performance index
K_A, K_C, K_F	AVR gain
K_d	generator damping ratio coefficient
K_s	conventional power system stabilizer gain
$K(nT)$	gain vector
$L(\circ)$	cost function
L	inductance
LQG	Linear Quadratic Gaussian
MIMO	Multi Input - Multi Output
N	array length
$N_1(nT)$, $N_2(nT)$	first norms
OAPSS	Optimal Adaptive Power System Stabilizer
PC	Personal Computer
PHSC2	Programmable High Speed Controller from ABB
PID	Proportional-plus-Integral-Plus-Derivative controller
$P(nT)$	correlation matrix
P_{Ei}	electrical power output from the generator
P_i	generator's electrical three phase power
P_{Mi}	turbine power applied to rotor
$P^{-}(nT)$	predicted covariance matrices
$Q_C(nT)$	symmetric positive semi-definite matrices
Q_e	reactive power
$Q_K(nT)$	process noise covariance
$\hat{Q}_K(nT)$	predicted process noise covariance

TABLE 0-1 List of Symbols

RLS	Recursive Least-Squares
R^n	real *n*-dimensional vector
$R_C(nT)$	positive definite matrices
R_C, X_C	voltage transducer compensation constants
$R_K(kT)$	measurement noise covariance
$\hat{R}_K(nT)$	predicted measurement noise covariance
R	resistance
SISO	Single Input - Single Output
$S_i(z)$	temporary variable
S_3	switch
$T_1, \ldots, T_4$	conventional power system stabilizer time constants
TCR	Time Constant Regulator
TMS320C30	Trademark of Texas Instrument Inc.
T_A, T_B, T_{B1}	AVR time constants
T_C, T_{C1}, T_F, T_R	AVR time constants
T_e	generator electrical power output
T_m	generator mechanical power input
$T_0', \ldots, T_4'$	time constants
$T_{\omega i}$	impulse moment of the rotor
T''_{do}	field transient time constant
U_{Cont}	control signal combined the U_{PSS} and the output of AVR
U_{PSS}	control signal for power system stabilization
U_{pi}	generator's internal voltage
V	Voltmeter
Vt	terminal voltage of the generator

TABLE 0-1 List of Symbols

V_a	rotor winding voltage
V_c	control signal voltage
V_{PSS}	power system stabilizer signal
V_{OEL},V_{UEL}	AVR over-excitation and under-excitation limits
V_{xMAX},V_{xMIN}	AVR V_x voltage variable upper and lower limits
V_T,V_{REF}	generator terminal volt. and AVR voltage reference settings
V_f	shunt winding voltage
$Y(z)$, $U(z)$, $\hat{E}(z)$	the *Z*-transforms of the discrete time functions
Z_{ii}	transmission line's driving point impedance
Z_{ij}	transfer impedance between machines i and j
a	acceleration
a, b	governor gain constants
a_c	acceleration limit
a_i, b_i *and* c_i	difference equation parameters
c	viscous damper coefficient
$\cos(\phi)$	power factor
e_d, e_q, e_f	generator d-axis, q-axis and field winding voltage
$\hat{e}(nT)$	prediction error
f_0', …, f_2'	digital conventional PSS coefficient
g	governor output
g'_0, …, g'_2	digital conventional PSS coefficient
i, j, k	numbers
i_d, i_q, i_f	generator d-axis, q-axis and field winding current
k	stiffness of spring
m	model order
m	mass

TABLE 0-1 List of Symbols

$p.u.$	per-unit (normalized value)
$r(nT)$	reference input
r_a	generator armature resistance
r_e, x_e	transmission line resistance and reactance
r_f, r_{kd}, r_{kq}	generator field, d-axis and q-axis damper windings resistance
t_f	final time
t_0	initial time
u_cpss	control signal when the CPSS is in control
u_oapss	control signal when the OAPSS is in control
$u(n)$	control signal
u_d, u_k, u_f	generator d-axis, q-axis and field winding voltage
$u_s(nT)$	external perturbation
v	velocity
vt	velocity limit
$v(nT)$	error in the measurement equation - measurement noise
$w(nT)$	error in the system model
y_cpss	system output signal when a CPSS is in control
y_oapss	system output signal when a OAPSS is in control
$y(n)$	plant output
x_d	generators d-axis reactance
x_f	generators field winding reactance
x_{kd}, x_{kq}	generator d-axis and q-axis damper winding reactances
x_{md}, x_{mq}	generator d-axis and q-axis mutual reactances
x_q	generators q-axis reactance
$\hat{x}^-(nT)$	prior estimate of the state variables

TABLE 0-1 List of Symbols

$\hat{x}(nT)$	estimate of the state variables
$x(t)$	state variable vector
z^{-1}	backward discrete time shift
zs	steady-state value of z
z	the z axis
ΔP_e	the variable part of the electric power
$\beta(nT)$	tracking constrained coefficient
β_0	empirically selected threshold
$\Theta(nT)$	parameter vector
ψ_d, ψ_q, ψ_f	generator d-axis, q-axis and field winding flux-linkage
ψ_{fq}, ψ_{1d}, ψ_{1q}	generator d-axis, q-axis damper winding flux-linkage
$\Psi(nT)$	measurement vector
δ_i	phase angle - load angle
δu	the variation in u
$\delta(nT)$	exogenous disturbance
λ_d, λ_q, λ_f	generator d-axis, q-axis and field winding flux-linkage
λ_{kd}, λ_{kq}	generator d-axis, q-axis damper winding flux-linkage
$\lambda(nT)$	forgetting factor
$\lambda(t)$	undetermined multiplier for the Hamiltonian
ξ	damping ratio of the system
ω	angular natural frequency
ω, ω_0	generator rotation speed and its rated value

1 Introduction

Electrical energy has become a major form of energy for end use consumption in today's society. To make electric energy generation and transmission more economic and reliable, the trend in electric power production is towards an interconnected network of transmission lines linking generators and loads into large integrated systems. The power station sites are selected close to a source of power, such as large coal mines and water power sources. Consequently, power transmission lines and networks have to meet the following requirements:

1. *ensure parallel operation of distant power stations connected together*
2. *transmit electrical power to large load centers over large distances*
3. *ensure satisfactory parallel operation with other interconnected power systems.*

For proper operation, this large integrated system requires a stable operating condition. Stability in power systems is generally regarded as the ability of generating units to maintain synchronous operation [1].

1.1 Nature of Power System Oscillations

Smaller power systems have hundreds of kilometers of transmission lines; while the largest (the eastern U.S./Canadian interconnected system) has thousands of kilometers of transmission lines. Most electric power systems are AC with a frequency that is almost uniform over the whole network. This is achieved by using synchronous AC generators. System frequency is held within tight limits by speed governing the generator prime movers, and system voltages are held by generator excitation system control. In small systems, there may be only tens of generators; in large systems there are thousands [2].

Interconnected AC generators produce torques that depend on the relative angular displacement of their rotors. These torques act to keep the generators in synchronism (synchronizing torques). Thus, if the angular difference between generators increases, an electrical torque is produced that tries to reduce the angular displacement. It is as though the generators were connected by torsional springs, and, just as in mass-spring systems, the moment of inertia of the rotors and the synchronizing torques cause the angular displacement of the generators to oscillate following a system disturbance. The angular displacements should settle to values that maintain the required power flows through the transmission network and supply the system load [2].

If the disturbance is large - say a prolonged three-phase fault on the transmission system- the nonlinear nature of the synchronizing torque may not be able to return the generator angles to a steady state. Some or all generators then lose synchronism and the system exhibits transient instability. On the other hand, if the disturbance is small, the synchronizing torques keep the generators nominally in synchronism, but the generators' relative

angles oscillate. In a correctly designed and operated system, these oscillations decay: the system is then called small-signal stable. In an overstressed system, small disturbances may result in oscillations that increase in amplitude exponentially: the system is then said to be small-signal unstable.

Unstable power system oscillations have occurred all over the word in the last 30 years. They appear first when a power system is pressed to supply increasing load. As transmission lines are loaded more and more, the generators need to rely more heavily on their excitation systems to maintain synchronism, and at some point, without supplementary control, the synchronizing oscillations become unstable. Also during the last 30 years, many power systems have been interconnected so as to be able to exchange power to keep operating cost to a minimum. However, the interconnecting ties between neighboring power systems, although they may not be overloaded, are often relatively weak when compared to the connections within each system. The synchronizing torques are lower across these weak ties; and this, coupled with the high aggregate inertia of each of the systems being interconnected, leads to low frequency interarea oscillations. Many of the early instances of oscillatory instability occurred at low frequencies when these interconnections were made [2].

1.2 Power System Stability Modeling

Stability calculation methods have always lagged behind interconnected power system size, so there has been a continuous striving for suitable simplifications. A kind of

“instinctive simplification” was to divide the theoretically unique problem of stability into two parts: steady-state and transient stability, for which analysis methods have been developed independently over many years. In American literature the steady-state stability and dynamic stability concept pair is in use. The analytical approach to synchronous machine’s fundamental behavior is best modeled by Park's reference frame. Those are the voltage equations, the flux-linkage equations and the torque equation, described in Appendix A “Park’s Equations”. In order to obtain same appreciation of power system oscillations it is important to include some discussion of stability analysis. However, this is not the main purpose of this study.

1.2.1 Steady-state stability

Steady-state stability analysis is the study of a power system and its generators in strictly steady state conditions and trying to answer the question of what is the maximum possible generator load that can be transmitted without loss of synchronism of any one generator. The maximum power is called the steady-state stability limit.

For an *n*-machine power system the active power fed in by the *i*th generator is defined by equation (1.1)

$$P_i = \frac{U_{pi}^2}{Z_{ii}} \sin\alpha_{ii} + U_{pi} \sum_{\substack{j=1 \\ i \neq i}}^{n} \frac{U_{pj}}{Z_{ij}} \sin(\delta_i - \delta_j - \alpha ij) \qquad (1.1)$$

where U_{pi} is the magnitude of the internal voltage (the voltage behind synchronous reactance) of the *ith* generator (line to line voltage); $Z_{ii}\left(\frac{\pi}{2}-\alpha_{ii}\right)$ is the driving point impedance "seen" from the internal voltage; $Z_{ij}\left(\frac{\pi}{2}-\alpha_{ij}\right)$ is the transfer impedance between machines i and j; δ_i is the phase angle lead (load angle) of the *ith* generator with respect to the reference phasor and P_i is the electrical three phase power of the *ith* generator [1].

Assuming that the load angles of all other machines are constant, the study-state stability limit can be predicted from equation (1.1).

A common problem is the insidious nature of oscillatory instability. Power flow over a tie-line may be increased to supply remote load with no noticeable problems until the stability limit is reached. A slight increase in power flow beyond this limit results in oscillations in which amplitude increases quickly with no need for any system fault. At best, system non-linearities limit oscillation amplitude. At worst, the oscillation amplitudes reach levels at which protective relays trip lines and generation, and this in turn causes partial or total system collapse [2].

1.2.2 Dynamic stability

Dynamic stability is a concept used in the study of transient conditions in power systems. Any electrical disturbances in a power system will cause electromechanical transient processes. Besides the electrical transient phenomena produced, the power balance of the

generating units is always disturbed, and thereby mechanical oscillations of machine rotors follow the disturbance.

To describe the transient phenomena, the well-known swing equation of the synchronous generators, derived from the torque equation for synchronous machine, can be used:

$$T_{\omega i}\frac{d^2\delta_i}{dt^2} = P_{Mi} - D_i\frac{d}{dt}\delta_i - P_{Ei} \tag{1.2}$$

where $T_{\omega i}$ is “the impulse moment” of the rotor of the generating unit, D_i is the damping coefficient (representing the mechanical as well as the electrical damping effect), δ_i is the phase angle (load angle), P_{Mi} is the turbine power applied to rotor and P_{Ei} is the electrical power output from the stator [1].

1.2.3 Synchronizing Oscillations

Two types of synchronizing oscillations are common in all interconnected AC power systems. The first is associated with a single generator (or a plant of identical generators) acting against the system. The second is more complex and involves many generators, in one area of the power system oscillating against other generators in other areas of the power system. Local or plant modes of oscillations have natural frequencies of about 1 to 2 Hz. Interarea modes of oscillation have lower natural frequencies on the order of 0.1 to 0.7 Hz. In small systems, interarea oscillations generally have higher natural frequencies than those of large systems [2].

The total number of modes of synchronizing oscillations is equal to one less than the number of interconnected generators. In a system having thousands of generators, there are thousands of modes of oscillations. All of these modes of oscillations must decay following a system disturbance. If any one mode increases in amplitude, the system's operators would have to take action to prevent either local or system-wide collapse.

Power systems must be designed to be stable under as wide a range of system load and operating conditions as possible. Generally, if the operation of the system is constrained, those constraints should be due to the thermal operating limits of the transmission system or loss of synchronism (transient instability) and not by oscillatory instability.

To determine the nature of system oscillations, analysis of the following system characteristics is required:

- Frequency and damping of the system’s synchronizing oscillation
- Pattern of generators that take part in each mode of oscillations

Generators that are able to have a controlling effect on the oscillations must be identified, and tools must be provided to allow for efficient and robust design of oscillation damping controls [2].

1.3 Damping Controls

Power system stabilizers are the most cost-effective power system oscillation damping controls. Essentially, they use the power amplification capability of the generators to generate a damping torque in phase with the speed change. This is achieved by injecting a stabilizing signal into the excitation system voltage reference summing junction. The

stabilizing signal is most often the change in generator rotor speed, phase advanced to counteract the phase lag between the exciter voltage reference and generator electrical torque [2].

Historically, in the late sixties, the need for such devices was demonstrated by some cases of sustained power swings in the western part of the USA. Subsequent analysis has shown that these swings were due to poor damping characteristics caused by modern voltage regulators of conventional structure, but with comparatively high gain from the stability point of view. To compensate for the unwanted effect of these voltage regulators, additional signals were introduced in the feedback loop of voltage regulators. The additional signals were mostly speed deviation, AC bus frequency or accelerating power. The devices set up to provide these signals through properly chosen transfer function have been called “power system stabilizers” [1].

The basic objective of power system stabilizer is to modulate the generator’s excitation in such a way as to provide additional damping to the electromechanical oscillations of generating units; thereby improving the steady-state stability of the whole power system. To do this the power system stabilizer has to produce a component of electrical torque in the synchronous machine that is in phase with the speed variation of rotors.

There have been problems in the past with power system stabilizers causing steam turbine shaft torsional modes to become unstable, but this risk has been eliminated in many modern power system stabilizer designs. However, there are still many problems with installed power system stabilizers that have been introduced by ineffective commissioning and tuning of the devices. Generally, in systems with both local and interarea modes, power system stabilizer parameters are determined through off-line analysis, and tuned further

during commissioning. The validity of the model used in the off-line studies should be checked on commissioning. Setting power system stabilizers to typical values is particularly dangerous for systems in which interarea modes are of concern. It is very easy for the stabilizer to have a destabilizing effect at low frequencies that cannot be observed during on-line commissioning test.

It is easy for controller settings to be inadvertently changed due to nonlinear changes in generators' and in transmission-lines' operating conditions. The models based on original manufacturers' information may not be accurate in few years [2]. This problem can be resolved by implementing an adaptive control system.

1.4 Optimal Adaptive Controller design

A power system is a sophisticated combination of multiple electrical and mechanical components. In general, these elements are highly nonlinear. Also, power system operation is characterized by a wide range of operating conditions and random load changes, and is subject to various unpredictable disturbances. The dynamics exhibited under different operating conditions make the design of power system stabilizer more challenging because it in no way can guarantee uniform performance under all operating conditions. Although various approaches have been proposed to deal with the power system stabilizer design problem, none of them provide an explicit way to handle the power system uncertainty problem under varying operating conditions.

An optimal control algorithm based on adaptive system identification and estimation provides a mechanism to deal with the problems in the face of system uncertainty and exter-

nal disturbances. The idea behind this design method is to provide satisfactory performance for the system under various operating conditions of the system within its operating range in terms of system stability and optimallity in control action, defined by the index of performance. This idea has lead to the research and development of the “Optimal Adaptive Power System Stabilizer”. The basic structure of the algorithm of this controller is shown in Figure 1-1

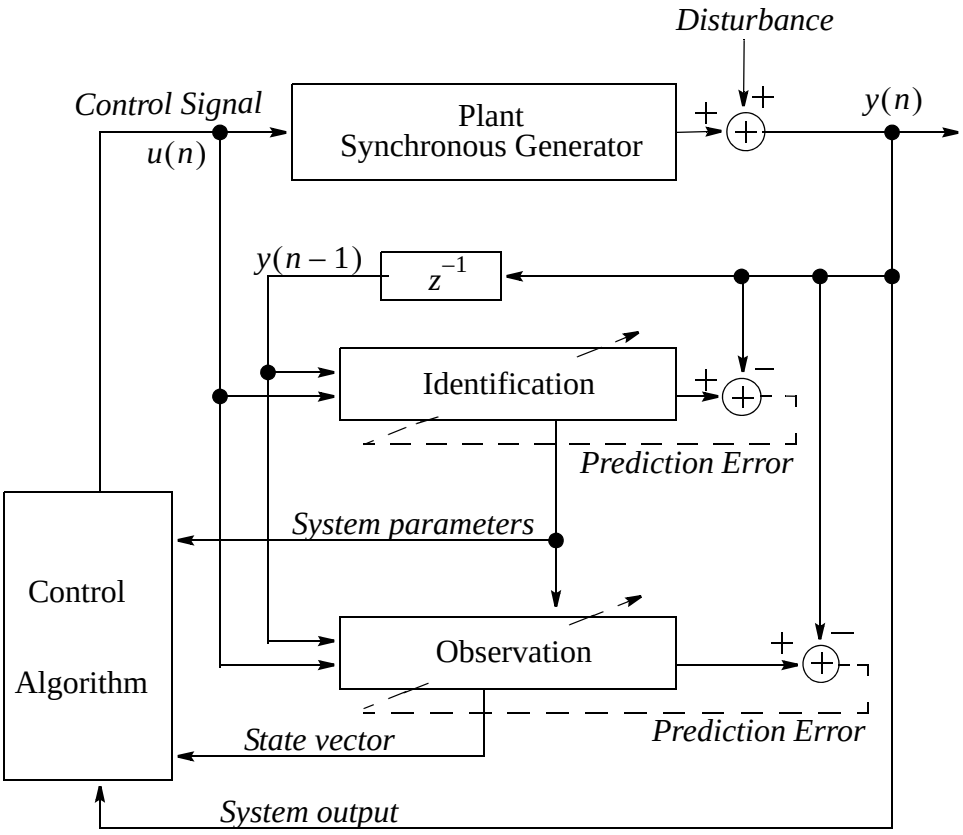

Figure 1-1 Adaptive Optimal Controller Structure

1.4.1 Adaptive Control

The adaptive controller is a controller that can modify its behavior in response to changes in the dynamics of the process and in the characteristics of disturbances. Adaptive controllers also have their own parameters, which must be chosen. Controllers without any externally adjusted parameters can be designed for specific applications in which the purpose of control can be stated a priory, autopilots for missiles and ships are typical examples.

In general an optimal control design requires a nominal system model, Figure 1-1, which represents the current operating point of the system. The implementation of optimal control with a non-adaptive system model can not be successful for a nonlinear system without continuous support.

1.4.2 Optimal Control

The controller design problem is specified by the process, by the criterion - formulated in the performance index - and by the admissible control signal. The assumption is that the process can be described by a discrete time model. The optimal design technique assumes that one can write a mathematical function which is called the cost function. This describes the requirements made for the behavior of the plant. The optimal design procedure minimizes this cost function, hence the term “optimal”. For systems represented by a discrete model the cost function is generally of the form (1.3), also called the performance index

$$J_N = \sum_{n=0}^{N} L[y(n), u(n)] \tag{1.3}$$

In this relation n is the sample instant, N is the terminal sample instant, $y(n)$ and $u(n)$ are the plant output and input respectively and L represents the cost function.

1.5 Thesis Objective

The objective of this thesis is to present a systematic methodology for building an adaptive and optimal control algorithm. The purpose of the applied control algorithm is to solve the power system stabilizer design problem in the face of nonlinear plant and exogenous disturbances. With the advance of modern control theory and digital signal processing techniques, it is hoped that this work will make a contribution to the development and application of adaptive optimal control algorithms. Even though this theory was introduced many years ago, its application was delayed by the lack of economical hardware. However, the advanced Digital Signal Processors (DSP) with their computational powers and economical prices would allow the more complex control algorithms to be used in a variety of control devices.

In order to develop an Optimal Adaptive Power System Stabilizer the following topics are discussed and studied in this thesis:

- The power system parameters are estimated by a Recursive Least-Squares (RLS) adaptive algorithm. It is a crucial requirement for the algorithm to operate satisfactorily with ill-conditioned input data, therefore robust behavior is required from the adaptive algorithm. Determination of the necessary modifications on the standard recursive least-square algorithm should be investigated.
- When the Recursive Least-Squares adaptive algorithm operates in a nonstationary environment, the algorithm is required to track parameter variations from the system. To achieve an adequate tracking performance, an adaptive forgetting factor should be used.
- A new adaptive state estimation algorithm, a Kalman filter with an on-line adaptive process-noise covariance and adaptive measurement-noise covariance assessment is proposed. With this approach the main drawback of Kalman filter implementation can be avoided, namely the requirement for the predetermination of the process noise covariance and measurement noise covariance values.
- To achieve the best control performance, a real-time optimization algorithm based on the on-line calculated system parameters and state-values is proposed. In this way, the optimal control (1.3) performance is approached even if the power system's parameters are changing due to nonlinearities in the power system.
- To achieve better performance with better accuracy, the control algorithm's model should be increased to fifth order, instead of third order as implemented in the past.
- In addition to the theoretical and simulation studies, investigate how the optimal adaptive power system stabilizer behaves in real-time on a physical model of a power system

1.6 Thesis organization

In addition to the first introductory chapter, this thesis is composed of eight chapters divided into three parts.

- Part I describes a time optimal, nonlinear approach to system control and consists of one chapter. This nonlinear control algorithm is the original idea by which this work started. However, after simulation it became evident that this algorithm was not appropriate for power system control.

- Part II describes an adaptive and optimal approach to system control and consists of four chapters. These are:

    1. “System Parameter Estimation” which depicts the theoretical base of an adaptive algorithm. Questions such as stability, convergence, and robustness are discussed.
    2. “State-Space Representation” is the next chapter, which explains the method of changing from the transfer function into the state space representation.
    3. “Kalman Filter” or state estimator is the third chapter in the second part. The state-space values of the system can be calculated in two ways. The first method is based on the direct recursive calculation of the state-space values, and the second method is the Kalman filter. The direct recursive method is discussed in the previous chapter. During simulation this method has shown acceptable results for the implementation of the control algo-

rithm, but the values calculated by the Kalman filter had less noise. Therefore the final version of the control algorithm is based on the Kalman filter, presented in this chapter.

4. "Optimal Control" is the last chapter of this part. This chapter presents the general theory available for an important class of optimization problems, namely, the class of control problems involving linear time-varying plans and quadratic performance criteria: the Linear Quadratic Gaussian (LQG) control algorithm.

- Part III describes the implementation of the optimal controller derived in part II, and consists of three chapters:

  1. "Real-time Control Environment" chapter describes the implementation of the optimal adaptive control algorithm in real time. The digital controller is based on a Texas Instruments floating point digital signal processor (DSP). With a physical model of a power system, this environment provides an excellent facility to implement any digital controller.
  2. "Experimental Studies" chapter describes and analyses the results achieved by the proposed Optimal Adaptive Power System Algorithm.
  3. "Conclusions and Future Work" chapter contains the conclusions and comments on further research topics in the area of adaptive optimal control algorithm implementation.

I Non-linear Control

In the period starting about 1953, a number of researcher, among them Bellman[1], Bushaw[2], Fel'Dbaum[3], LaSalle[4], and Pontriagin[5], proved, with increasing rigor and generality, that an on-off control system is the time-optimal system [3]. This means that a system that employs its maximum available effort at all times and switches the polarity of this effort at the optimum moments can follow an arbitrary input in a better fashion (at least in the time-optimal sense) than a system with any other conceivable use of the same range of effort.[3]

The first part of this chapter describes the relevant theory for time optimal control, based on Pontriagin's Maximum Principle. In the second part of this chapter a feedback version of this controller is introduced and tested.

1. Bellman Richard, 1920-, American mathematician
2. Bushaw W. Donald, American mathematician
3. Fel'Dbaum A. A., Russian applied mathematical scientist
4. LaSalle P. Joseph, 1916-1983, American applied mathematical scientist
5. Pontriagin Lev Semenovich, 1908-, Russian mathematician, (blind from age 14)

2 Time Optimal Control

The class of optimization problems for which the sole measure of performance is the minimization of transition time from an initial state to a target state is called the class of minimum-time (or brachistochrone) problems [4]. A suitable performance index for these problems is

$$J = \int_{t_o}^{t_f} 1 dt = t_f - t_0 \tag{2.1}$$

where t_0 is the initial and t_f is the final time of interest [6]. The equation (2.1) is derived from equation (B.2), by defining $\phi(x(t_f), t_f) = 0$ and $L(x, u, t) = 1$, presented in Appendix B - “Continuous Nonlinear Optimal Controller”.

A state variable model for a nonlinear time-varying dynamical system is given by:

$$\frac{dx}{dt} = f(x, u, t) \tag{2.2}$$

where $x(t) \in R^n$ is the vector of internal states and $u(t) \in R^1$ is the control input. After linearizing equation (2.2) around the operating point, the linear system model becomes

$$\frac{dx}{dt} = Ax + Bu \tag{2.3}$$

with $x \in R^n$, $u \in R^1$ and the control signal u is limited by the normalized value

$$-1 \le u(t) \le 1 \tag{2.4}$$

A requirement when the control is constrained to an admissible region, like (2.4), arises in many problems where the control magnitude is limited by physical considerations [7].

The general final condition includes the cases where the final states are required to be equal to a certain value. In this case the final state will be required to satisfy the prescribed function

$$\Psi(x(t_f), t_f) = 0 \tag{2.5}$$

where $\Psi \in R^p$.

The optimal control problem posed here is to find a control *u(t)* that minimizes the performance index (2.1), satisfies the constraint on control signal (2.4) at all time, and drives given $x(t_0)$ to the final state $x(t_f)$ satisfying (2.5) for a given function Ψ [6].

By using the pure minimum time index performance (2.1), where t_f is free, the Hamiltonian is defined in Appendix (B.4):

$$H = 1 + \lambda^T(Ax + Bu) \tag{2.6}$$

where $\lambda(t) \in R^n$ is an undetermined multiplier. The objective is to determine *u(t)* such that *H(t)* is minimized subject to the constraint (2.4). The stationary condition depicted in Appendix by (B.7), can not be simply used at this point due to the fact that the extreme of *H(t)* (2.7) is not a function of *u(t)*.

$$0 = \frac{\partial H}{\partial u} = \lambda^T B \tag{2.7}$$

Pontriagin and co-workers have shown that in the case of constrained control, the necessary conditions for optimal control, given in Appendix B, still apply if the stationary condition is replaced by a more general condition, known as "Pontriagin's Maximum Principle" [6]

$$H(x^*, u^*, \lambda^*, t) \le H(x^*, u^* + \delta u, \lambda^*, t), \quad \text{for all admissible } \delta u \tag{2.8}$$

where δu is the variation in u, and the starred quantities(*) denote the optimal values. This my also be written as

$$H(x^*, u^*, \lambda^*, t) \le H(x^*, u, \lambda^*, t), \quad \text{for all admissible } u \tag{2.9}$$

According to Pontriagin's maximum principle, the optimal control $u^*(t)$ must satisfy

$$1 + (\lambda^*)^T(Ax^*+\mathrm{Bu}^*) \le 1 + (\lambda^*)^T(Ax^*+\mathrm{Bu}) \tag{2.10}$$

or after simplification

$$(\lambda^*)^T Bu^* \le (\lambda^*)^T Bu \quad \text{for all admissible } u(t) \tag{2.11}$$

This condition allows $u^*(t)$ to be expressed in terms of the costate. It is easy to chose $u^*(t)$ to minimize the value of $\lambda^T(t)Bu(t)$. (Note: Minimize means that $\lambda^T(t)Bu(t)$ should take on a value as close to $-\infty$ as possible.)

If $\lambda^T(t)B$ is positive, select *u(t)=-1* to get the largest possible negative value of $\lambda^T(t)Bu(t)$. But on other hand, if $\lambda^T(t)B$ is negative, select *u(t)* as its maximum admissible value of *u(t)=1* to make $\lambda^T(t)Bu(t)$ as negative as possible. If $\lambda^T(t)B$ is zero at a sin-

gle point *t* in time, then *u(t)* can take any value at that time, since then $\lambda^T(t)Bu(t)$ is zero for all values of *u(t)*.

Then the time optimal control is given by

$$u^*(t) = -sign(B^T\lambda(t)) \tag{2.12}$$

where *sign()* is defined as:

$$sign(x) = \begin{cases} 1 & x > 0 \\ any & x = 0 \\ -1 & x < 0 \end{cases} \tag{2.13}$$

In both its computation and its final appearance, bang-bang control is fundamentally different from smooth control. Pontriagin's Maximum Principle leads to expression (2.12) for $u^*(t)$, but it is difficult to solve this equation explicitly for the optimal control. Instead, it can be seen that (2.12) specifies several different control laws, and that one must then select which among these is the optimal control. Thus, the Pontriagin Maximum Principle keeps one from having to examine all possible control laws for optimality, giving a small subset of potentially optimal controls to be investigated.

In the following, based on the knowledge of the time optimal control characteristic, a simplified feedback version of a bang-bang controller is presented.

2.1 Time-optimal Control of the Harmonic Oscillator

Since power system oscillation is a lightly damped electromechanical oscillation, a mechanical system model can be used to provide a better understanding. In this example a one-degree-of-freedom spring-mass oscillator, Figure 2-1, is used. In this model the dis-

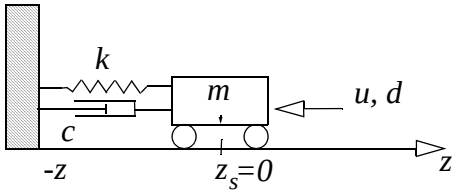

Figure 2-1 Spring-mass System

placement of mass from the origin can represent either the electrical power of the generator or the frequency-offset of the AC voltage in the power lines. The z_s point will represent the steady-state value of this parameter, but under the disturbance force *d* the mass will start to oscillate around this point just like the real electrical values will in the case of a disturbance on an electrical distribution line.

Consider the mechanical system model in Figure 2-1 where a body of mass *m*, moving along the *z* axis with velocity $v = \frac{d}{dt}z(t)$, is connected by a spring, of stiffness *k*, and a viscous damper with coefficient *c*, to a fixed support. The motion can be described by the second order differential equation of forces [8]

$$m\frac{d^2}{dt^2}z(t) + c\frac{d}{dt}z(t) + kz(t) = u(t) \qquad \xi = \frac{c}{2m} \qquad \omega = \sqrt{\frac{k}{m} - \left(\frac{c}{2m}\right)^2} \qquad (2.14)$$

$$\xi > 0 \qquad \omega > 0$$

where *z(t)* is the deviation of the body from the equilibrium position z_s, ω is the angular natural frequency of oscillations around the equilibrium point, and ξ is the damping ratio of the system. The motion of the body around the equilibrium point is an exponentially decaying harmonic oscillation with angular frequency ω as shown in Figure 2-2.

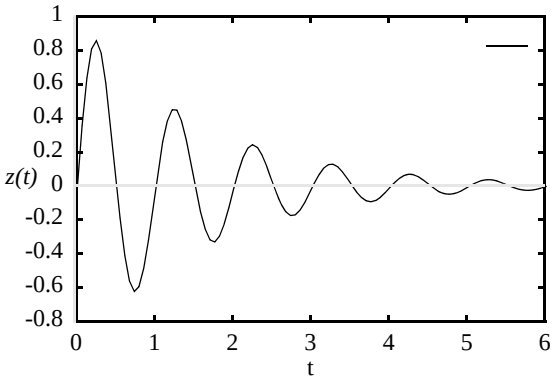

Figure 2-2 Free Damped Oscillations

Let

$$z_1(t) = z(t) \qquad z_2(t) = \frac{d}{dt}z(t) \tag{2.15}$$

be a set of state-variables, where $z_1(t)$ represents the deviation from equilibrium and $z_2(t)$ is the speed of the mass. The $z_i(t)$ satisfies the vector differential equation

$$\begin{bmatrix} \frac{dz_1}{dt} \\ \frac{dz_2}{dt} \end{bmatrix} = \begin{bmatrix} 0 & 1 \\ -(\xi^2 + \omega^2) & -2\xi \end{bmatrix} \begin{bmatrix} z_1 \\ z_2 \end{bmatrix} + \begin{bmatrix} 0 \\ K \end{bmatrix} u(t)$$
$$z(t) = \begin{bmatrix} 1 & 0 \end{bmatrix} \begin{bmatrix} z_1 \\ z_2 \end{bmatrix} \tag{2.16}$$

where $K = \frac{1}{m}$ and ξ is the damping coefficient of oscillation.

It is convenient to use the canonical form [4][3], to define a new set of state variables $x_1(t)$ and $x_2(t)$ by applying a suitable linear transformation,

$$\begin{bmatrix} x_1(t) \\ x_2(t) \end{bmatrix} = \frac{1}{K} \begin{bmatrix} \omega & 0 \\ \xi & 1 \end{bmatrix} \begin{bmatrix} z_1(t) \\ z(t) \end{bmatrix} \tag{2.17}$$

or the inverse transformation from canonical model back to the physical model:

$$\begin{bmatrix} z_1(t) \\ z_2(t) \end{bmatrix} = K \begin{bmatrix} \frac{1}{\omega} & 0 \\ -\frac{\xi}{\omega} & 1 \end{bmatrix} \begin{bmatrix} x_1(t) \\ x_1(t) \end{bmatrix} \tag{2.18}$$

The x variables satisfy the vector differential equations in canonical form

$$\begin{bmatrix} \frac{dx_1}{dt} \\ \frac{dx_2}{dt} \end{bmatrix} = \begin{bmatrix} -\xi & \omega \\ -\omega & -\xi \end{bmatrix} \begin{bmatrix} x_1 \\ x_2 \end{bmatrix} + \begin{bmatrix} 0 \\ 1 \end{bmatrix} u(t) \tag{2.19}$$

Now the time-optimal control algorithm for the damped harmonic oscillations can be formulated. The Hamiltonian H based on (B.4) from Appendix B is given by

$$H = 1 - \xi x_1(t)\lambda_1(t) + \omega x_2(t)\lambda_1(t) - \omega x_1(t)\lambda_2(t) - \xi x_2(t)\lambda_2(t) + u(t)p\lambda_2(t) \tag{2.20}$$

The control which absolutely minimizes the Hamiltonian is

$$u(t) = -sign(\lambda_2(t)) \tag{2.21}$$

The solution of this equations is presented in the literature [4][3] and given by the relation

$$\lambda_2(t) = e^{\xi t}(\lambda_1(0)\cos(\omega t) + \lambda_2(0)\sin(\omega t)) \tag{2.22}$$

which means that (since $\xi > 0$) the function $\lambda_2(t)$ is the product of an increasing exponential and a sinusoid. Figure 2-3 illustrates a typical function $\lambda_2(t)$ and the control $u(t)$ defined by equation (2.21) as a function of $\lambda_2(t)$.

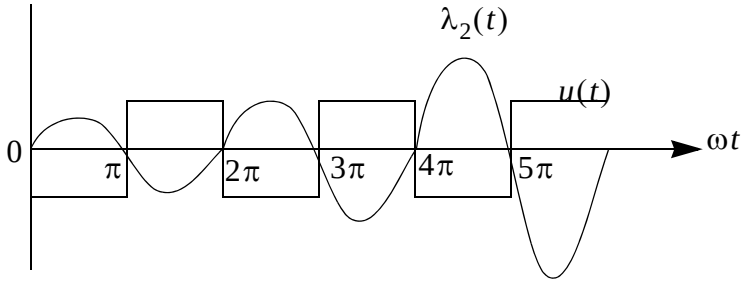

Figure 2-3 A typical function $\lambda_2(t), u(t)$

The control $u(t)$ has the following properties [4]:

1.It must be piecewise constant and must switch between the values *+1* and *-1*.

2.It cannot remain constant for more than π/ω units of time.

3.There is no upper bound on the number of switching.

After extensive algebraic manipulation, the control $u(t)$ can be defined throughout the state-space. It divides the state space into two regions, thus forming a switching boundary, shown in Figure 2-4, created based on the literature [4].

While in principle the method above may be applied to higher-order systems with complex roots, the computational difficulties are immense and therefore some sort of approximation is usually made [3].

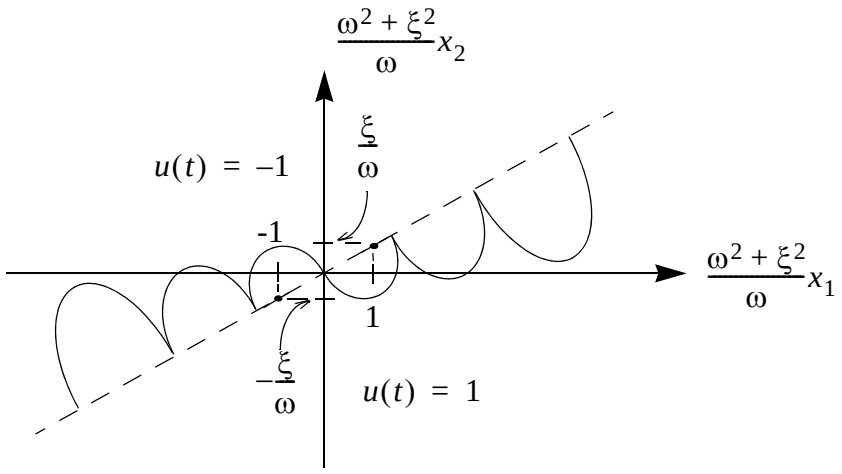

Figure 2-4 Switching curve for damped harmonic oscillator

2.2 Bang-Bang Control Law

The control objective is to bring the state from any initial point to the desired final state in the minimum time. How this objective can be achieved for second order systems is described in the previous section. The following two sections will introduce some approximations in the optimal control law [10].

The oscillation of the body is due to the exchange of the body's kinetic energy and the spring's potential energy. The oscillations can be eliminated by reducing, or eliminating, this energy by the control force *u(t)* acting against the movement of the body. The simple feedback control law, which is identical to that derived from equation (2.12) is:

$$u = -sign(v) \qquad v = \frac{dz}{dt} \tag{2.23}$$

The resulting changes in the body movement can be represented in the phase plane of displacement and velocity, Figure 2-5. The control action behaves optimally only far from

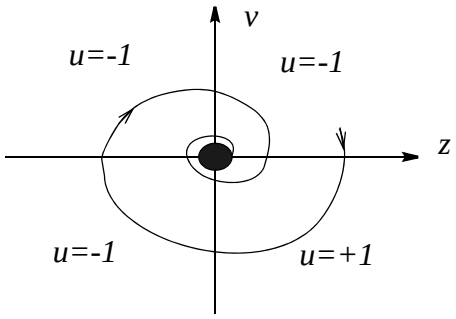

Figure 2-5 Phase-plane - I

the equilibrium point and causes persistent control switching near the equilibrium point, since the control value can never be zero. In order to prevent this outcome, one can introduce a suitable dead band in the control law, delimited by a velocity threshold v_t (2.24). However, it is apparent that without mechanical damping, the system is not asymptotically stable at any point.

$$u = \begin{cases} 0 & |v| \le v_t \\ -sign(v) & |v| > v_t \end{cases} \tag{2.24}$$

The resulting control transient can be divided into two phases In the first phase, far away from the origin, the system trajectory is a spiral of quickly decreasing radius. The second

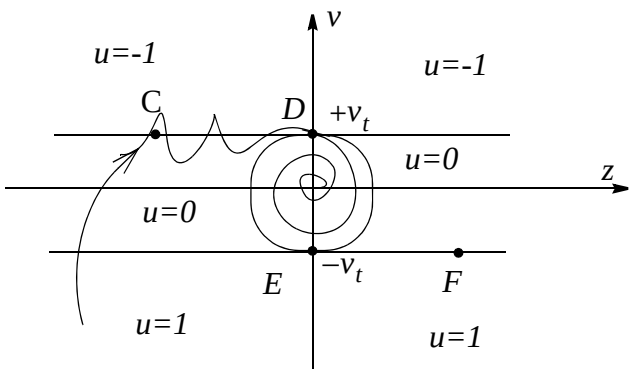

Figure 2-6 Phase-plane - II

phase (Figure 2-6) begins when the trajectory first crosses one of the two segments, CD or EF, i.e. when the elastic force becomes weaker than the control force, so the controller will succeed in keeping the velocity small even if the position is “far” away from the origin. Due to the particular kind of discontinuity in the control law, the differential equations (2.14) and (2.24) have no solution in the classical sense. If it is required that the residual velocity be small, the threshold has to be kept low, causing the control transient to lengthen and much more control action to be used. In some cases the high frequency commutations could be harmful when applying this control law.

2.3 Modified Bang-Bang Control Law

Some simple consideration suggests a suitable modification to the above described control law. For example, let $z<0$ and $v>0$, so that $-kz>0$ and $u=-1$. The elastic force of the spring

F_s is pulling the body towards the origin, while the control force is directed away from the origin. If the velocity towards the origin is low enough, it can become lower than the threshold v_t, before the origin has been reached, thus starting the high frequency control commutation. The simplest way to avoid this is to inhibit the activation of the control force whenever it is greater than the elastic force acting on the body.The resulting control law and control system trajectory are shown in Figure 2-7.

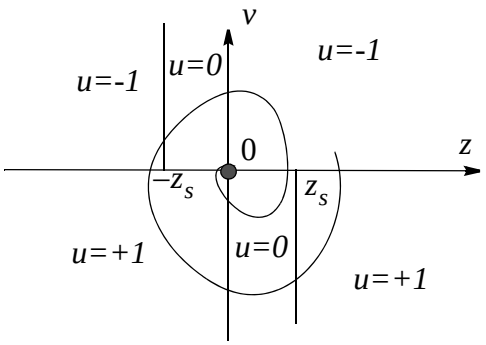

$$F_s = zk$$

$$z_s = \frac{u}{k} \qquad (u = 1)$$

Figure 2-7 Modified law

Finally, in order to avoid persistent control action in the neighborhood of the origin, this control law can be suitably modified by adding an acceleration dead band [10]. The resulting control law is then defined on the acceleration-velocity plane, where $a_c = \frac{u}{m}$ is the acceleration that the control force can impress on the body as shown on Figure 2-8. The control force is activated with the maximum available intensity in opposition to the velocity. A switching logic based on the value of the elastic acceleration term and of the veloc-

ity itself may inhibit the activation of the control force. This control law has been tested on a seventh order power plant model, described in the next section.

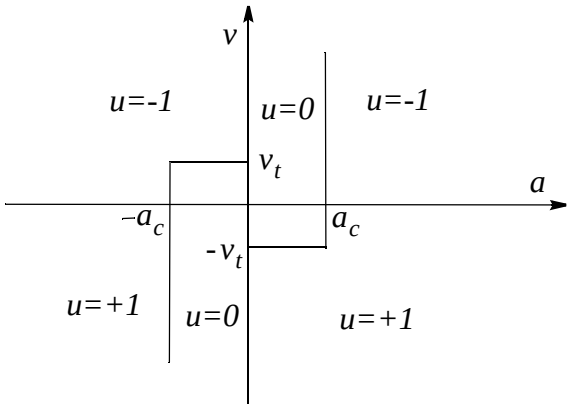

Figure 2-8 The control law

2.4 Simulation Studies

Behavior of the proposed controller has been verified by means of simulation under ideal conditions, by using a seventh order mathematical model which simulates power system behavior.

2.4.1 Single-Machine Infinite-Bus System

A single-machine infinite-bus system is the simplest form of a power system model[10]. It is useful to understand the dynamic behavior of an electrical power system and to design and test a controller to improve its performance and stability.

A simple schematic representation of a single-machine infinite-bus system is shown in Figure 2-9.

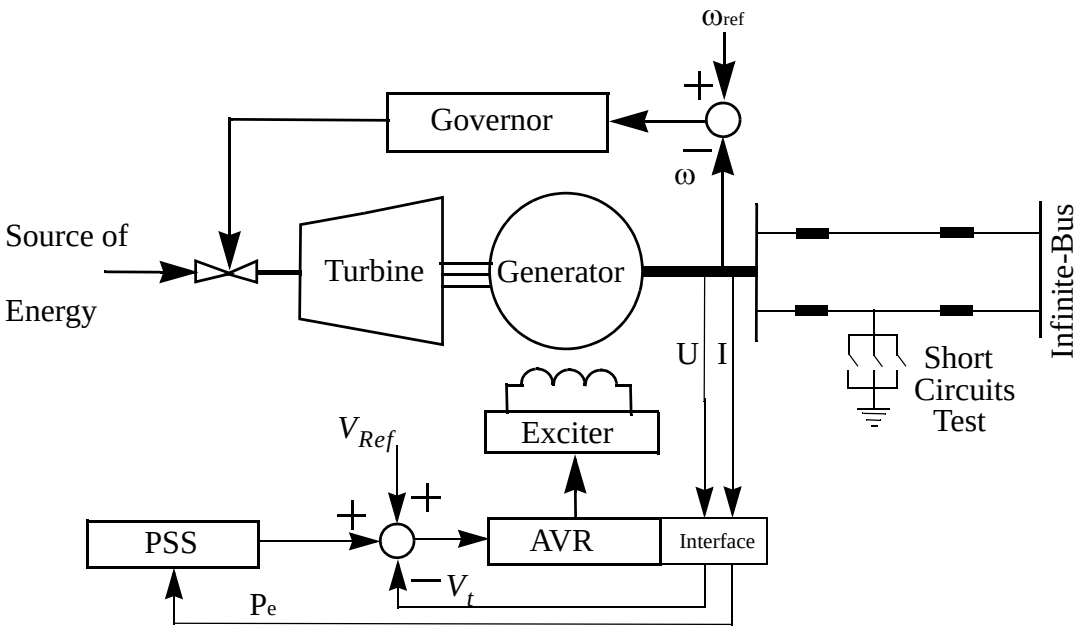

Figure 2-9 Diagram of basic power system

The system consists of a generating unit connected to a constant voltage bus through two parallel transmission lines. An excitation system and Automatic Voltage Regulator (AVR) are employed to control the terminal voltage (V_t). An infinite-bus is a source of invariable frequency and voltage. A bus of very large capacity compared to the rating of the machine under consideration approximates an infinite bus [36]. A detailed mathematical model of this system is given in Appendix C.

2.4.2 Studies

A nonlinear modified bang-bang controller, based on an approximation of the Pontriagin's Maximum Principle, has been proposed to serve as the power system stabilizer. The resulting control system has been tested by means of simulation. Results of the simulations are given in Figure 2-10 to Figure 2-13, for two different types of disturbances.

Speed deviation for a three phase to ground fault disturbance is shown in Figure 2-10. In this test a generator with the power system stabilizer is connected to an infinite bus (very big generator) by a double transmission line, presented in Figure 2-9. With both lines in operation, a three phase to ground fault in the middle of one transmission line was applied at *2.4 s*, and cleared *100 ms* later by the disconnection of the faulted line and successful reclosure at *8 s*. The control action shown in Figure 2-11 responds correctly in the initial stages of this disturbance. Later, as the system starts to settle and the control force exceeds the disturbance, the control algorithm does not switch off properly. Instead it attempts to stabilize the speed at a point away from the equilibrium.

Speed deviation for a mechanical power step change is shown in Figure 2-12. The mechanical power is changed by *0.1 p.u.* at *2 s* and by *-0.1 p.u.* at *6 s.* Similar to the previous case, the control action, presented in Figure 2-13, responds correctly in the first stages of this disturbance. Later, as the system starts to settle and the control force exceed the disturbance, the control algorithm does not switch off properly. Instead it attempts to stabilize the speed at a point away from the equilibrium. When it finally comes to switching off the control action, the generator's speed deviation still contains significant oscillations.

These results imply that the control signal, $u = 0.1$ p.u. or $u = -0.1$ p.u., has too strong action on the power system; and therefore the proposed algorithm is not the best power system stabilizer.

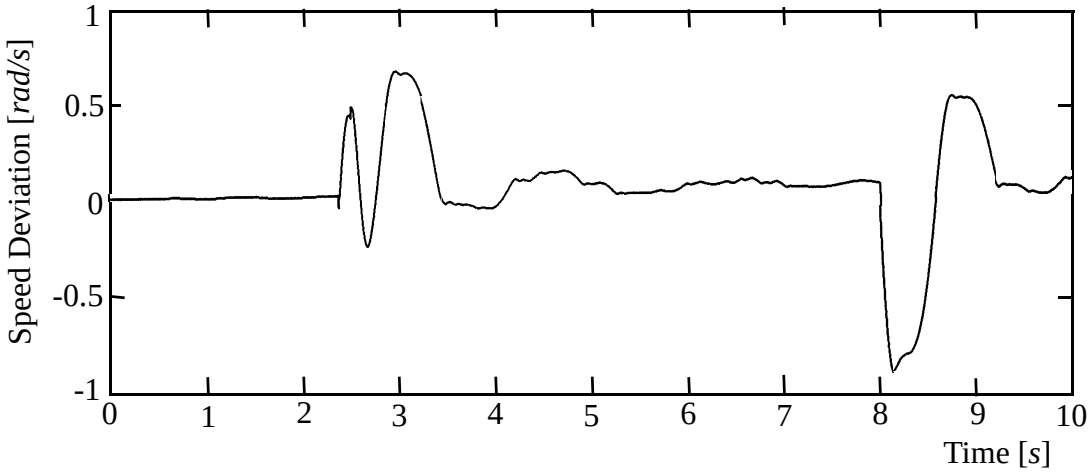

Figure 2-10 Speed Deviation - Three Phase to ground fault test (0.1s)

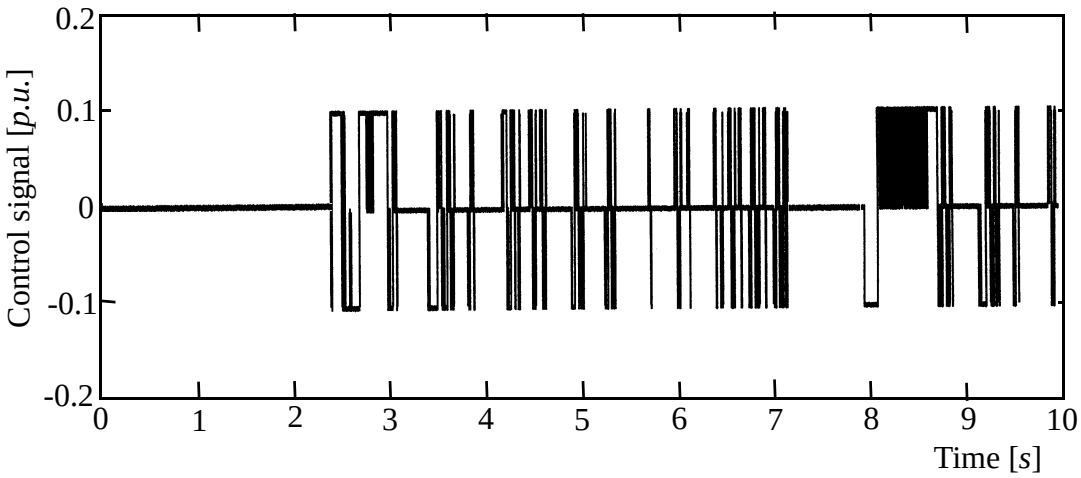

Figure 2-11 Control Signal - Three Phase to ground fault test (0.1s)

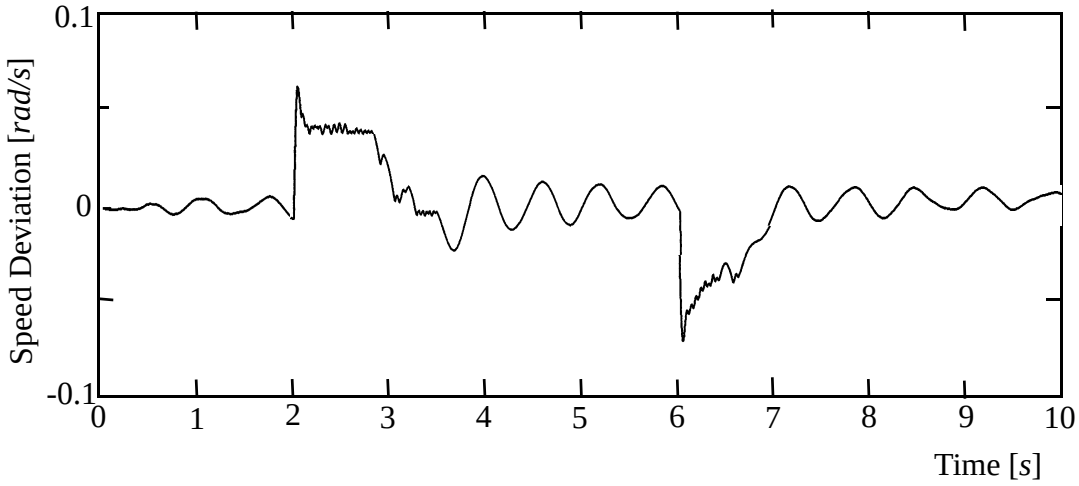

Figure 2-12 Speed deviation - Mechanical power step change: 0.1/-0.1 p.u.

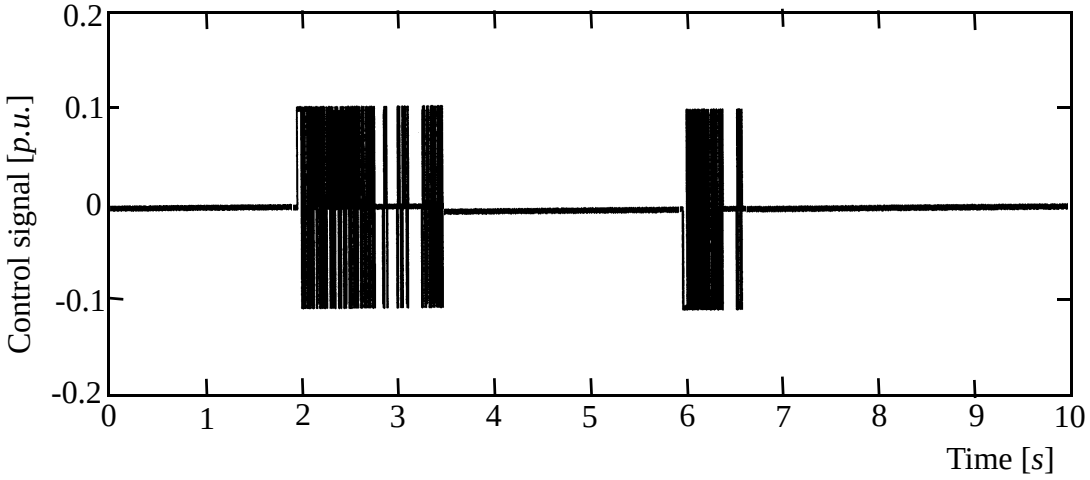

Figure 2-13 Control signal - Mechanical power step change: 0.1/-0.1 p.u.

2.4.3 Discussion

The problem of the too strong action of the control signal originates from the situation where the control force is stronger than the system's oscillatory force and in this case the control force can stabilize the system even far from the stability point by high frequency chattering of the control signal.

This case is illustrated in Figure 2-14: z_s is the correct equilibrium point, but the body is stabilized some distance z_d from this point. During the research, experiments were done with different mechanisms to switch the control to zero at the appropriate time, but none of these experiments provided satisfactory results. If they worked well for one type of disturbance they did not work well for other types.

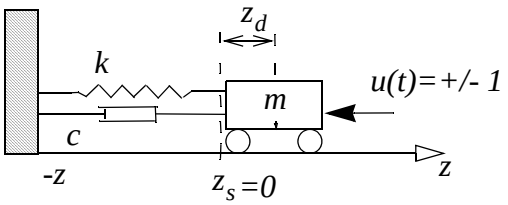

Figure 2-14 Stabilization in wrong place

In conclusion, the major problem, which exists in all optimum switched-system designs, is eliminating the inevitable high speed chattering around the origin.

Based on these experiments one can conclude that the applied approximation on the time optimal control law is invalid for this particular case of the power system stabilization. However similar approximations may be useful for different control systems.

One possible solution to eliminate this high speed chattering is to switch on a linear control algorithm when the error is close to the origin. This algorithm is the so called dual-mode control algorithm. A dual-mode control system combines many of the good features of both the linear system and the optimum switched or relay system. It consists of two parallel path being active for small signals, and a relay path active for large signals. The major advantages of such device are [3]:

1. It uses a simple relay amplifier for large error, where a linear system would require a high-power linear amplifier. The amplitude range and power requirement of the small-signal linear amplifier are thus reduced.
2. It uses a small-range (economical) linear system so to eliminate the complicated switching boundaries required by a high-order optimum-relay servo and to ensure local asymptotic stability.

Probably the major disadvantage unique to the dual-mode system is the possibility of indecision, i.e., oscillation, at the mode switching boundary. The major argument against using this type of approximation of the time optimal control is in the fact that relay mode and the linear mode are stable by themselves but this does not mean that in combination the result will be stable [3].

Time-optimum control is, of course, only one special example of the general optimum-control problem. Rather than time, the design of optimal linear control systems with quadratic criteria might be more suitable for power system stabilization.

II Adaptive Optimal Control

One of the most exciting developments in automatic control in the past half century is the emergence of a new concept called adaptive control. Rather than being designed to do a certain function as is a conventional control system, the adaptive controller is allowed to organize itself, in a restricted sense, so as to yield optimum performance with respect to one or several indices of performance selected by the designer[3].

When fast Digital Signal Processors (DSP) are used to implement a controller it is possible to implement a more complicated control algorithm. A natural step is to include both a parameter estimation method and control design algorithms. In this way it is possible to obtain an adaptive control algorithm that determines the mathematical models and then performs control system design on-line[12].

The necessary theoretical information is described in the following. It is assumed that the system is observable and controllable. The control algorithm is based on the Linear Quadratic Gaussian theory. The states of the system are estimated by a Kalman filter, and a Recursive Least Squares adaptive algorithm is implemented to identify the system model by using the input-output measurements.

3 System Parameter Estimation

All techniques for analysis and design of control systems are based on the availability of appropriate models for the process dynamics. The model structures are derived from prior knowledge of the process and the disturbances. In some cases, only a priori knowledge is available so that the process can be described as a linear system in a particular operating range. It is then natural to use the general representation of linear systems. Such representations are called black-box models. A typical example is the difference-equation model

$$\sum_{i=1}^{m} a_i y((n-i)T) = \sum_{i=1}^{m} b_i u((n-i)T) + \sum_{i=1}^{m} c_i \hat{e}((n-i)T) \qquad (3.1)$$

where u is the input, y is the output, and $\hat{e}$ *is a white-noise disturbance. The parameters, as well as the order of model, are considered as the unknown parameters [12].*

For real time identification, recursive parameter estimation methods have been developed for linear time invariant and time variant processes, for some classes of nonlinear processes and for stationary and some classes of nonstationary signals [13]. A large number of methods have been developed for recursive parameter estimation. However, there is no method that is universally best. In this thesis the method used is the Recursive Least Squares (RLS) method which is one of the basic techniques for parameter estimation. The RLS method is characterized as one of the faster converging. However, it is one of the most computationaly complex algorithms. The computational complexity problem was eliminated by using a fast DSP based controller for the calculation of the control action.

3.1 Least Squares Identification

Least-squares is an old method dating back to Gauss[1] in the eighteenth century where he used it to determine the orbit of planets. The basic idea behind least-squares is fitting a mathematical model to an observed sequence by minimizing the sum of the squares of the difference between the observed and the estimated data. In doing so, any noise or inaccuracies in the observed data are expected to have less effect on the accuracy of the mathematical model. The basic structure of the least-squares parameter estimation algorithm is presented in Figure 3-1. The feedback of $\hat{e}(nT)$ with an arrow through the identifier box

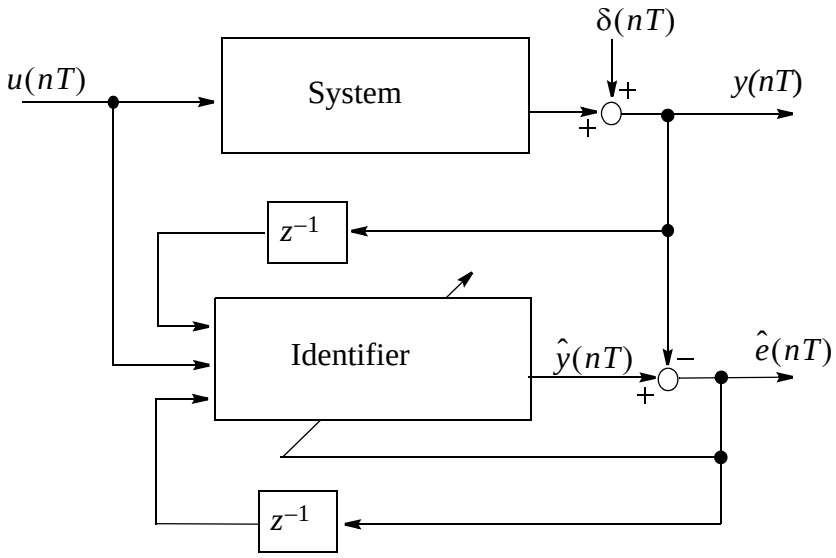

Figure 3-1 Recursive Least Squares parameter estimation

1. Karl Friedrich Gauss, 1777-1855. German mathematician & astronomer

indicates that the prediction error is the performance information used to adjust the identifier parameters. The computed variable, the predicted value of the system output, is calculated by the model in difference equation form as

$$\hat{y}(nT) = \sum_{i=1}^{m} b_i u((n-i-1)T) - \sum_{i=1}^{m} a_i y((n-i)T) + \sum_{i=1}^{m} c_i \hat{e}((n-i)T) \qquad (3.2)$$

where $m \geq 1$ is the model order, a_i, b_i and c_i are unknown parameters and $u(jT), y(jT), \hat{e}(jT)$ are known functions in time. It is allowed that the parameters a_i, b_i and c_i take value *zero* if $i > k_a, i > k_b$ and $i > k_c$, respectively. The values of $\{k_a, k_b \text{ and } k_c\} \leq m$ are determined by the dynamics of the plant model. The model represented by equation (3.2) is called an ARMAX process, i.e., an autoregressive moving average ARMA process with an exogenous signal [12].

The function $\hat{e}(jT)$ is defined by the equation

$$\hat{e}(jT) = \hat{y}(jT) - y(jT) \qquad (3.3)$$

The task is to determine the unknown parameters in such a way that the variable $\hat{y}(nT)$, computed from the model of (3.2) agrees as closely as possible with the measured variable $y(nT)$. In the method of exponentially weighted least squares, the parameters should be selected in such a way that the cost function

$$J(n) = \sum_{i=1}^{n} \lambda^{n-i} |\hat{e}(i)|^2 \qquad (3.4)$$

is minimum, where λ is the forgetting factor, close to, but less than, *1*. The use of a forgetting factor is intended to ensure that data points in the distant past are “forgotten” in order

to afford the possibility of following the statistical variations of the observable data when the filter operates in a nonstationary environment [14]. The relation between the forgetting factor and the “memory” length is given by [15]

$$\lambda = e^{-1/l} \tag{3.5}$$

where l is the memory length measured in samples and e is the base of natural logarithm.

3.2 The Recursive Least-Squares (RLS) Algorithm

In adaptive control the observations are obtained sequentially in real time. Computation of a least-squares estimate can be arranged in such a way that the result obtained at time *(n-1)T* can be used to calculate the estimate at time *nT*. In this section, the Recursive Least-Squares (RLS) algorithm based on the above method is described. The RLS algorithm is represented by the diagram in Figure 3-2. The simplest way to implement and describe the

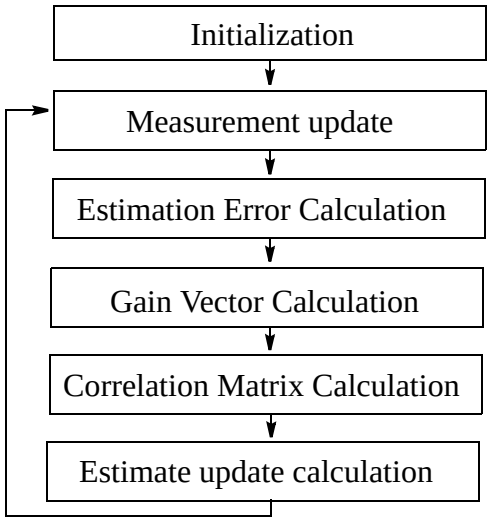

Figure 3-2 RLS algorithm

RLS algorithm is to use matrix notation and calculation. The RLS algorithm should estimate the parameter vector

$$\Theta(nT)^T = \left[b_1 \ \ldots \ b_m \ a_1 \ \ldots \ a_m \ c_1 \ \ldots \ c_k\right] \tag{3.6}$$

3.2.1 Initialization

For the RLS algorithm the recursion is initialized by choosing a starting value $P(0)$ that assures the nonsingularity of the correlation matrix $P(0)^{-1}$ It is recommended that it should be initialized as

$$P(0) = \delta I \tag{3.7}$$

were I is an m-by-m identity matrix, and δ is a large positive constant (for example $\delta = 10^{12}$ for this research). If the selected constant δ is relatively small the convergence of identification at the start is much slower.

The rest of the vectors should be initialized to zero or updated by the measurement variables.

3.2.2 Measurement Update

At the start of each recursion the measurement vector

$$\Psi(nT)^T = \left[u(nT) \ \ldots \ u(n-m+1)T) \ -y(n-1)T) \ \ldots \ -y(n-m)T) \ \hat{e}(n-1)T) \ \ldots \ \hat{e}(n-k)T)\right] \tag{3.8}$$

should be updated with the measurement variables $u(nT), y((n-1)T)$ and with the estimated error from the previous recursion $\hat{e}((n-1)T)$.

3.2.3 Estimation Error Calculation

The estimation error is defined by

$$\hat{e}(nT) = y(nT) - \Psi(nT)^T \Theta((n-1)T) \tag{3.9}$$

where the product $\Psi(nT)^T \Theta((n-1)T)$ represents an estimate of the desired response $y(nT)$, based on the old least-squares estimate of the parameters $\Theta((n-1)T)$. In other words, $\hat{e}(nT)$ can be interpreted as the error in predicting the signal $y(nT)$ one step ahead based on the estimate $\Theta((n-1)T)$.

3.2.4 Gain Vector Calculation

The gain vector is defined as

$$K(nT) = \frac{P((n-1)T)\Psi(nT)}{\lambda + \Psi(nT)^T P((n-1)T)\Psi(nT)} \tag{3.10}$$

where λ is the forgetting factor. Hence, as the memory of the algorithm is shortened by reducing the exponential weighting factor λ, the misadjustment is correspondingly increased. In other words, fast adaptation of the RLS algorithm, in general, results in a more noisy adaptive process [14]. To achieve a compromise in the implementation of the

forgetting factor an adaptive solution is implemented. The on-line calculated variable forgetting factor is a function of the estimation error given in the following form

$$\lambda(nT) = \begin{cases} \lambda((n-1)T)\lambda_d + (1-\lambda_d) & if(\hat{e}(nT)^2 < e_d) \\ \lambda_r & if(\hat{e}(nT)^2 \geq e_d) \end{cases} \tag{3.11}$$

where $\lambda_d, \lambda_r, e_d$ are experimentally selected constants, respectively *0.995*, *0.97* and *0.005*. As an example, the $\lambda(nT)$ variation in time can be presented as in Figure 3-3. The

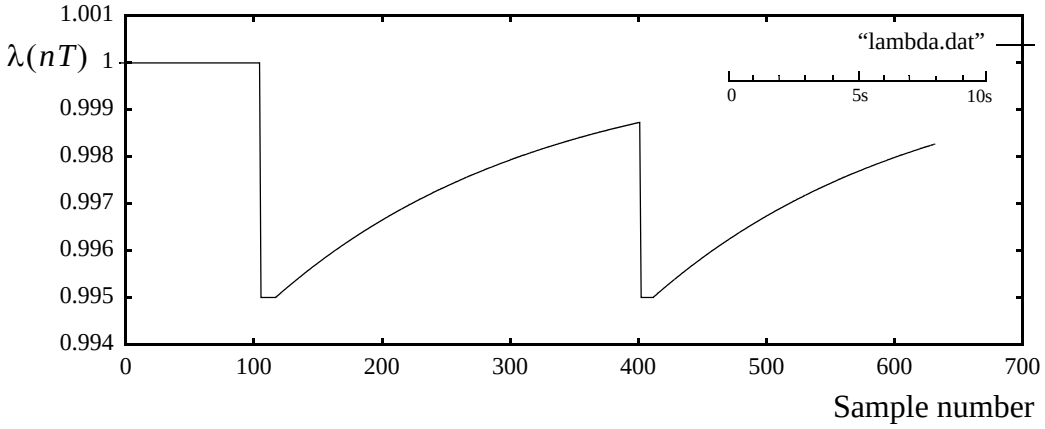

Figure 3-3 Forgetting factor $\lambda(nT)$ variation in time

forgetting factor was constant with value *1* until the *100th* sample, where a disturbance increased the estimation error beyond the e_d limit and λ was set to the value λ_r. By applying (3.11), λ approaches the level *1* but at the *400th* sample, a new disturbance again sets the value of λ to λ_r. With this solution, the algorithm is well balanced between the longer and shorter "memory".

3.2.5 Correlation Matrix Calculation

The correlation matrix is updated as

$$P(nT) = \frac{1}{\lambda}(P((n-1)T) - K(nT)\Psi(nT)^T P((n-1)T)) \tag{3.12}$$

The matrix $P(nT)$ can be interpreted as the correlation matrix of the coefficient-error vector $\Theta(nT) - \Theta_0$, where Θ_0 is the optimum Wiener value of the coefficient vector. That is

$$P(nT) \approx E[(\Theta(nT) - \Theta_0)(\Theta(nT) - \Theta_0)^T] \tag{3.13}$$

This result, however, only holds if the error $\hat{e}(nT)$ has zero mean and its elements are uncorrected [14]. To satisfy this requirement it is necessary to remove the DC components from the input signal $y(nT)$ and $u(nT)$.

3.2.6 Estimate Update Calculation

The robust RLS estimate update is defined by recursive equation

$$\Theta(nT) = \Theta((n-1)T) + K(nT)\hat{e}(nT)\beta(nT) \tag{3.14}$$

The estimate $\Theta(nT)$ is obtained by adding a correction to the previous estimate $\Theta((n-1)T)$. The components of the vector $K(nT)$ are weighting factors that tell how the correction and the previous estimate should be combined. The correction term is proportional to the prediction error modified by the ***tracking constrained coefficient*** $\hat{e}(nT)\beta(nT)$. The net effect of this weighting is to decrease the impact of large errors.

The least-squares estimate is optimal if the disturbances are Gaussian and this causes the prediction error to appear as white noise. In practice the least-squares estimates have some drawback because the assumptions are violated. It is a direct consequence of the least-squares formulation that a single large error will have a drastic influence on the result because the errors are squared in the criterion [15]. To correct this impact, the tracking constrained coefficient is introduced in the algorithm:

$$\beta(nT) = \begin{cases} 1 & \text{if} \quad N_2/N_1 \le \beta_0 \\ \beta_0/N_2 & \text{if} \quad N_2/N_1 > \beta_0 \end{cases} \tag{3.15}$$

where

$$N_1 = \|\Theta((n-1)T)\|_1 \tag{3.16}$$

$$N_2 = \|K(nT)\hat{e}(nT)\|_1 \tag{3.17}$$

and the norm is defined as

$$\|X\|_1 = \sum_{i=1}^{m} |x_i| \tag{3.18}$$

The β_0 variable is selected empirically as an appropriate threshold to eliminate the influence of large disturbances. Here β_0 is set to 0.006. However, it is very important that in the first period, when the adaptation is starting after the initialization, the tracking constrained coefficient should be disabled by setting $\beta(nT) = 1$. In contrast, the adaptation will be disabled by the action of this constraint.

The RLS algorithm described above was implemented as a part of a power system stabilizer for the micro-synchronous generator power system model. The environment for the

control system implemented, together with the applied disturbances are described in detail in Chapter 7 “System Parameter Estimation”. The following graphs demonstrate a typical case when the RLS algorithm is running in steady state with the prediction error around 10^{-3}. At the 100th and 400th sample, two disturbances occur which cause the estimation error to increase by approximately 100 times.

In Figure 3-4 the estimation error is illustrated including two large disturbances at the 100th and 400th samples.

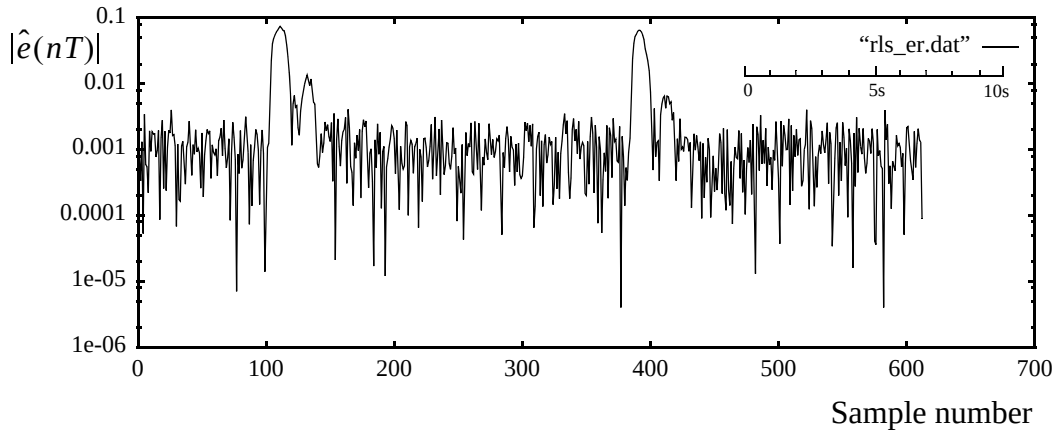

Figure 3-4 Estimation error (the absolute value)

Figure 3-5 and Figure 3-6 represent the first norm, $\|\Theta((n-1)T)\|_1$, changes for the

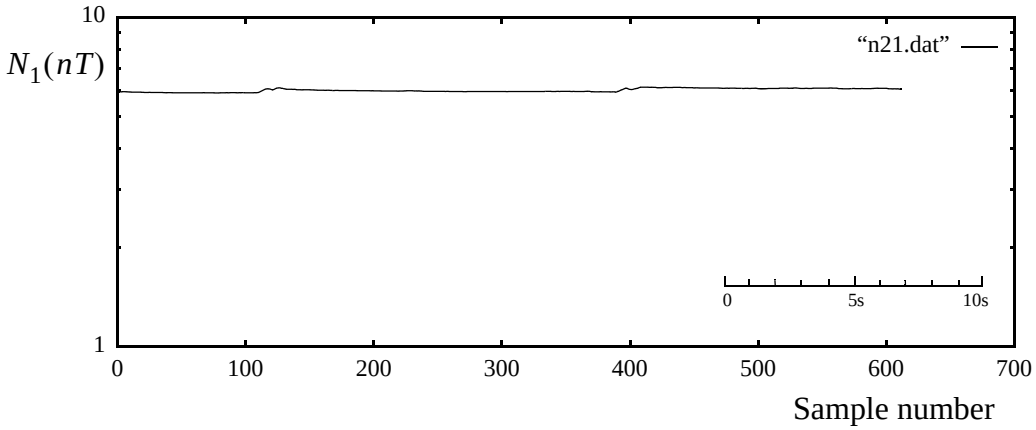

Figure 3-5 Changes of N_1, (3.16), in time

parameter vector $\Theta((n-1)T)$ and for the vector received as a product of the multiplication of the gain vector with the estimation error $N_2(nT) = \|K(nT)e(nT)\|_1$, for the same disturbances as in Figure 3-4.

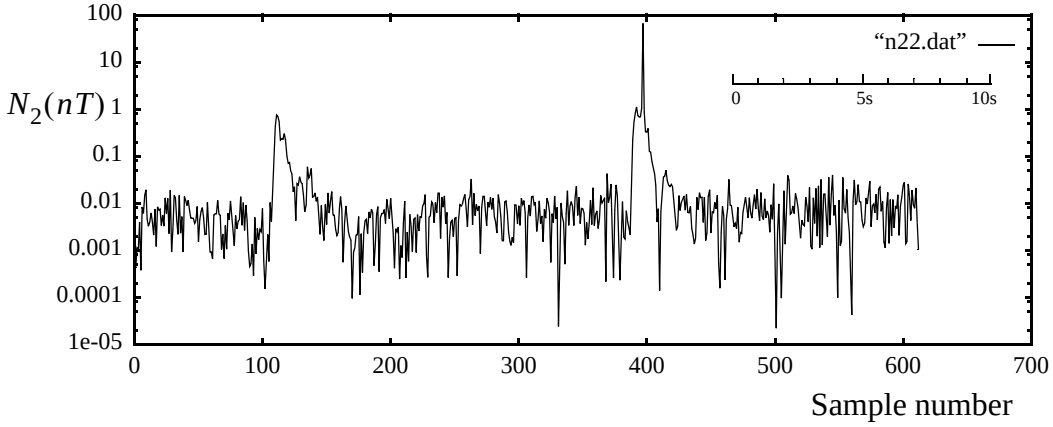

Figure 3-6 Changes of N_2, (3.17), in time

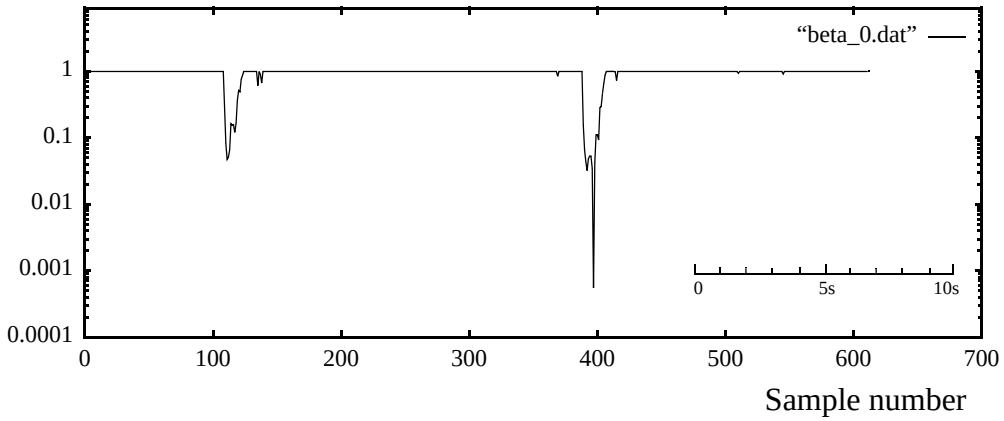

Figure 3-7 Changes of $\beta(nT)$ in time

The effect of the robust adaptation is well presented in Figure 3-7. If a large disturbance happens, the $\beta(nT)$ constraint changes from 1 to a small number and reduces the effect of the suddenly increased estimation error.

3.2.7 Results of Identification

The estimated a_i and b_i parameters with this robust estimation algorithm behave smoothly even with the disturbances and prediction error represented in Figure 3-4. In this research a fifth order model was selected without the extended part $c_i = 0 \forall i$. The typical estimated parameter can be represented as in Figure 3-8 and Figure 3-9.

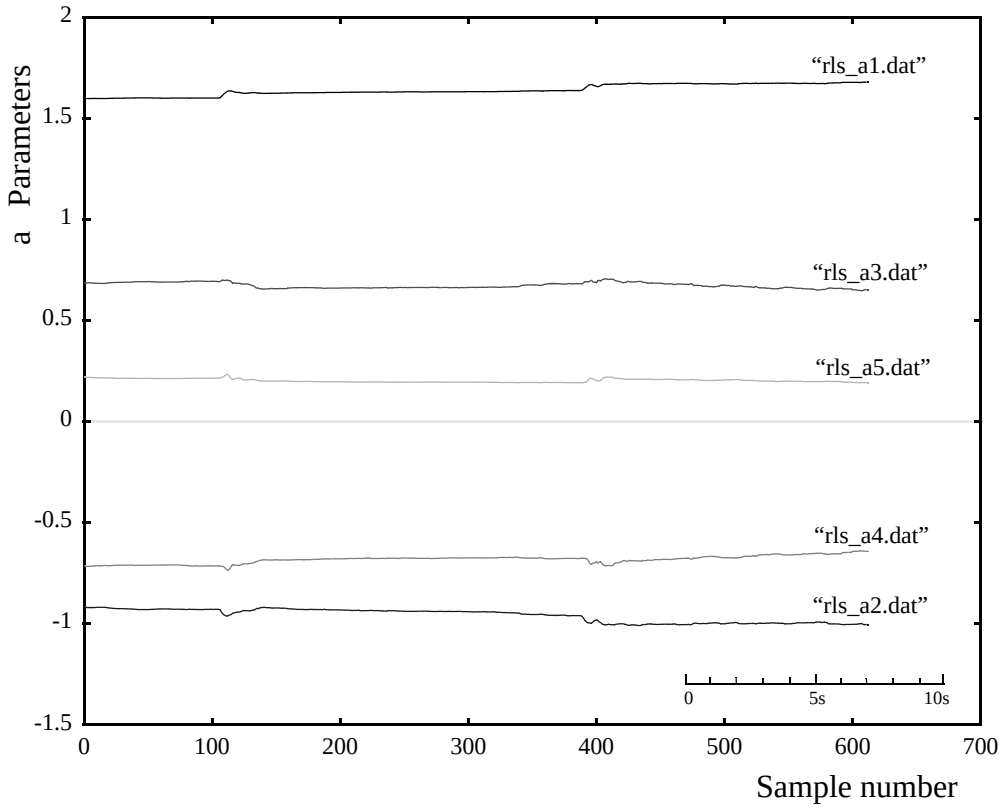

Figure 3-8 Identified a_i parameters

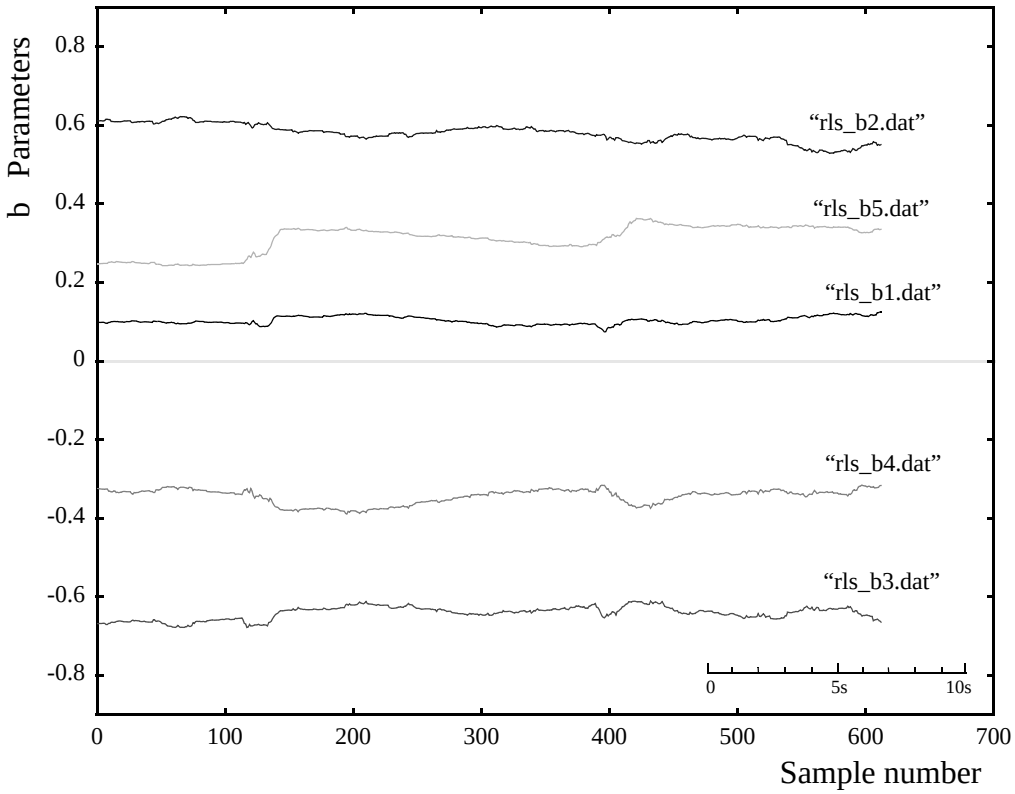

Figure 3-9 Identified b_i parameters

The proposed control algorithm is based on the estimated a_i and b_i parameters, in state-space representation, to calculate the control signals. How to form a state-space representation of the system if these parameters are known, is described in the following chapters.

3.3 Stability Test

The selected discrete model represented by equation (3.2) can be characterized as an infinite-duration impulse response (IIR) filter. The feature that distinguishes an IIR filter is the inclusion of a feedback part, through the $y(iT)$ system output and a_i parameters. Indeed, it is the presence of feedback that makes the duration of the impulse response of an IIR filter (model) infinitely long. Furthermore, the presence of feedback introduces a new problem, namely, that of the possibility of instability. In particular, it is possible for an IIR filter output to become unstable (i.e., break into oscillation), for some estimated parameters a_i during the exogenous disturbances [12]. The straightforward way to analyze the stability of the estimated parameters is by using the characteristic equation:

$$1 + a_1 z^{-1} + a_2 z^{-2} + \ldots + a_m z^{-m} = 0 \tag{3.19}$$

For a stable model it is required that the roots of equation (3.19) lie inside the unit circle, or in another words, the zeros $z_i, \quad i = 1 \ldots m$ of characteristic equations must be inside the unit circle.

During the simulation it was recognized that the exogenous disturbance caused at least one pole of the model to move outside the unit circle. This instability was eliminated by introducing a tracking constraining coefficient, $\beta(nT)$, described in section 3.2.6.

3.4 On-line Identification in Closed Loop

In the proposed adaptive control system, the control is based on the identified process model, but the process identification has to be performed in a closed loop. Identifiability could be lost if the input was generated by feedback from the output. The problem is quite obvious if a correlation analysis is considered because the feedback is an integral part of the overall system. For convergence of the cross correlation function, on what the least squares algorithm is based, it is required that the error signal $\hat{e}(nT)$ is not correlated with the elements of the data vector $\Psi(nT)$ [13]. Feedback, however, generates such a correlation. To satisfy this requirement it is necessary to introduce into the input signal $u(nT)$ an external perturbation $u_s(nT)$. The perturbation signal is a noise signal and acts on the closed loop as shown in Figure 3-10. The perturbation signal is a random sequence of ±1

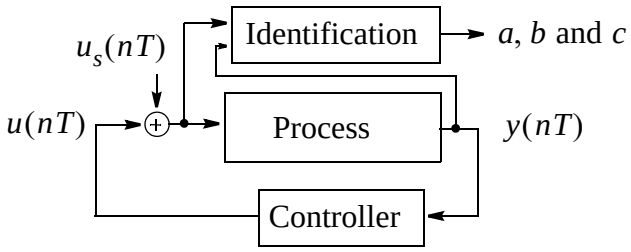

Figure 3-10 Closed loop identification

scaled to *5%* of the control signal. In this way the process is directly identifiable. The 5% external perturbation is sufficient to excite the process, in order that it is identifiable, without causing performance degradation or instability of the power system.

4 State-Space Representation

Since their introduction by Leibnitz[1] and Newton[2] in the seventeenth century, differential equations have provided concise mathematical models for many dynamic systems. A very important event in the late fifties was the development, based on this technique, of state-space theory for control system design by Kalman[3]. This is a modern approach for the analysis and synthesis of control systems in the time domain. State variables completely describe the dynamics of the system with the minimum amount of information which is necessary to determine both the future states and the system outputs for any given input function.

The power of modern control has its roots in the fact that the state-space model can represent both multi input - multi output (MIMO) systems and single input - single output (SISO) systems. That is, the inputs and outputs are generally represented by vectors whose entries are the individual scalar inputs and outputs. This vectors can be related by matrix functions which describes the system dynamics.

The objective in this chapter is to characterize the measurable outputs of dynamic systems as functions of the internal states and inputs of the system [17].

---

1. Gottfried Wilhelm Leibnitz, 1646-1716, German philosopher and mathematician
2. Isaac Newton, 1642-1727, English mathematician, scientist and philosopher
3. Rudolf Emil Kalman, 1930-, Hungarian born mathematical systems theorist

4.1 Discrete-Time State-space System Model

It will be shown in Chapter 6, that digital control laws are conveniently designed using the linear discrete-time state-space model given by a process equation (4.1) and by a measurement equation (4.2).

The *process equation* can be defined by the difference equation

$$x((n+1)T) = A(nT)x(nT) + B(nT)u(nT) + G(nT)w(nT) \tag{4.1}$$

The state of the system is represented by a vector $x(nT)$ of length m equal to the order of the system model. The system input is represented by a vector $u(nT)$ of length p equal to the number of inputs to the system. The process noise variable $w(nT)$ represents the error in the system model. The state transition matrix $A(nT)$, an $[m \times m]$ matrix, relates the system's present states to the future states. The input gain matrix $B(nT)$ is an $[m \times p]$ matrix, and represents the effect of the system input on a particular state of the system. The process noise gain vector $G(nT)$ is an $[m \times 1]$ vector, and connects the process noise to a particular state of the system.

The *measurement equation* is defined by

$$y(nT) = C(nT)x(nT) + v(nT) \tag{4.2}$$

where the system output represented by the vector $y(nT)$ of length $[r \times 1]$ *is* equal to the number of the system outputs. The measurement noise vector $v(nT)$ of length r represents the error in the measurement equation. The parameter of the measurement equations is an $[\mathrm{m} \times r]$ measurement matrix $C(nT)$. The dimension r is the number of outputs.

In this work the number of inputs p and the number of outputs r is assumed to be one.

4.2 Model Transformation

Up to this point the discussion have been concerned with the estimation of the parameters of the system difference equation model (3.2). In the following it is assumed that the estimated a_i, b_i and c_i are available from section 3.2, and that they model the system with the required accuracy. The transformation of the model represented by equation (3.2) to the state-space form, is shown in the following starting by rewriting this equation as

$$\hat{y}(nT) = \sum_{i=1}^{m} b_i u((n-i)T) - \sum_{i=1}^{m} a_i y((n-i)T) + \sum_{i=1}^{m} c_i \hat{e}((n-i)T) \qquad (4.3)$$

where $u(nT)$ is the system input, $y(nT)$ is the system output, $\hat{e}(nT)$ is the estimation error in system model, and a_i, b_i and c_i are the estimated model parameters. For a given system, there is no unique state-variable formulation. In fact there exist countless choices of the state variables for the equation (4.3) to be presented. However, for certain analysis and design procedures, certain formulations present advantages with respect to calculations. The *observer canonical form* is the one which is chosen for state-space representation. This realization is a direct structure. Direct structures for digital filters are those in which the real coefficients, *a*, *b* and *c*, from equation (4.3), appear as multipliers in the block-diagram implementation, or in the state-space representation. These coefficients are used directly in the state equations; with no calculations required. The observer form means that the state vector $x(nT)$ and all the feedback signals come from the observed

(output) signal. The canonical form refers to the structure in which the number of time-delay elements or the state vector length is minimal.

To get to the observer canonical form representation one can start by taking the ***Z*** transformation of equation (4.3)

$$Y(z) = \sum_{i=1}^{m} b_i z^{-i} U(z) - \sum_{i=1}^{m} a_i z^{-i} Y(z) + \sum_{i=1}^{m} c_i z^{-i} \hat{E}(z) \tag{4.4}$$

where z^{-i} represents a delay by iT, and $Y(z)$, $U(z)$ and $\hat{E}(z)$ are the *Z*-transforms of the discrete time functions $y(nT)$, $u(nT)$ and $\hat{e}(nT)$, respectively. After rearranging equation (4.4) as

$$Y(z) = \sum_{i=1}^{m} z^{-i} [b_i U(z) - a_i Y(z) + c_i \hat{E}(z)] \tag{4.5}$$

and by introducing a new variable for substitution

$$S_i(z) = b_i U(z) - a_i Y(z) + c_i \hat{E}(z) \tag{4.6}$$

equation (4.4) can be written as

$$Y(z) = \sum_{i=1}^{m} z^{-i} S_i(z) \tag{4.7}$$

Equation (4.7), by expanding the summation, can also be written in the form

$$Y(z) = z^{-1}\{S_1(z) + z^{-1}\{S_2(z) + \ldots + z^{-1}\{S_{m-1}(z) + z^{-1} S_m(z)\}\ldots\}\} \tag{4.8}$$

Under this correspondence the state variables are defined as

$$
\begin{aligned}
X_m(z) &= z^{-1}S_m(z) \\
X_{m-1}(z) &= z^{-1}\{S_{m-1}(z) + z^{-1}S_m(z)\} \\
&\circ \\
&\circ \\
&\circ \\
X_2(z) &= z^{-1}\{S_2(z) + \ldots + z^{-1}\{S_{m-1}(z) + z^{-1}S_m(z)\}\ldots\} \\
X_1(z) &= z^{-1}\{S_1(z) + z^{-1}\{S_2(z) + \ldots + z^{-1}\{S_{m-1}(z) + z^{-1}S_m(z)\}\ldots\}\}
\end{aligned}
\tag{4.9}
$$

Substituting in equation (4.6) gives

$$
\begin{aligned}
X_m(z) &= z^{-1}\{b_m U(z) - a_m Y(z) + c_m \hat{E}(z)\} \\
X_{m-1}(z) &= z^{-1}\{[b_{m-1}U(z) - a_{m-1}Y(z) + c_{m-1}\hat{E}(z)] + X_m(z)\} \\
&\circ \\
&\circ \\
&\circ \\
X_2(z) &= z^{-1}\{[b_2 U(z) - a_2 Y(z) + c_2 \hat{E}(z)] + \ldots + z^{-1}X_3(z)\ldots\} \\
X_1(z) &= z^{-1}\{[b_1 U(z) - a_1 Y(z) + c_1 \hat{E}(z)] + X_2(z)\}
\end{aligned}
\tag{4.10}
$$

and by equating equations (4.8) and (4.9) it follows that

$$Y(z) = X_1(z) \tag{4.11}$$

Taking the inverse *Z* transformation of equation (4.10) leads to the time domain representation

$$
\begin{aligned}
x_m((n+1)T) &= b_m u(nT) - a_m x_1(nT) + c_m \hat{e}(nT) \\
x_{m-1}((n+1)T) &= b_{m-1} u(nT) - a_{m-1} x_1(nT) + c_{m-1} \hat{e}(nT) + x_m(nT) \\
&\circ \\
&\circ \\
&\circ \\
x_2((n+1)T) &= b_2 u(nT) - a_2 x_1(nT) + c_2 \hat{e}(nT) + x_3(nT) \\
x_1((n+1)T) &= b_1 u(nT) - a_1 x_1(nT) + c_1 \hat{e}(nT) + x_2(nT)
\end{aligned}
\tag{4.12}
$$

The output from the model is defined by equation (4.11) as

$$y(nT) = x_1(nT) \tag{4.13}$$

For better understanding, equations (4.8), (4.6), (4.12) and (4.3), can be represented by the block diagram in Figure 4-1, where: time-delay elements are represented by z^{-1}, adders as summation points, and multipliers by their coefficient values.

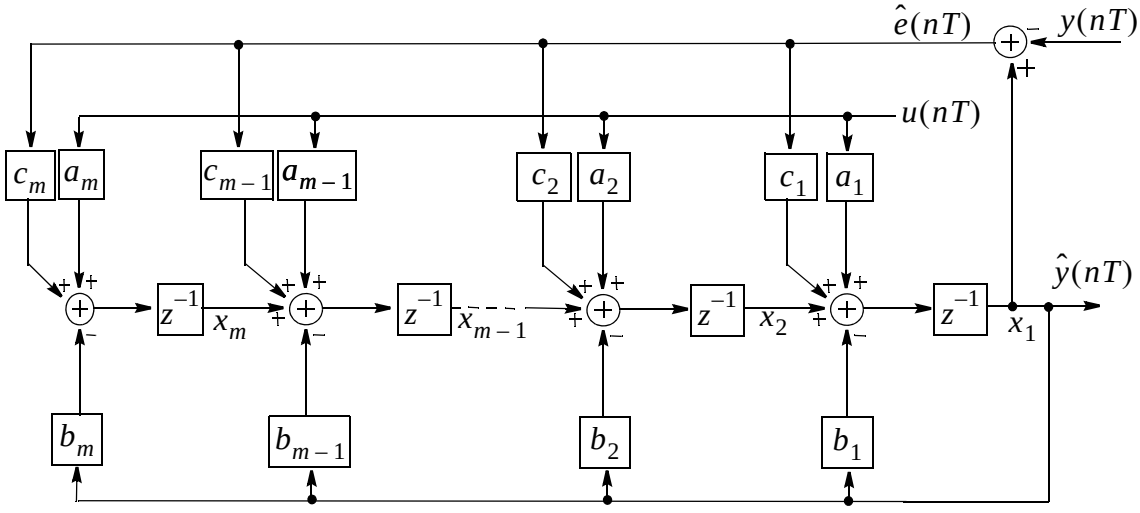

Figure 4-1 System model in observer canonical form

Equations (4.12) and (4.13) are well known in the matrix form as

$$\begin{bmatrix} x_1((n+1)T) \\ x_2((n+1)T) \\ \cdots \\ \cdots \\ \cdots \\ x_m((n+1)T) \end{bmatrix} = \begin{bmatrix} -a_1 & 1 & 0 & \ldots & 0 \\ -a_2 & 0 & 1 & \ldots & 0 \\ -a_3 & 0 & 0 & \ldots & 0 \\ \ldots & \ldots & \ldots & \ldots & \ldots \\ -a_{m-1} & 0 & 0 & \ldots & 1 \\ -a_m & 0 & 0 & \ldots & 0 \end{bmatrix} \begin{bmatrix} x_1(nT) \\ x_2(nT) \\ \cdots \\ \cdots \\ \cdots \\ x_m(nT) \end{bmatrix} + \begin{bmatrix} b_1 \\ b_2 \\ \cdots \\ \cdots \\ \cdots \\ b_m \end{bmatrix} u(nT) + \begin{bmatrix} c_1 \\ c_2 \\ \cdots \\ \cdots \\ \cdots \\ c_1 \end{bmatrix} \hat{e}(nT) \quad (4.14)$$

$$\hat{y}(nT) = \begin{bmatrix} 1 & 0 & 0 & \ldots & 0 & 0 \end{bmatrix} \begin{bmatrix} x_1(nT) \\ x_2(nT) \\ \cdots \\ \cdots \\ \cdots \\ x_m(nT) \end{bmatrix} \quad (4.15)$$

The relationship between the estimated parameters a_i, b_i and c_i and the state-space representation depicted by equations (4.1) and (4.2), is defined by equations (4.14) and (4.15).

4.3 The State-Space Variables

The variables $x_1(nT)$, …, $x_m(nT)$ are called the state variables of the dynamic system, as defined by equation (4.12). When they are collected into a single *m*-dimensional vector, shown in equation (4.14), it is called the state vector of the dynamic system. Given the values $x_i(n_0T)$ at some initial time n_0T, equation (4.14) will uniquely determine the values

of $x_i(nT)$ on some closed time interval $[n_0T, nT]$ with initial time n_0T and final time nT. In this sense, the initial value of each state variable represents an independent degree of freedom of the dynamic system [17].

The state values which correspond to the selected model can be calculated based on input and output directly from equation (4.12), with a little modification,

$$\begin{aligned}
x_m((n+1)T) &= b_m u(nT) - a_m y(nT) + c_m \ddot{e}(nT) \\
x_{m-1}((n+1)T) &= b_{m-1} u(nT) - a_{m-1} y(nT) + c_{m-1} \hat{e}(nT) + x_m(nT) \\
&\circ \\
&\circ \\
&\circ \\
x_2((n+1)T) &= b_2 u(nT) - a_2 y(nT) + c_2 \hat{e}(nT) + x_3(nT) \\
x_1((n+1)T) &= b_1 u(nT) - a_1 y(nT) + c_1 \hat{e}(nT) + x_2(nT)
\end{aligned} \tag{4.16}$$

The disadvantage of the direct method is that it may be sensitive to disturbances. An alternative to direct calculation, using the Kalman Filter algorithm, is discussed in chapter 5.

5 Kalman Filter

Kalman filtering is an optimal state estimation technique, which has the ability to incorporate noise from both measurement and modeling. The Kalman filter was introduced in 1958 by Rudolf E. Kalman, but has only achieved wider application in recent years because of more accessible, faster and cheaper means which are used for its computation.

The discrete Kalman filter is a recursive predictive update technique used to determine the correct states of a process model. Given some initial estimates, it allows the states of a model to be predicted and adjusted with each new measurement, providing an estimate of the error at each update. It has been proven that, in the right situation, when certain assumptions about the noise model are satisfied, it performs better than any other linear filter [17].

A feature of the Kalman filter, not present in other statistical predictors, is its ability to adjust its own parameters automatically according to the statistics of the measurements, and according to the current confidence in the accuracy of the state parameters.

The discrete Kalman filter is used in situations where a continuous process is sampled at discrete time intervals or for purely discrete processes.

5.1 Description of the Kalman Filter

The dynamic system with noise described by the process equation (4.1), and by the measurement equation (4.2) is introduced in section 4.1. These equations are:

$$x((n+1)T) = A(nT)x(nT) + B(nT)u(nT) + G(nT)w(nT) \tag{5.1}$$

$$y(nT) = C(nT)x(nT) + v(nT) \tag{5.2}$$

In addition to the description for these equations in section 4.1, it is necessary to define more strict requirements for the quantities $w(nT)$ and $v(nT)$.

The process noise $w(nT)$ represents disturbances or modeling inaccuracies. It is assumed that it is a white noise process with zero mean, and its covariance is defined by

$$E\{w(kT)w^T(iT)\} = \begin{cases} Q_K(kT) & i = k \\ 0 & i \neq k \end{cases} \tag{5.3}$$

where $E\{\circ\}$ is the statistical expectation, superscript T denotes transpose, and $Q_K(kT)$ is the process noise covariance [17].

The measurement noise $v(nT)$ is due to sensor inaccuracy, and is assumed to be a white noise process with zero mean and its covariance matrix is defined by

$$E\{v(kT)v^T(iT)\} = \begin{cases} R_K(kT) & i = k \\ 0 & i \neq k \end{cases} \tag{5.4}$$

where $R_K(kT)$ is the measurement noise covariance.

It is assumed that $x(nT)$, $w(nT)$ and $v(nT)$ are mutually uncorrelated so that

$$E\{x(jT)v^T(kT)\} = 0 \qquad \text{for all } j \text{ and } k \qquad (5.5)$$
$$E\{w(jT)v^T(kT)\} = 0$$

that is, the processes and measurement noises arise in the system from independent effects.

The state estimator can be presented in a simplified way as in Figure 5-1, where the symbols $A(nT)$, $B(nT)$ and $C(nT)$ are the system parameters from the state space representation and $K(nT)$ represents the Kalman gain of the state estimator. The Kalman gain

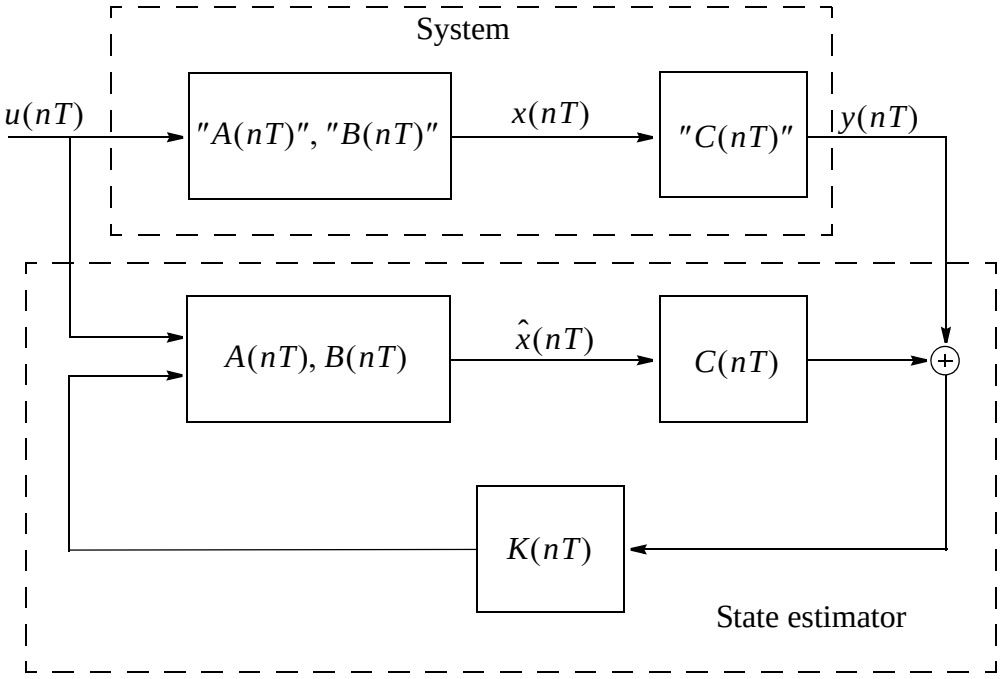

Figure 5-1 A simplified state estimator model

vector $K(nT)$ can be explained as furnishing a correction input to the system model in the

state estimator, to account for unknowns in the system. If the unknowns are significant, $K(nT)$ should be relatively large. However, if the measurement noise in $y(nT)$ is significant, the estimation cannot rely heavily on the measurement $y(nT)$, and $K(nT)$ should be relatively small [25]. The discrete Kalman Filter represents an iterative procedure, based on the above described assumptions and contains several elements which are described in the following sections as depicted in Figure 5-2.

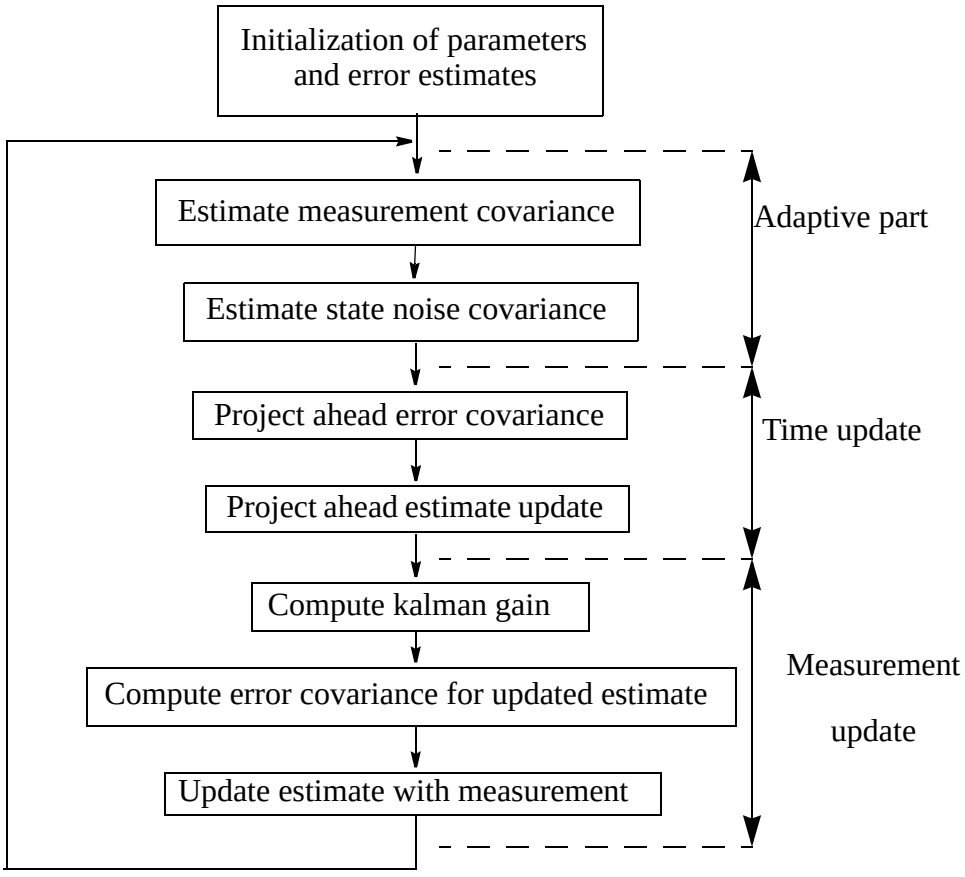

Figure 5-2 Kalman filter loop

5.2 Kalman Filter Equations

The equations used in the discrete Kalman filter are detailed in the literature [6][17][18], and are described below. The Kalman filter consists of two parts; the time update, which takes into account the error in modeling the system dynamics, and the measurement update, which takes into account the effect of error in the measurement of the system output. In other words, the discrete Kalman filter has two steps at each sampling time nT, the first is the time update or a prior update, by which $\hat{x}((n-1)T)$ is updated to $\hat{x}^{-}(nT)$, and the other is the measurement update, by which the measurement $y(nT)$ at time *n* is incorporated to provide the updated estimate $\hat{x}(nT)$ [6]. The a priori estimate will be denoted as $\hat{x}^{-}(nT)$ where the "hat" denotes estimate, and the "super minus" is a reminder that this is the best estimate prior to the assimilation of the measurement $y(nT)$.

5.2.1 Time Update

The a priori prediction of the state parameter values and error for the next time instant is calculated with the time update equation.

The Predicted Error Covariance is calculated by the equation

$$P^{-}(nT) = A(nT)P((n-1)T)A^{T}(nT) + G(nT)Q_{K}(nT)G^{T}(nT) \tag{5.6}$$

The covariance $P(\circ)$ indicates how closely distributed a random variable is about its mean, with a larger covariance indicating greater uncertainty in its value. The error covari-

ance $P^{-}(nT)$ is the sum of two terms; the first term is due to the system dynamics involving the plant matrix $A(nT)$, and the second term is an increase in uncertainty due to the process noise $w(nT)$. The $Q_K(nT)$ matrix is used to represent modeling error. In addition, the use of a larger $Q_K(nT)$ value forces the $P((n-1)T)$ matrix to stay 'significantly' larger so that the estimate becomes more sensitive to the most recent measurements [17]. The error covariance matrix $P^{-}(nT)$ is associated with $\hat{x}^{-}(nT)$ and it is defined as

$$P^{-}(nT) = E[(x(nT) - \hat{x}^{-}(nT))(x(nT) - \hat{x}^{-}(nT))^{T}] \tag{5.7}$$

where $x(nT)$ is the true value of the process state vector and $\hat{x}^{-}(nT)$ is an a priori estimate.

The Estimate Update is calculated by the equation

$$\hat{x}^{-}(nT) = A(nT)\hat{x}((n-1)T) + B(nT)u((n-1)T) \tag{5.8}$$

This equation provides a "predictive estimate" $\hat{x}^{-}(nT)$ of $\hat{x}(nT)$ in that the most current measurement $y(nT)$ is not used. The equation (5.8) automatically incorporates a delay of one sample period for computation purposes.

5.2.2 Measurement update

The Kalman Gain determines the proportion of the error (between predicted and measured parameters) that will be used to update the state vector. It is defined based on the

minimization of the mean-square estimation error of the Kalman filter. It is calculated by the equation

$$K(nT) = P^{-}(nT)C^{T}(nT)[C(nT)P^{-}(nT)C^{T}(nT) + R_K(nT)]^{-1} \quad (5.9)$$

The gain matrix $K(nT)$ is computed by using the predicted error covariance $P^{-}(nT)$ of those elements in the state parameter vector that are obtained from the system, determined by the measurement vector $C(nT)$. The predicted error of these parameters is divided by itself with the addition of the measurement error covariance $R_K(nT)$. This has the effect of reducing the value of the gain matrix $K(nT)$ as $P^{-}(nT)$ becomes smaller relative to the measurement error, and it can be seen that as the $P^{-}(nT)$ error decreases (showing growing confidence in the state parameters) the influence of measurement data also decreases. In other words, the more confidence there is in the state parameters, the less notice is taken of the error between the predicted states.

The Updated Error Covariance is calculated by the equation

$$P(nT) = [I - K(nT)C(nT)]P^{-}(nT) \quad (5.10)$$

The portion of the gain matrix that is associated with elements obtained from the system is subtracted from an identity matrix to yield a proportion of update-gain. This is multiplied with the estimated error covariance to produce an updated error covariance, that reflects the remaining uncertainty about the state parameters.

The error covariance matrix $P(nT)$ is associated with a posteriori estimate $\hat{x}(nT)$ and it is defined as

$$P(nT) = E[(x(nT) - \hat{x}(nT))(x(nT) - \hat{x}(nT))^T] \quad (5.11)$$

where $x(nT)$ is the true value of the process state vector and $\hat{x}(nT)$ is a posterior estimate of it.

The Measurement Update Estimate is calculated by the equation

$$x(nT) = x^-(nT) + K(nT)y(nT) - K(nT)C(nT)x^-(nT) \quad (5.12)$$

The difference between the estimated and measured parameters can be considered to be a prediction error for the Kalman filter, and is caused by an inaccurate measurement, an inaccurate prediction, or a combination of these. This prediction error is derived by the subtraction of the estimated state parameter data from the associated measured value of the output of the system $y(nT) - C(nT)x^-(nT)$. A proportion of the prediction error is added to the parameter estimate $x^-(nT)$ to produce an updated state parameter vector $x(nT)$. The proportion is determined by the values held in the gain matrix $K(nT)$, which in turn is determined by the current degree of confidence in the state parameters, as well as the known measurement error.

5.2.3 Adaptive Kalman Filter

The Kalman Filter, described above, is developed with certain assumptions about the system's mathematical model. These assumptions include complete information about noise statistics $Q_K(nT)$ and $R_K(nT)$. In practice, this information is usually not known totally. The role of the noise covariance, $Q_K(nT)$ and $R_K(nT)$, in the Kalman Filter is to adjust

the Kalman gain in such a way that it controls the filter “bandwidth” as the state and the measurement error vary [19]. By using a curve-fitting method, it is possible to get an estimate of these covariances.

Estimation of the Measurement Noise Covariance

The idea of this estimation is based upon the measurement equation (5.2). Rearranging this equations leads to the definition of the measurement noise

$$v(nT) = y(nT) - C(nT)\hat{x}(nT) \tag{5.13}$$

In equation (5.13), $v(nT)$ represents the residual at time nT. The conventional estimate of the covariance of this residual $R_K(nT)$, can be calculated using the N most recent residuals [20], as

$$\hat{R}_K(nT) = \frac{1}{N-1}\sum_{i=0}^{N-1}[v((n-i)T) - \bar{v}]^2 \tag{5.14}$$

where

$$\bar{v} = \frac{1}{N}\sum_{i=0}^{N-1} v((n-i)T) \tag{5.15}$$

Estimation of the State Noise Covariance

For the estimation of $Q_K(nT)$, which is proposed as an original idea of this thesis, the residual estimation error $\hat{e}(nT)$, as obtained in adaptive RLS algorithm, could be used. The adaptive RLS algorithm and the calculation of the estimation error $\hat{e}(nT)$ is described in chapter 3 “System Parameter Estimation”. The state space representation of the system model is a modified representation of that algorithm. This logically leads to the assump-

tion that the prediction error $\hat{e}(nT)$ and the process noise $w(nT)$ represent the same characteristics of the model - the error of the model. The estimation error is defined by the equation

$$\hat{e}(jT) = \hat{y}(jT) - y(jT) \tag{5.16}$$

where $\hat{y}(jT)$ is the predicted system output from the RLS algorithm, and $y(jT)$ is the measured output from the plant. By using the prediction error $\hat{e}(nT)$ of the adaptive algorithm as an "estimate" of the error in the system model, the estimate of the state noise covariance can be obtained with the equation

$$\hat{Q}_K(nT) = \frac{1}{N-1} \sum_{i=0}^{N-1} [\hat{e}((n-i)T) - \bar{e}]^2 \tag{5.17}$$

where

$$\bar{e} = \frac{1}{N} \sum_{i=0}^{N-1} \hat{e}((n-i)T) \tag{5.18}$$

5.3 Implementation of the Kalman Filter

The Kalman filter described above has been implemented as a part of a power system stabilizer for the micro-synchronous generator power system model. The environment for the control system implementation, together with the applied disturbances are described in detail in Chapter 7 "Real-time Control Environment". In the following some characteristic graphs for the Kalman filter are shown in the implemented environment.

One of the characteristic graphs for Kalman filter is the time variation of the measurement noise $v(nT)$, which characterizes the error in the predicted system output as defined by equation (5.14). Figure 5-3 presents the variation of the Kalman filter's "prediction error" for the case when an exogenous disturbance is not present.

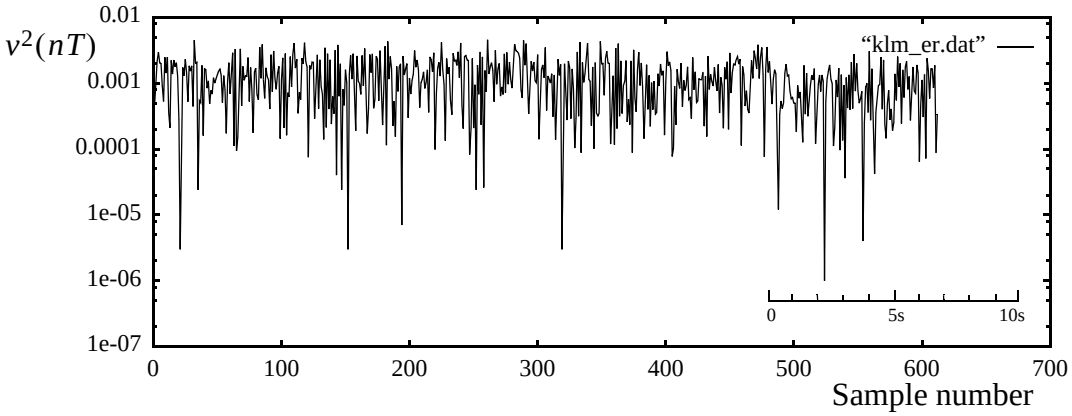

Figure 5-3 Variation of measurement noise without disturbance

The Kalman filter's "prediction error" increases when an exogenous disturbance is on the output signal $y(nT)$. Figure 5-4 presents a case when a mechanical torque step change is applied on the micromachine power system model. The micromachine is operating at 0.85 lag power factor, and the power is changing from 0.9 p.u. to 0.5 p.u. and back at the 100th and 400th sample time, respectively.

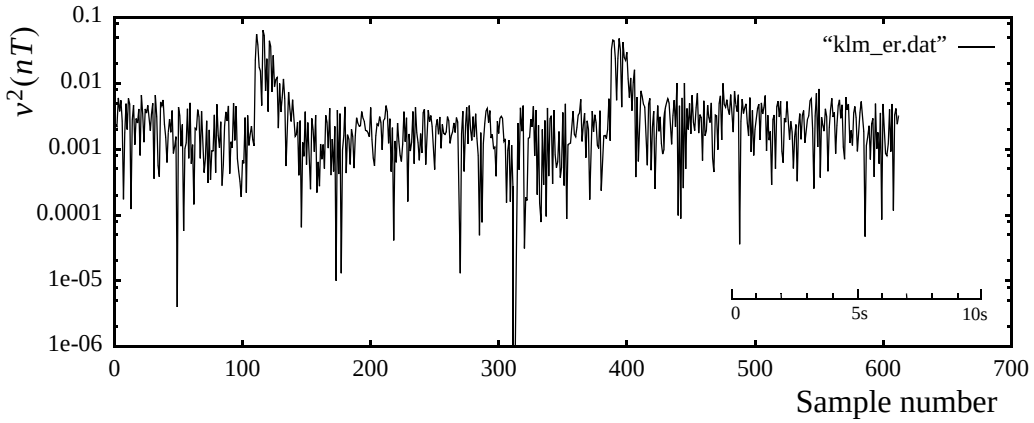

Figure 5-4 Variation of measurement noise squared for a torque step change

The above disturbances would also cause a typical change in the state-space values from $\hat{x}_1(iT)$ to $\hat{x}_5(iT)$. These patterns are presented in Figure 5-5 through Figure 5-9, respectively.

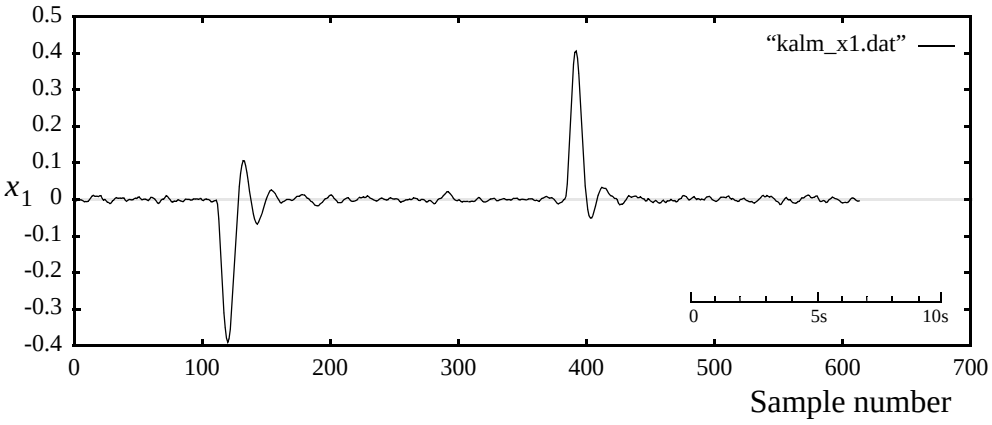

Figure 5-5 State-space vector variable - x_1, for a typical disturbance

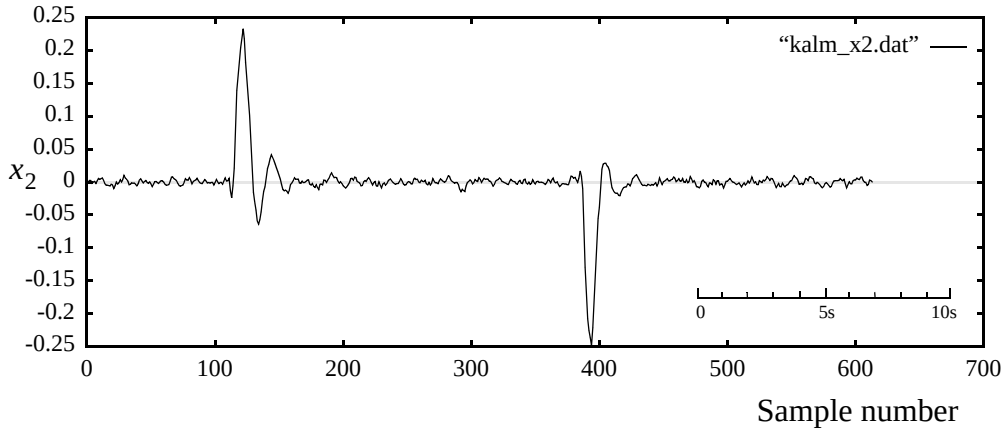

Figure 5-6 State-space vector variable - x_2, for a typical disturbance

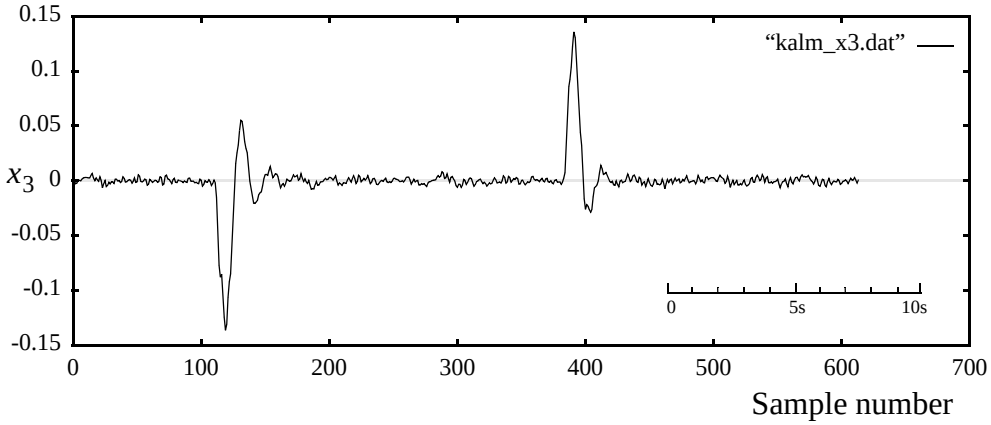

Figure 5-7 State-space vector variable - x_3, for a typical disturbance

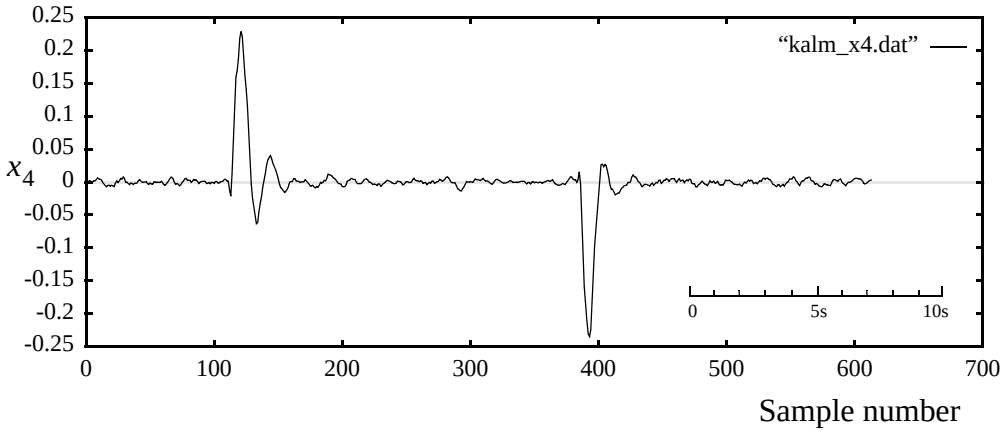

Figure 5-8 State-space vector variable - x_4, for a typical disturbance

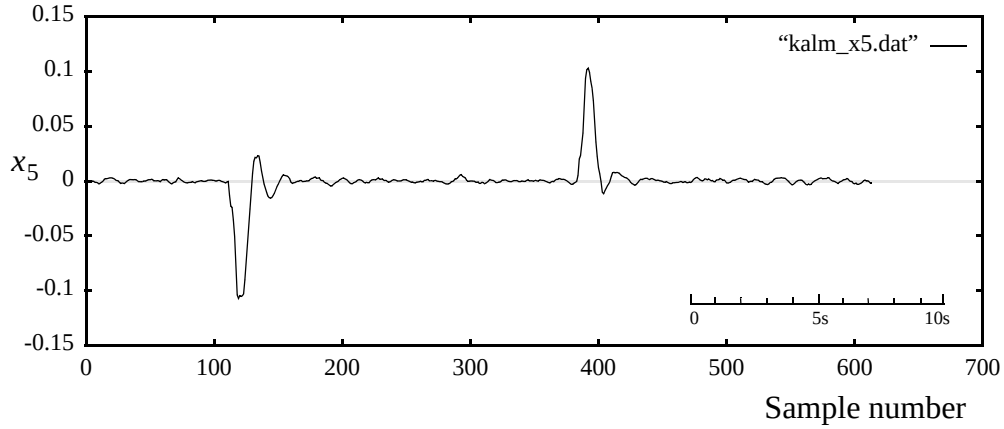

Figure 5-9 State-space vector variable - x_5, for a typical disturbance

6 Optimal Control

In this chapter the main characteristics of the Linear Quadratic Gaussian (LQG) control are described. It is a time-domain approach, making it applicable for time-varying linear systems as well as nonlinear systems. The mathematical model of this optimal control uses linear algebra and matrices, so the systems with multiple inputs and outputs can easily be treated. Linear quadratic gaussian control employs the concept of internal system state; thus, the approach is one that is concerned with the internal dynamics of a system and not only it's input/output behavior. The optimal behavior of this control is formalized by minimizing a very general quadratic function called performance index.

The guaranteed performance obtained by solving the matrix design equations means that it is often possible to design a control system without gaining any engineering intuition about the problem. On the other hand, the frequency-domain techniques of classical control theory impart a great deal of intuition [6].

The major contributor to the theory of Linear Quadratic Regulators was Rudolf E. Kalman by publishing the "Contribution to the Theory of Optimal Control" in 1960, where in he discussed the optimal control of systems and provided the necessary equations for their design [6].

6.1 The Quadratic Cost Function

The modern optimal control design is fundamentally a time-domain technique. It requires a state-space model of the system to be controlled. The state-space model for the linear discrete plant described by the process equation (4.1) and by the measurement equation (4.2), was introduced in Section 4.1 “Discrete-Time State-space System Model”. These equations are

$$x((n+1)T) = A(nT)x(nT) + B(nT)u(nT) + G(nT)w(nT) \tag{6.1}$$

$$y(nT) = C(nT)x(nT) + v(nT) \tag{6.2}$$

The goal of optimal control is to determine the feedback control as a function of the internal states

$$u((n+1)T) = f(x(nT)) \tag{6.3}$$

that minimizes a quadratic function of the states and control signal, usually called the quadratic cost-function or quadratic performance index, given by

$$J = \sum_{k=0}^{N} x^T((n-k)T)Q_C(kT)x((n-k)T) + u^T((n-k)T)R_C(kT)u((n-k)T) \tag{6.4}$$

where N is finite, $Q_C(k)$ is symmetric positive semi-definite and $R_C(k)$ is positive definite. With this algorithm both the plant and the cost-function matrices are allowed to be *time varying*.

This problem, which is stated formally above, is called the Linear Quadratic Gaussian (LQG) control problem [12]. The resulting optimal control is linear, but time varying.

The design results in a control law of the form

$$u((n+1)T) = -K(nT)x(nT) \tag{6.5}$$

and hence it is linear, time-varying, full state feedback.

The solutions for $K(nT)$ can be expressed with the Algebraic Riccati Equation [25], and the solution can be obtained by the following recursive equation

$$K(nT) = [B^T(nT)P((n-1)T)B(nT) + R_C(nT)]^{-1}B^T(nT)P((n-1)T)A(nT) \tag{6.6}$$

where $P(nT)$ is the solution of the algebraic Riccati equation

$$P(nT) = A^T(nT)P((n-1)T)[A(nT) - B(nT)K(nT)] + Q_C(nT) \tag{6.7}$$

The recursion is started with the initial values $P(0) = Q_C(0)$ and $K(0) = 0$.

The Linear-Quadratic Gaussian design relies on the fact that the linear-quadratic regulator with full state-variable feedback and the Kalman filter can be used together to design a dynamic regulator. An important advantage of the Linear-Quadratic Gaussian design is that the compensator structure is automatically given by the procedure, so that it need not be known beforehand [6]. The closed loop structure for Linear-Quadratic Gaussian control

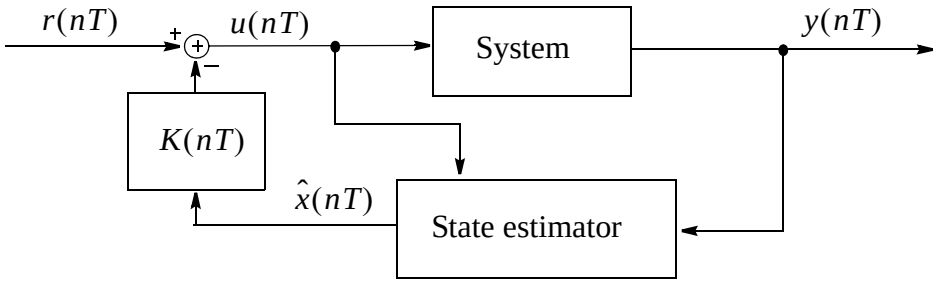

Figure 6-1 Linear-Quadratic Gaussian Control block diagram

is shown in Figure 6-1. According to the literature [6], the closed loop poles and the transfer function from $r(nT)$ to $y(nT)$ are the same as if full state feedback (requiring measurement of the state-space vector) had been used. The importance of this is that the feedback $K(nT)$ and the state estimation $\hat{x}(nT)$ may be designed separately to yield desired closed-loop plant behavior and state estimator behavior. This is the *Separation Principle* which is at the heart of modern control design [6].

In the following, Figure 6-2 through Figure 6-6 presents the changes in the feedback gain $K_i(nT)$ when a mechanical torque step change is applied to the micromachine power system model. The environment for the control system implementation, together with the applied disturbances are described in detail in Chapter 7 “Real-time Control Environment”. The setup is 0.85 lag power factor, and the power is changing from 0.9 p.u. to 0.5 p.u. and back at 100 and 400 sample time, respectively.

These figures clearly demonstrate that the feedback gain responds to the changes in the system.

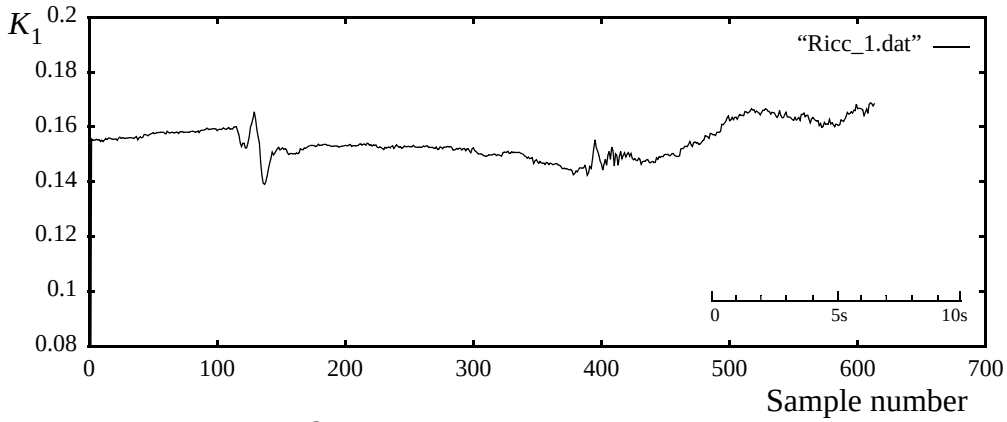

Figure 6-2 State feedback gain $K_1(iT)$

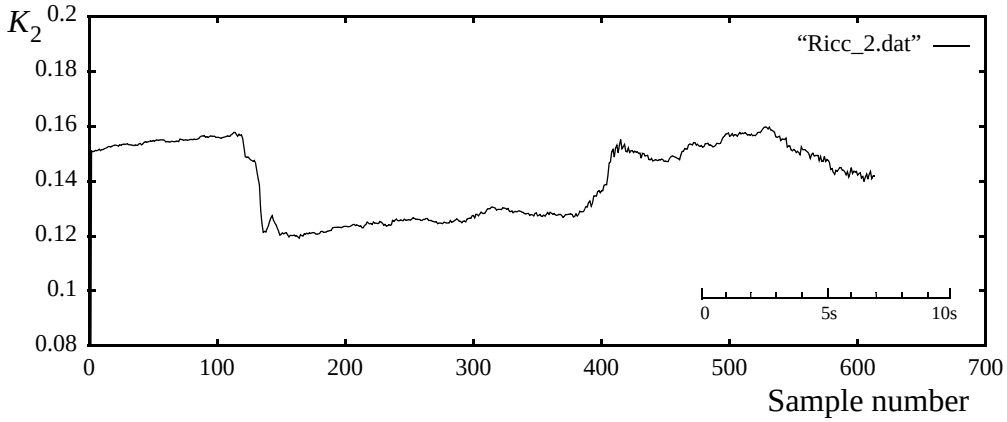

Figure 6-3 State feedback gain $K_2(iT)$

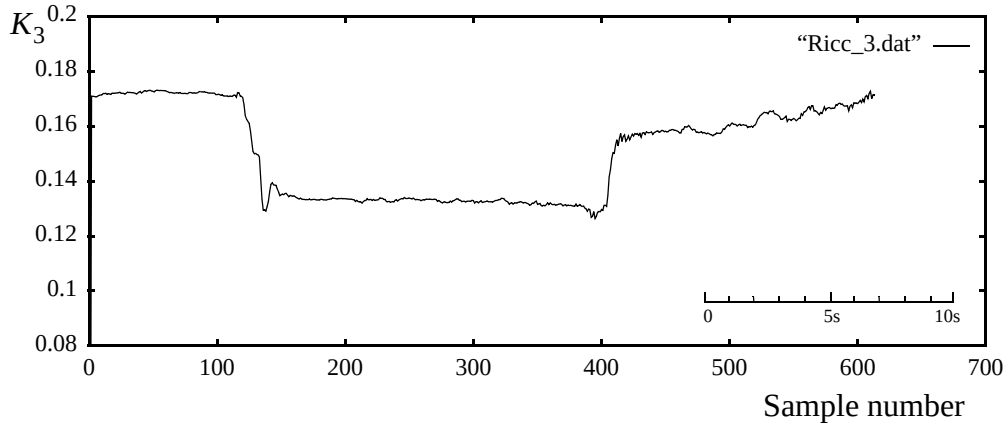

Figure 6-4 State feedback gain $K_3(iT)$

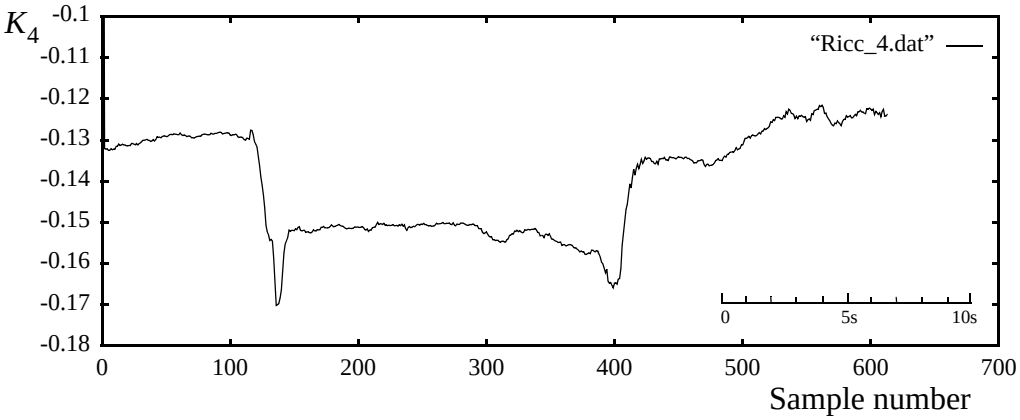

Figure 6-5 State feedback gain $K_4(iT)$

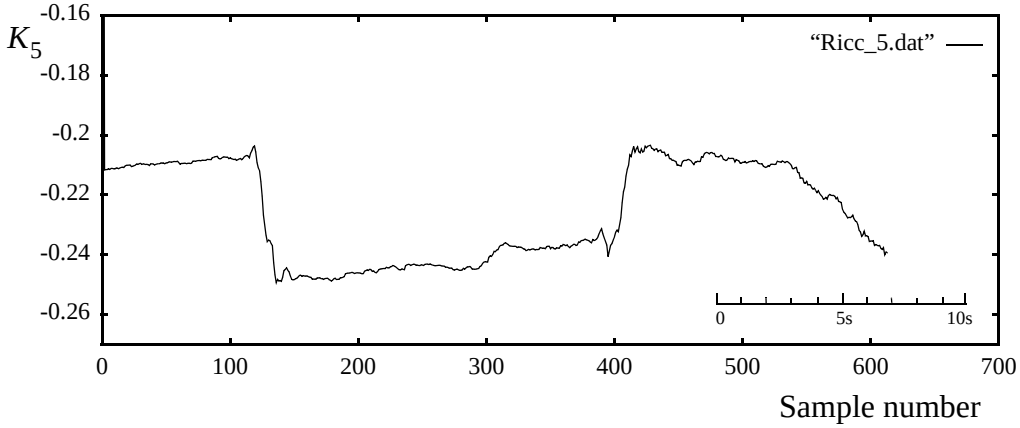

Figure 6-6 State feedback gain $K_5(iT)$

6.2 The Q and R Selection Process

To say a control system is “optimal” means only that the control law minimizes a given performance index. In the case of linear quadratic Gaussian control the system performance depends on the weighting matrices $Q_C(k)$ and $R_C(k)$ [26].

In the design, a trade-off must be made between control activities and output performance. Trade-off studies are made by repeatedly varying the $Q_C(k)$ and $R_C(k)$ weight parameters in the selected performance index (6.4). The closed-loop system obtained in this manner is then analyzed with respect to: transient response, typical disturbance response, frequency response, robustness, etc. The elements of the performance index are modified until the desired result is obtained. Such a procedure may seem a strange use of optimization theory; however, it has been found empirically that linear quadratic control is quite easy to use in this way [12]. The response of the closed-loop system to typical disturbances is evaluated to achieve the best system behavior.

The initial guess of weights can be made using the following rule of thumb [31]. Specially, if the specifications are given in terms of the maximum allowed deviations in the states and the control signals for a given disturbance, the weights, in equation (6.4), can be selected as

$$Q_C = diag(q_1, q_2, \ldots, q_m) \tag{6.8}$$

$$R_C = diag(r_1, r_2, \ldots, r_p) \tag{6.9}$$

where *m* is the order of the system and *p* is the number of control signals. In this work *p=1*. The diagonal elements can be defined according to a rule of thumb [12],[26] as

$$q_i = \frac{1}{[(x_i)_{max}]^2} \tag{6.10}$$

$$r_i = \frac{1}{[(u_i)_{max}]^2} \tag{6.11}$$

where the index *max* selects the maximum allowed deviation in the state or control signal for possible disturbances [26].

The effect of $R_C(k)$ and $Q_C(k)$ on the control system can be described by two extreme situations:

- As $R_C(k)$ goes to infinity or as $Q_C(k)$ approaches zero, the control system approaches the open loop mode of operation as the feedback control gain $K(k)$ approaches zero. With these conditions the control law approaches the fuel-optimal control law [26].
- As $R_C(k)$ goes to zero or as $Q_C(k)$ approaches infinity, the bandwidth of the resulting closed-loop system increases rapidly because the feedback control gain $K(k)$ increases drastically. In other words, if $R_C(k) = 0$, the system is not penalized for control-energy expenditure. The optimal control, in this case, will bring the state to zero as fast as possible, since no magnitude restriction has been placed on the control signal. The optimal control will turn out to be impulsive. In order to obtain a meaningful engineering solution, it is necessary to place magnitude constraints upon the components of the control vector [4]. With these conditions the control law approaches the time-optimal control law.

6.3 Robustness of the Linear-Quadratic Regulator

It is necessary to consider the robustness of the linear quadratic Gaussian regulator in a control system. The issue is that in any actual situation the system dynamics may not be exactly known, and there may exist disturbances and measurement noise in the system. It is a basic requirement for this regulator to provide not only good performance under ideal conditions, but also performance robustness in the face of disturbances and stability robustness in the presence of unmodeled system dynamics. The design equations for linear quadratic Gaussian control involve several design parameters - namely, the performance index weighting matrices $Q_C(nT)$ and $R_C(nT)$, and the noise covariances $Q_K(nT)$ and $R_K(nT)$ for the Kalman filter. These matrices, and especially the Kalman filter design matrices $Q_K(nT)$ and $R_K(nT)$, may be selected so that the dynamic regulator recovers the desirable robustness properties of a full state feedback system [6].

The robust design can be done either as a *recovery of robust state-feedback loop gain* or as a *recovery of robust loop gain at output* design:

- *Recovery of robust state-feedback loop gain* - The essence of this design is first to design the regulator with the desired response, by selecting the weighting matrices $Q_C(nT)$ and $R_C(nT)$; and second to modify the Kalman filter, through the noise covariances $Q_K(nT)$ and $R_K(nT)$, so that the robustness and time response of the target feedback loop are suitable.

- *Recovery of robust loop gain at output* - The essence of this design is first to design the Kalman filter, by selecting the noise covariances $Q_K(nT)$ and $R_K(nT)$, and to design the regulator with the desired response; and then to modify the feedback regulator, through the weighting matrices $Q_C(nT)$ and $R_C(nT)$, so that the robustness and time response of the target feedback loop are suitable.

This technique is called the Linear-Quadratic Gaussian/Loop-Transfer Recovery (LQG/LTR) design, since the loop gain of a full state feedback is recovered in the regulator [6].

6.4 Properties of the Linear-Quadratic Regulator

The controller has several good properties [6]:

- It is applicable to multivariable and time-varying systems, using the same matrix calculations.
- By changing the relative magnitude of the elements in the weighting matrices, it is easy to obtain a compromise between the speed of recovery and the magnitudes of the control signals.
- Given that the system is observable, controllable and that the performance index is symmetric and positive definite, the controller will always results in a stable closed-loop system.
- The closed loop poles of the system $(A - BK)$ may be placed arbitrarily as desired [6].

6.5 Overall Control Algorithm

The linear quadratic control algorithm combined with a parameter estimation and state reconstruction method can be used to control processes on-line by means of a digital computer. The general structure is given by Figure 1-1. The control signal is recalculated each sampling period, based on new measurement of the plant output and on updated estimations of the process parameters and of the state variables.

The control algorithm cycles through the following steps:

- The process parameters $\{a_i, b_i\}$ are estimated by a recursive least-square algorithm, described in section: 3.2 “The Recursive Least-Squares (RLS) Algorithm”. In the implemented RLS algorithm the $\{c_i\}$ parameters are not estimated.
- The estimated difference equation (4.3) parameters $\{a_i, b_i\}$ are transformed into state-space matrices $A(nT)$, $B(nT)$ and $C(nT)$ as presented in section 4.2 “Model Transformation”- with the equations (4.14) and (4.15).
- The state variables $\{x_i(nT)\}$ are estimated by a Kalman filter, as described in section 5.2 “Kalman Filter Equations”.
- The feedback gain $K(nT)$ is calculated with equations (6.6) and (6.7), using the matrices $A(nT)$, $B(nT)$ and $C(nT)$. The control signal $u(nT)$ is calculated with equation (6.5), where the state variables $\{x_i(nT)\}$ are solution of the Kalman filter.

6.6 Summary

In this second part of the thesis the relevant theory for the proposed Optimal Adaptive Power System Stabilizer has been presented. In the thirt part, the results of an experiment using a physical model of a power system to test the proposed control algorithm will be presented and discussed.

III Experimental Tests

An excellent way to gain an intuitive feel for control system design and performance is to perform computer simulations. It is conceptually a short step from simulation to actual implementation, since the subroutines that are used on today's digital signal processors are very similar to those used for simulation. However, a numerical system model can only approximate the dynamics of a system to a certain extent. There is always some unexpected dynamic behavior inherent in a system that is not accounted for by any given mathematical model. Generally, it is necessary to do some laboratory and/or field tests to further assess the evidence from the computer simulation before the installation of the proposed control algorithm on an actual system. This is especially true for a power system in which damage could be very expensive. For this kind of system the solution is to build a scaled physical model of the target system. This scaled physical model is able to emulate the behavior of the actual power plant in the laboratory environment.

A real-time digital control system and the physical power system model for implementation and testing of the Optimal Adaptive Power System Stabilizer are described in this third part.

7 Real-time Control Environment

After the theoretical development and computer simulation studies, a novel control strategy should be tested on the plant on which the control will be applied or at least a physical model of it. Scaled physical models, which can simulate the behavior of the plant in the laboratory environment, are extensively used in research laboratories to test novel instrumentation and control schemes. Virtually every phenomenon encountered in large power systems can be qualitatively duplicated with the small machines [32].

Implementation of the optimal adaptive power system stabilizer with a real-time digital control system applied on a laboratory power system is described in this chapter.

The control algorithm is implemented on a single board computer, which uses a Texas Instruments TMS320C30 digital signal processor to provide the necessary computational power.

To enhance the control environment, a windows based human-machine interface package has been developed to fully utilize the resources of the personal computer and to provide a convenient interface for the operator to monitor changes in the controller's parameters.

7.1 Power System Model

In this section the physical model of the power system to be simulated is presented. The model is available in the Power System Research Laboratory at the University of Calgary and consists of a 3-phase 3kVA micro-synchronous generator connected to an infinite bus-bar through a double transmission line simulator. An overall schematic diagram of this physical model is given in Figure 7-1. The major units of this model are: the turbine

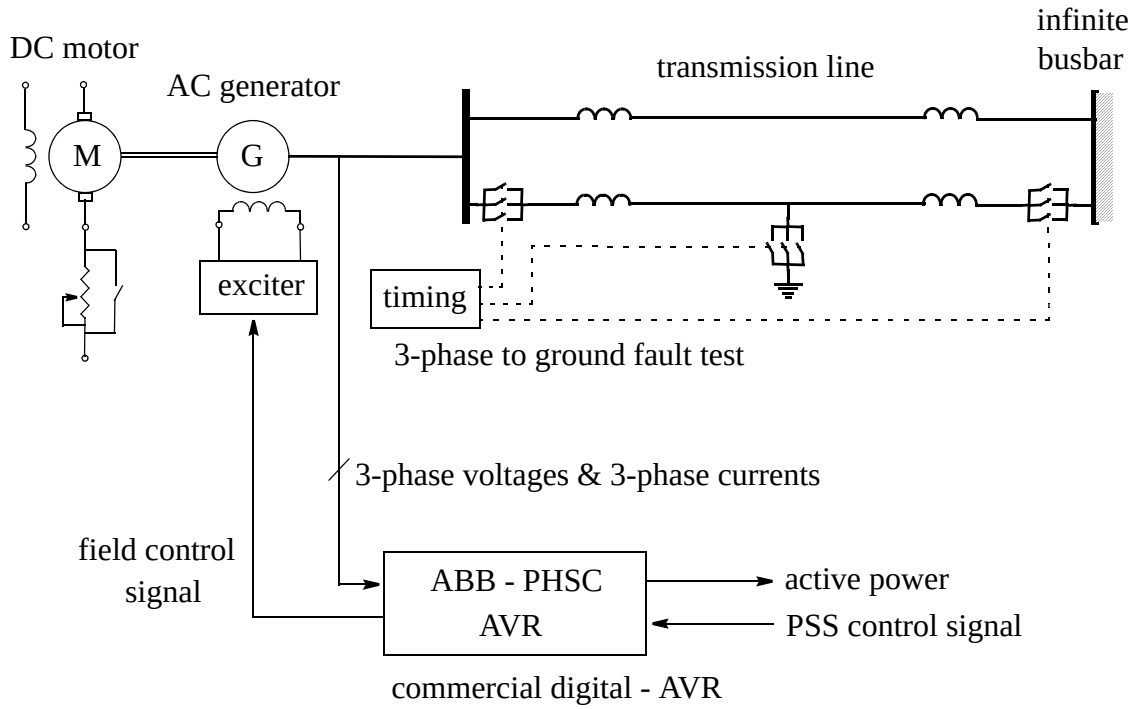

Figure 7-1 Configuration of laboratory power system

model, the generator model, the transmission line model and the automatic voltage regulator.

7.1.1 Turbine Model

The mechanical energy source, in practice, usually a turbine, is modeled by a 5.5 kW (7.5 h.p.) separately excited DC motor, made by Madsley's Ltd. in 1968. The technical parameters of this DC motor are: *220 V, 30 A, 1800 RPM, 7.5 h.p. (5592.75 W)*, excitation *40/20/10 V.* The connection diagram with the measurement points is represented in Figure 7-2.

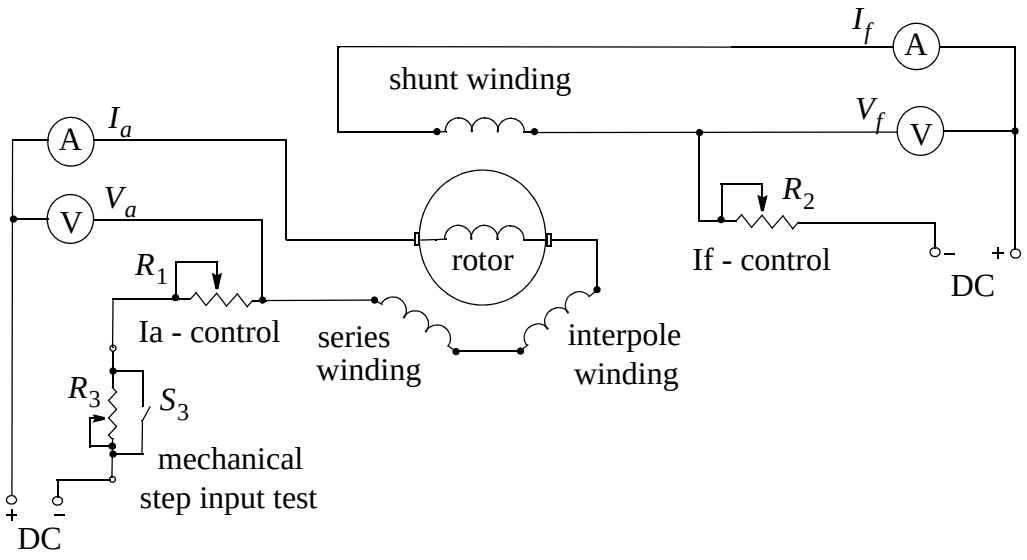

Figure 7-2 DC motor as a turbine model

The active electrical power P_e of the micro-synchronous generator shown in Figure 7-3 can be set by varying the field current of the DC motor by the resistances R_1 and R_2. A

large power step disturbance or input torque step, can be produced by using the switch S_3. The corresponding power step is adjusted by the resistor R_3.

7.1.2 Generator Model

A generator unit is modeled by a three phase 3 kVA, 220 V micro-synchronous generator, made by Madsley's Ltd. The technical parameters of this alternator are: 220/127 V, 7.9 A, 3 kW, 3 phase, 60 Hz with a power factor of 0.8. The measurable parameters for the micro-synchronous generator are shown in Figure 7-3.

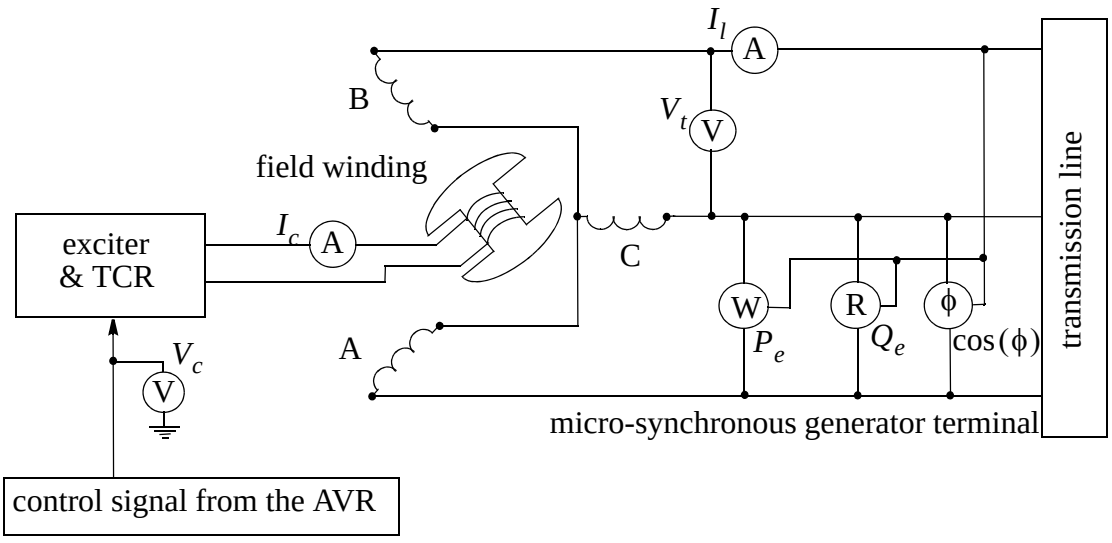

Figure 7-3 Micro-synchronous generator model

The field winding resistance of these synchronous machines, on per unit basis, is much higher than that of the large machines to be simulated. This results in a comparatively low field transient time constant $T"_{do} = 0.765\,s$, where the transient time constant of the mod-

ern large machines is in the neighborhood of *5 s*, thus adversely affecting the performance of the machine under transient conditions. An electrical device called the Time Constant Regulator (TCR) has been designed to reduce the effective field resistance and thereby alter $T"_{do}$ to the order of that required for the simulation of large machines. With the time constant regulator, the effective field time constant of the micro-synchronous generator can be increased up to *10 s* [38].

The voltage reference step disturbance can be simulated using this generator model, to conduct a dynamic performance study and evaluate the performance of a proposed power system stabilizer. The generator's terminal voltage, V_t, can be stepped up and down by changing the voltage reference setting of the AVR.

7.1.3 Transmission Line Model

The main objective of the transmission line is the power flow through an AC line, which is a function of the phase angle, the line end voltages, and the line-impedance [40].

The transmission line is modeled by a lumped element transmission line. The physical model consists of six π sections as presented in Figure 7-4, and gives a frequency response

that is close to the actual transmission line response up to 500 Hz [43]. This model simu-

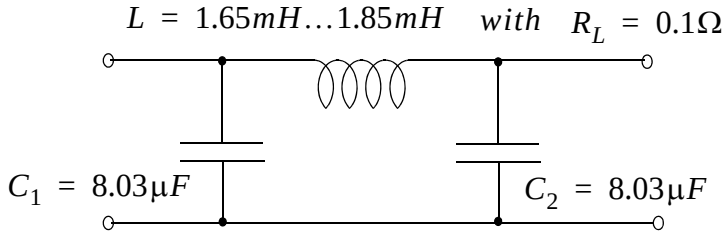

Figure 7-4 pi section

lates the performance of a 300 km long 500 kV, double circuit transmission line connected to a constant voltage bus (infinite busbar), as shown in Figure 7-1.

Large disturbances such as various three phase to ground faults can be simulated using relays controlled by short circuit simulation logic, presented in Figure 7-1.

7.1.4 Automatic Voltage Regulator (AVR)

The terminal voltage V_t and speed of a synchronous generator are two important quantities on which the operation of the power system depends, and special means are necessary to control them if the best operating conditions are to be obtained. The terminal voltage of a generator operating by itself can be wholly controlled by an automatic voltage regulator actuated by voltage feedback. When the generator is connected to a large power system (infinite busbar), its voltage and speed are largely determined by the voltage and frequency of the system. The main effect of the automatic voltage regulator is to control the reactive power Q_e of the generator [39].

In the power system model a commercial automatic voltage regulator made by ABB of Switzerland is used. This is the PHSC2 Programmable Logic Controller (PLC), specially designed for power systems.

Based on the measurement of the three phase voltages and three line currents the PHSC2 calculates the field control signal and also the electric power of the generator P_e for the proposed power system regulator. The proposed power system stabilizer setup is shown in the Figure 7-5.

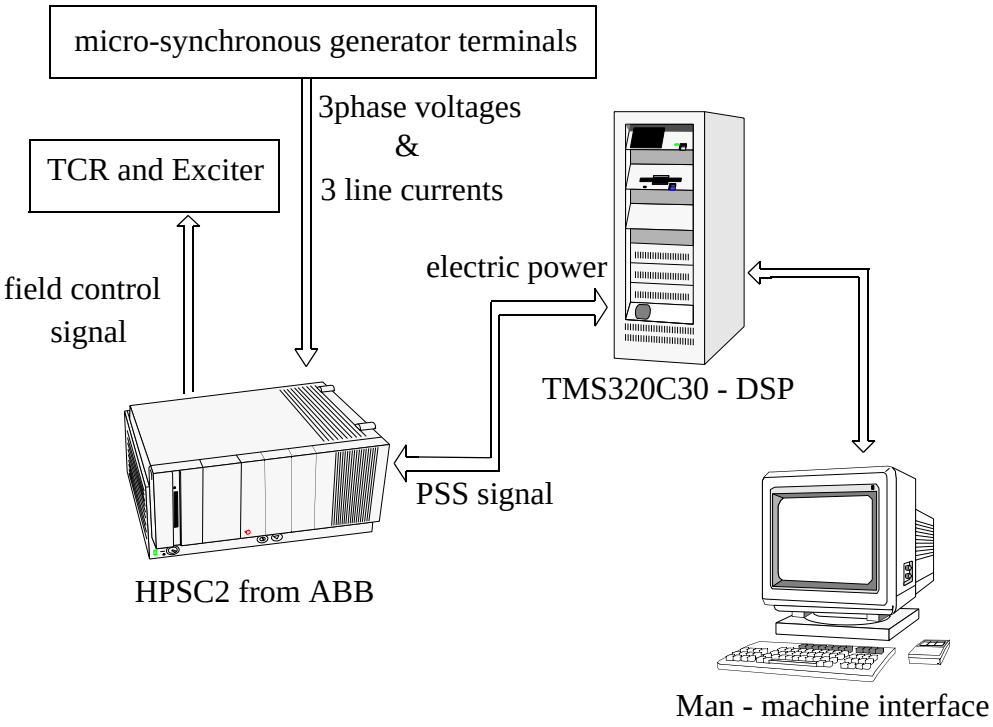

Figure 7-5 The control system

7.2 Real-Time Power System Stabilizer Implementation

The real-time control environment, for the power system stabilizer, is based on a single board computer from Spectrum Signal Processing Inc., Burnaby, BC. The board contains a TMS320C30 digital signal processor from Texas Instrument Inc., Dallas, TX., which is a 32 bit floating-point device, capable of 30 million floating point calculations or 15 million instructions per second. The digital signal processor board is installed in a personal computer, with the corresponding development software and debugging application program. For data acquisition, the board is equipped with two 16 bit dynamic range

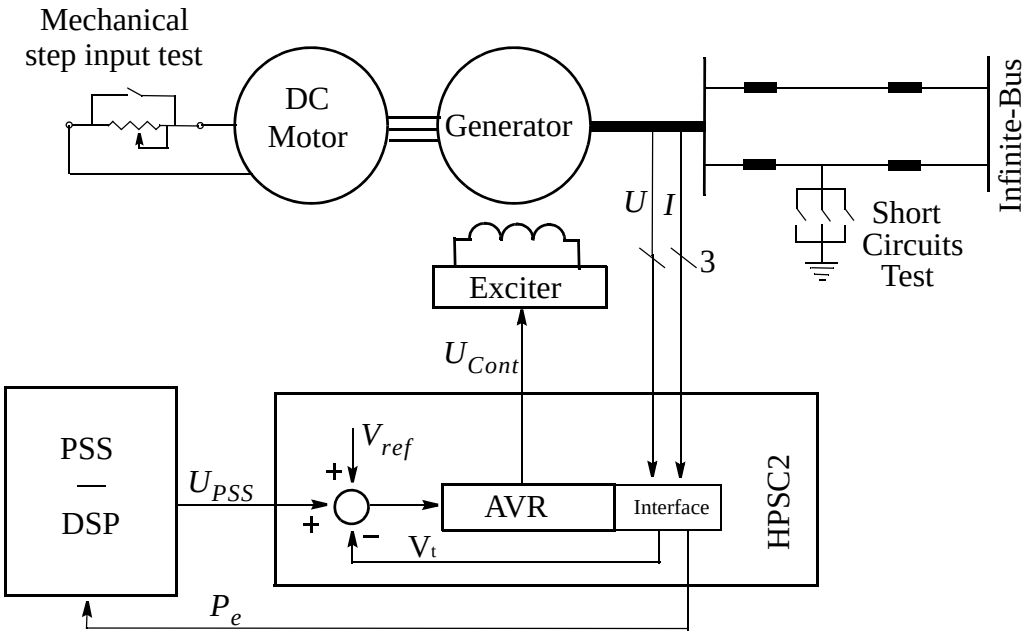

Figure 7-6 Power system stabilizer connection

analogue interface channels. These channels have a selectable sampling rate, with a maximum of 200 kHz.

The communication between the digital signal processor and the PHSC2 programmable logic controller is through analogue signals, as shown in Figure 7-6. The electrical power P_e produced by the micro-synchronous generator, is calculated by the PHSC2 programmable logic controller. The analog to digital (A/D) input channel of DSP board receives the P_e signal, sampled at a 50 ms interval, and calculates the control signal U_{PSS}. The calculation time of the OAPSS is less than *37ms*. The control signal is placed into the output channel and converted by the digital to analogue converter (D/A). This output signal is connected to the analog input of the PHSC2 programmable logic controller. Combining the U_{PSS} signal obtained from the DSP board and the AVR signal acquired from the PHSC2 programmable logic controller internal calculation, it sends the U_{Cont} control signal to the TCR-exciter, thus forming a closed-loop control system.

7.2.1 Embedded Software Structure

The real-time control application program is primarily interrupt driven, with a basic structure as shown in Figure 7-7.

The control system is initiated by the execution of the *pss.exe* on the personal computer. *pss.exe* boots the digital signal processor (DSP) by loading *oapss.out* into the digital signal processor board memory through the personal computer's ISA bus.

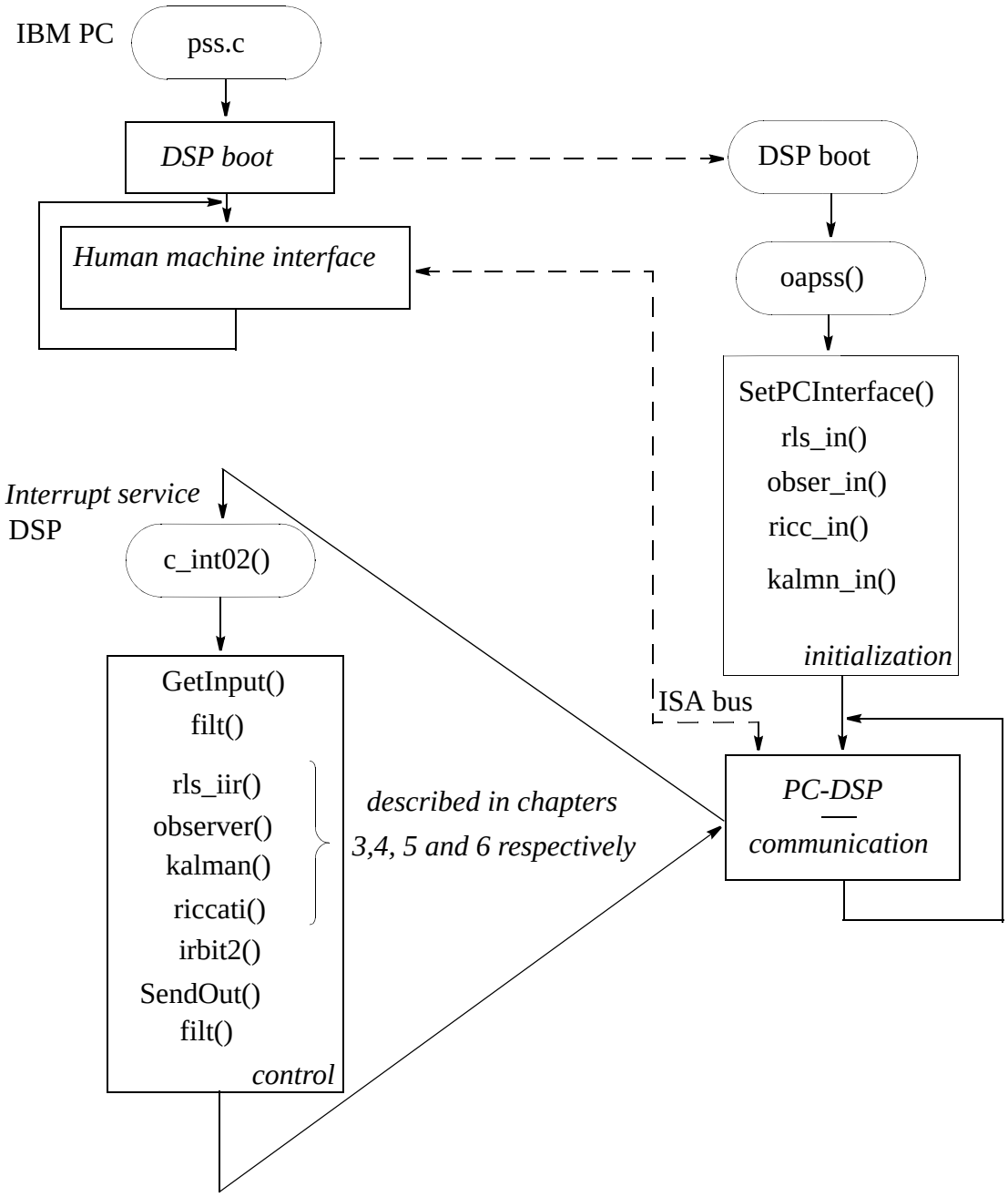

Figure 7-7 Application program structure for the power system stabilizer

The *oapss.out* file contains the compiled and linked *C*-language program prepared for the digital signal processor, which is the control element of the system. After this load is successful, the personal computer executes the human-machine interface. This interface allows the user to select control algorithm variables to display as real time graphs on the computer's monitor and to select control algorithm. For future reference, these graphs can be saved on the hard disk.

The DSP boot procedure initializes the board and establishes the communication between the two computers by executing the *SetPCInterface()* function. *rls_in(), obser_in(), ricc_in() and kalm_in()* allocate and initialize the required matrices and vectors for the control part of the program. After initialization the DSP enables the interrupt service mechanism, and the control executes as an interrupt service routine.

When the analog to digital converter finishes a conversion, every *50 ms*, it strokes interrupt 2, -causing the interrupt service routine to be called (*c_int02()*), which contains the controller program. This interrupt routine starts with the *GetInput()* function, which reads and converts the value of the generator's electric power, P_e, from the analogue to digital converter in per unit, normalized for the 3 kW generator. P_e contain a steady-state component and possibly high frequency components. The parameter estimation function *rls_iir()* requires that the input data for the adaptation contain only the deviation from the steady-state value. To achieve this requirement the *filt()* function is included in the algorithm. The *filt()* function is a band-pass filter which removes the steady-state value (DC) and attenuates the higher frequency components below the Nyquist[1] frequency. This band pass filter

1. Nyquist Harry, 1889-1976, Swedish born communications engineer

is designed for the frequency components in the range of 0.3 Hz to 1.6 Hz because the frequency response of the power system is in that range.

The functions *rls_iir(), observer(), kalman() and riccati()* are described in Chapters 3 to 6 respectively and implement the optimal control algorithm.

Since the RLS adaptation algorithm in *rls_iir()* requires that the input of the system not be in correlation with the output of the system, a white noise signal generated by the white noise generator *irbit2()* is added to the control signal. The function *irbit2()* is a random bit generator *(*± 1*)* which provides a constant level of excitation for the plant, independent of the plant output. The generated noise is *0.005 p.u.* or *5%* of the maximum control signal *(0.1 p.u.).*

The control signal calculated by these functions is output to the digital to analog converter by *SendOut()* function. The *irbit2()* function at the end of control algorithm is identical to the above described band pass filter. It is used for the same purposes on the control signal U_{PSS} as it is used on the input signal P_e.

7.3 Conventional Digital Power System Stabilizer

For comparison, a conventional power system stabilizer (CPSS) with the following transfer function

$$U_{PSS}(s) = K_s \cdot \frac{sT_5}{1+sT_5} \cdot \frac{1+sT_1}{1+sT_2} \cdot \frac{1+sT_3}{1+sT_4} \cdot \Delta P_e(s) \qquad (7.1)$$

was implemented in the same environment. Since the control setup is for the development of the digital controller, the CPSS transfer function was discretized with the sampling period of $\tau = 1ms$. Using the bilinear transformation

$$s = \frac{2}{\tau} \cdot \frac{z-1}{z+1} \tag{7.2}$$

the transfer function of the CPSS can be transformed from the complex continuous s-domain to the discrete z-domain as

$$U_{PSS}(z) = \frac{g'_0 + g'_1 z^{-1} + g'_2 z^{-2}}{f_0' + f_1' z^{-1} + f_2' z^{-2}} \cdot \Delta P_e(z) \tag{7.3}$$

where the coefficients $g'_0, \ldots, g'_2$ and $f_0', \ldots, f_2'$ are explicit functions of the gain, K_s, and the time constants $T_0', \ldots, T_4'$ [41]. The same interface was used, but the control algorithms *rls_in(), obser_in(), ricc_in() and kalm_in()* were replaced and the sample rate was increased.

8 Experimental Studies

Using the real-time digital control environment and physical power system model described in Chapter 7, result of experimental studies with the proposed optimal adaptive power system stabilizer are presented in this chapter. The behavior of the proposed adaptive stabilizer has been investigated on a physical model of a single machine infinite bus power system under different operating conditions and disturbances. For comparison, a digital conventional power system stabilizer has been implemented in the same environment and tested under the same conditions.

All experimental data was collected through the human-machine interface and saved on a disk for further analysis. For easy comparison, the time axis has been adjusted so that the disturbance occurs coincidentally.

The experimental results are consistent with the theoretical and simulation results, and demonstrate that the proposed adaptive stabilizer outperforms the conventional PID stabilizer.

8.1 Voltage Reference Step Change

In this experiment the micro-synchronous generator was operated at power P_e = *0.9 p.u.* and a power-factor $\cos\phi$ = *0.85 lag.* A *10%* step increase in the reference voltage was applied at *2 s* and removed at *8 s*. The micro-synchronous generator's electrical power P_e with the proposed optimal adaptive power system stabilizer (OAPSS) and with the conventional power system stabilizer (CPSS) is shown in Figure 8-1.

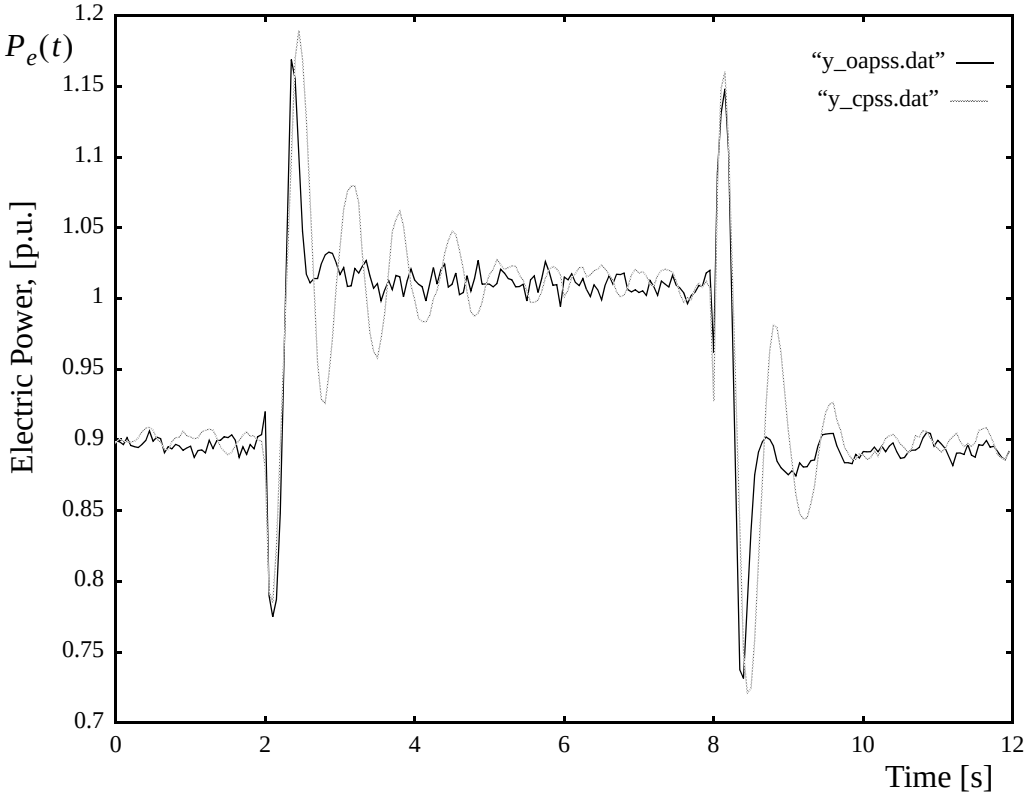

Figure 8-1 Comparison of OAPSS and CPSS responses to a 10% step reference voltage disturbance at Pe = 0.9 p.u., cosϕ=0.85 lag.

From the illustration in Figure 8-1 it can be observed that the conventional CPSS controller damps very slowly as compared to the proposed OAPSS controller. The conventional controller exhibits an oscillatory damping which lasts for *3 s* before dying out. This response can be seen at *2 s* and at *8 s* corresponding to the voltage input step. The proposed controller exhibits a faster and more controlled damping. The duration of this damping is one cycle. The fluctuation on the micro-synchronous generator's electric power is due to the random bit generator associated with the adaptive estimation algorithm and it is not related to the control algorithm. Comparison of the control signals for OAPSS and CPSS is given in Figure 8-2.

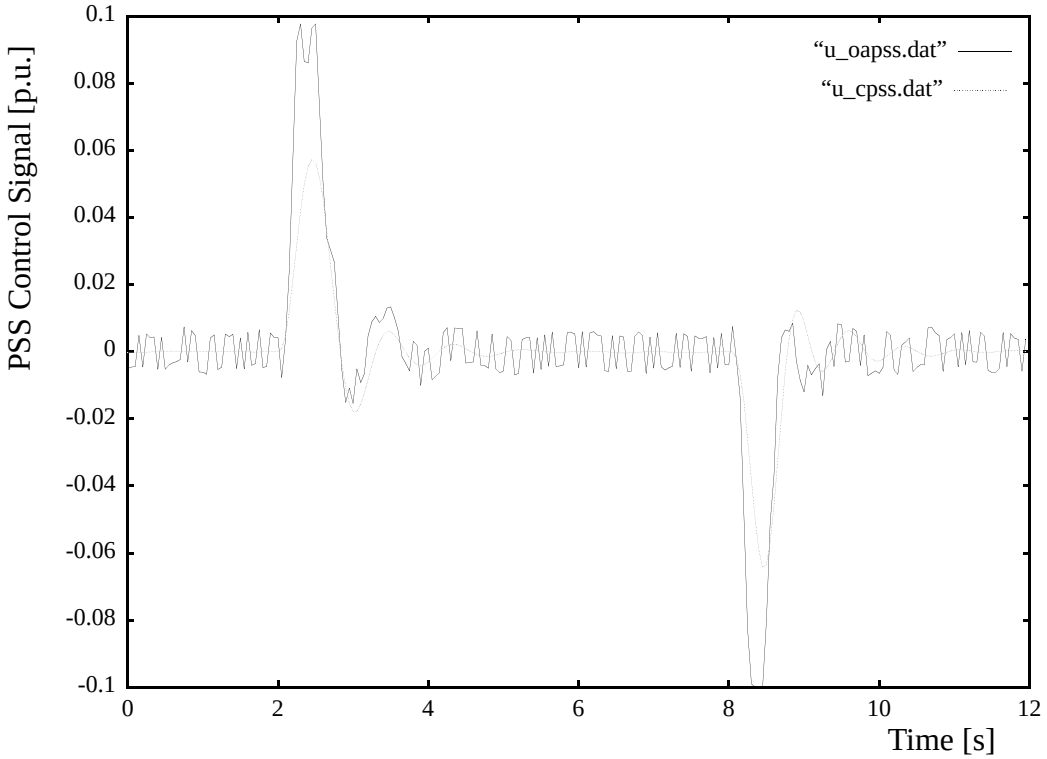

Figure 8-2 Control signal of OAPSS and CPSS for a 10% step reference voltage disturbance at Pe = 0.9 p.u., cosϕ=0.85 lag

The experiment was repeated with $P_e = 0.5$ *p.u.* and $\cos\phi = 0.8$ *lag*. Results are shown in Figure 8-3 and in Figure 8-4.

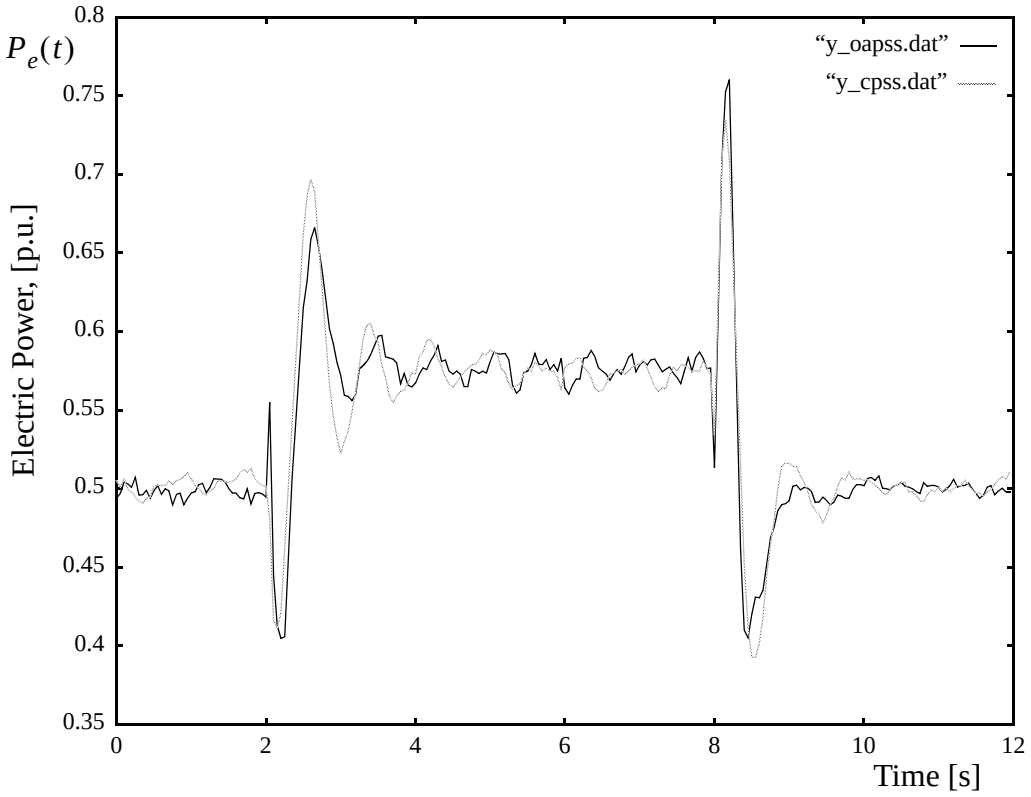

Figure 8-3 Comparison of OAPSS and CPSS responses to a 10% step reference voltage disturbance at Pe = 0.5 p.u., cosϕ=0.8 lag.

The responses in Figure 8-3 are much more similar than those in Figure 8-1. The improvement in the CPSS response is due to the fact that it is optimized at this operating point.

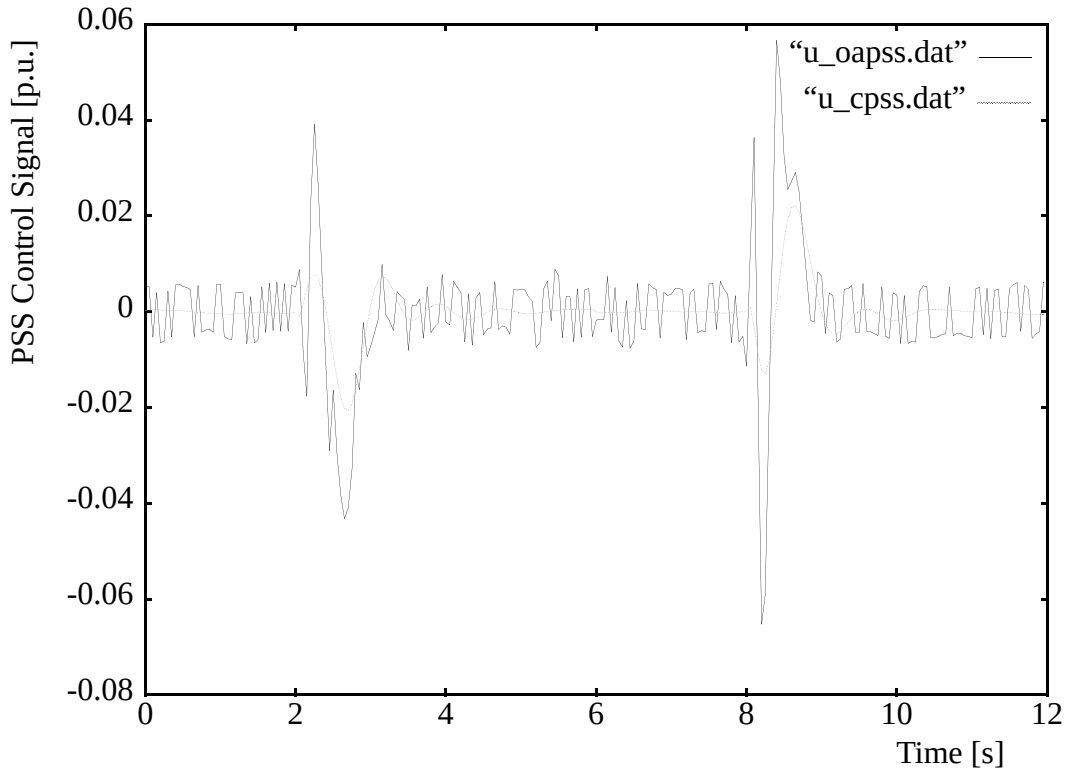

Figure 8-4 Control signal of OAPSS and CPSS for a 10% step reference voltage disturbance at Pe = 0.5 p.u., cosϕ=0.8 lag

The voltage reference step change of 10% was also tested with a leading power factor. The experiment was repeated a second time with $P_e = 0.5$ *p.u.* with power-factor $\cos\phi = 0.9$ *lead.* Results are shown in Figure 8-5.

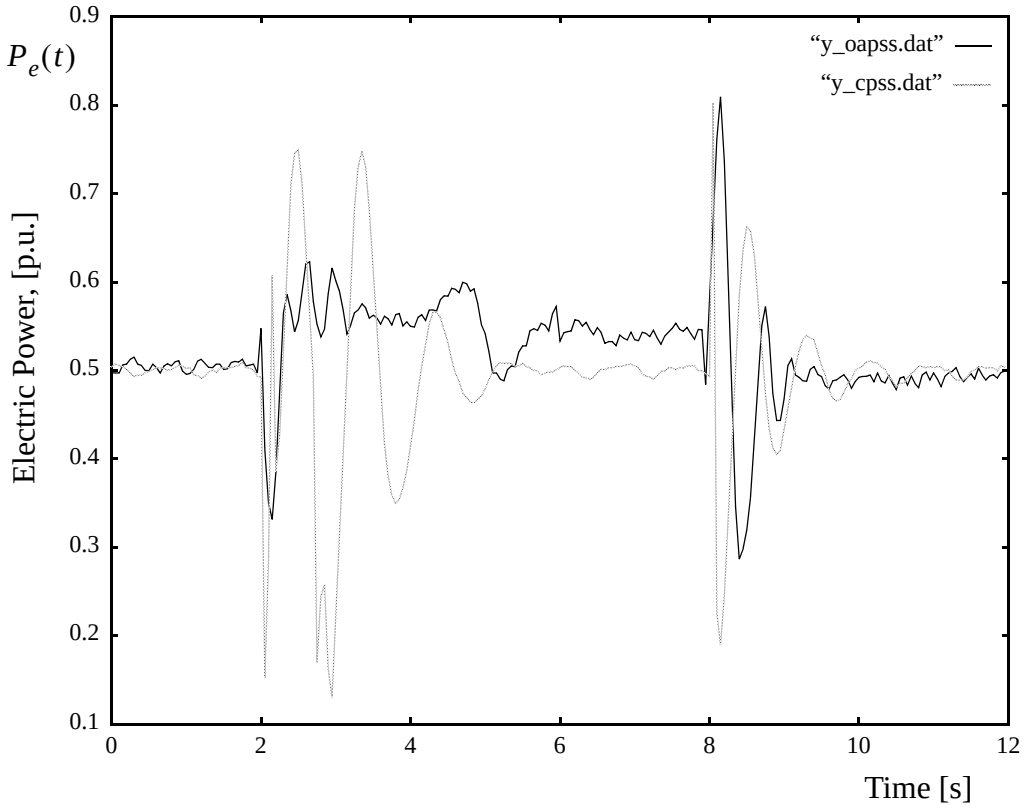

Figure 8-5 Comparison of OAPSS and CPSS responses to a 10% step reference voltage disturbance at Pe = 0.5 p.u., cosϕ=0.9 lead.

In Figure 8-5 the conventional controller is observed to dampen inadequately. The controller does not start to dampen the oscillations for at least 3 cycles. The proposed controller performs much more effectively. The damping occurs within approximately one cycle of the power system oscillations.

8.2 Input Torque Reference Step Change

In this experiment the micro-synchronous generator was operated at power $P_e = 0.9$ *p.u.* and a power-factor $\cos\phi = 0.85$ *lag.* A step decrease in the input torque was applied at *2 s* and removed at *8 s*. The micro-synchronous generator's electrical power P_e with the proposed optimal adaptive power system stabilizer (OAPSS) and with the conventional power system stabilizer (CPSS) is shown in Figure 8-6.

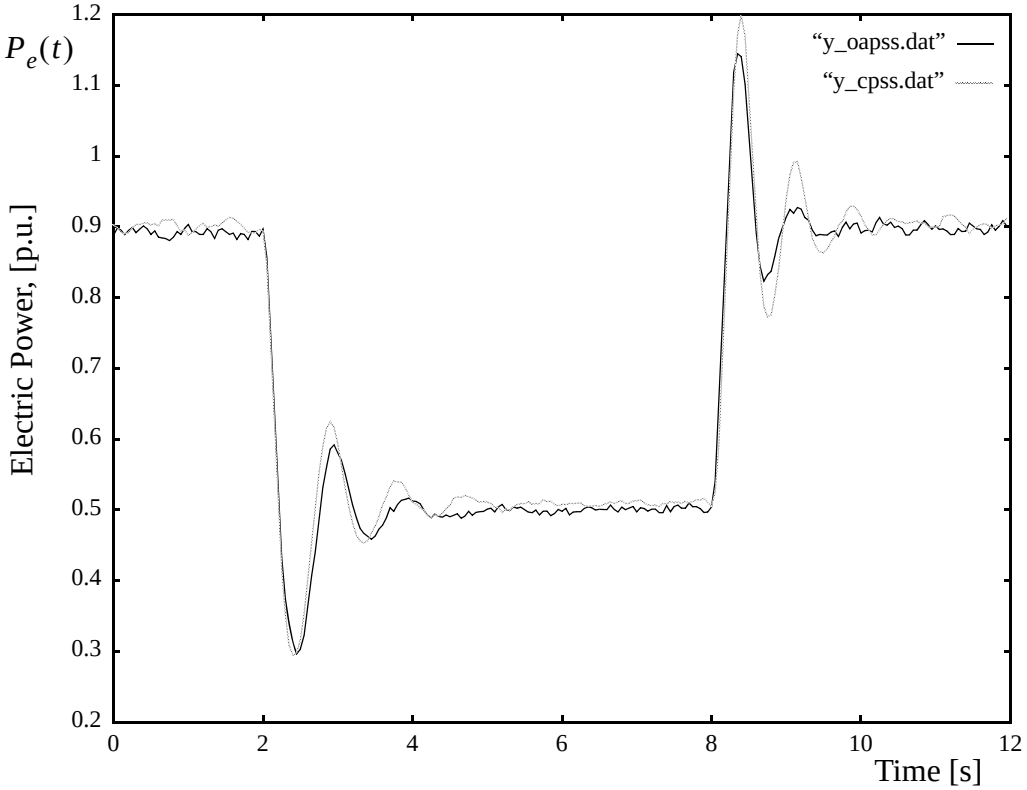

Figure 8-6 Comparison of OAPSS and CPSS responses to a 0.4 p.u. step torque disturbance at Pe = 0.9 p.u., cosϕ=0.85 lag.

Differences in the performance of these two stabilizers can be seen in Figure 8-6. When the generator condition changes to a lower operating point at *2 s* both control algorithms provide good damping. However, when a *0.4 p.u.* electric power step increase is applied to the system at *8 s*, the system's stability margin is decreased due to the higher operating point and the performance with the OAPSS is considerably better. Comparison of the control signal for OAPSS and CPSS is given in Figure 8-7.

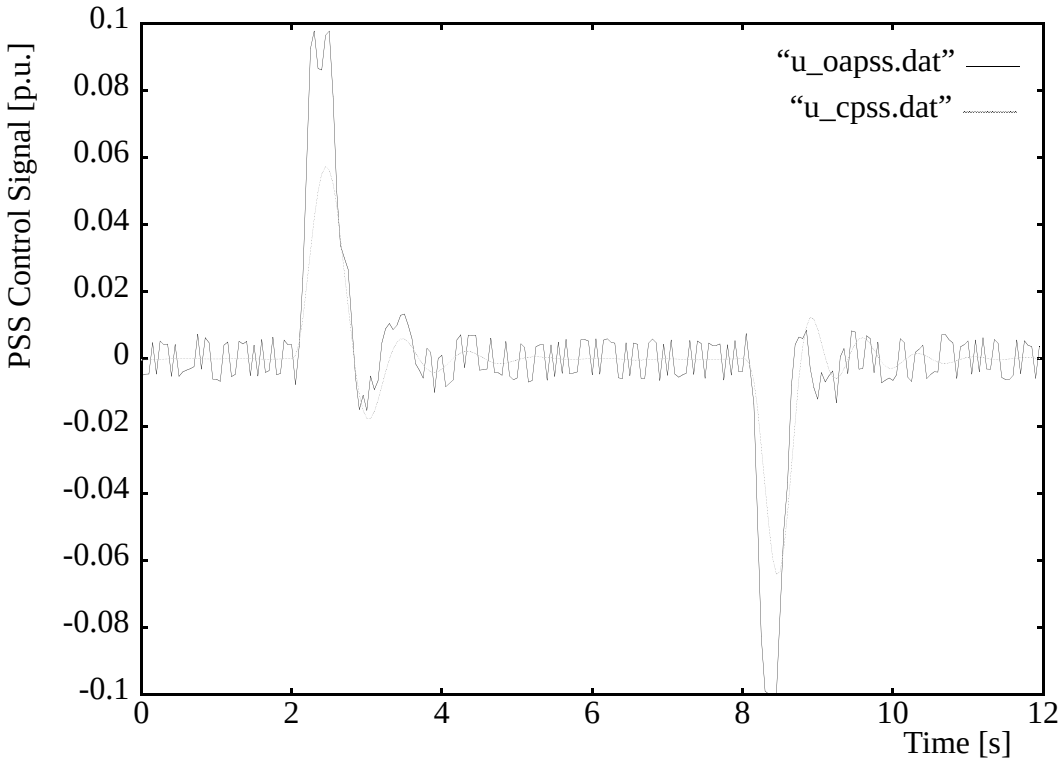

Figure 8-7 Control signal of OAPSS and CPSS for a 0.4 p.u. step torque disturbance at Pe = 0.9 p.u., cosϕ=0.85 lag.

The experiment was repeated with P_e = *0.5 p.u.* and $\cos\phi$ = *0.8 lag.* The system response is shown in Figure 8-8.

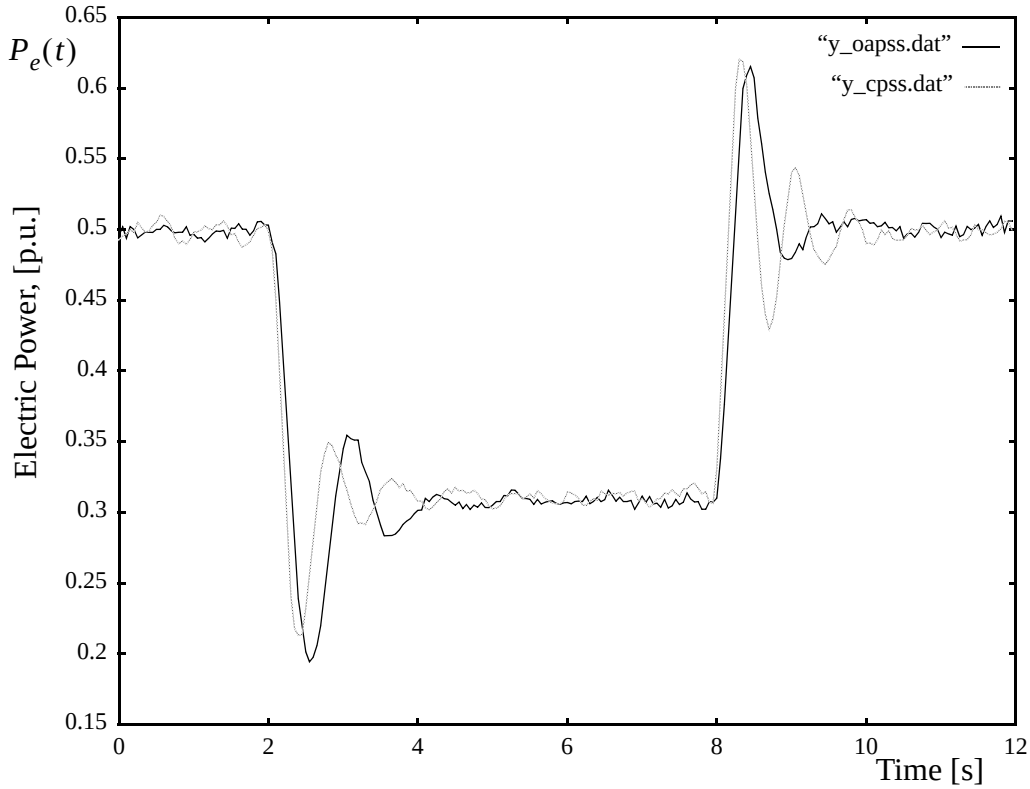

Figure 8-8 Comparison of OAPSS and CPSS responses to a 0.2 p.u. step torque disturbance at Pe = 0.5 p.u., cosϕ=0.8 lag.

When the generator's power changes to a lower operating point at *2 s*, the CPSS provides better damping than the OAPSS, in terms of overshoot on system's response. However, when the system's operating point is in less stable region, with the *0.2 p.u.* step increase in generator's electric power P_e at *8 s*, the system response with the OAPSS becomes more acceptable.

The *0.2 p.u.* step decrease in the input torque was also tested with a leading power factor. The experiment was repeated a second time with P_e = *0.5 p.u.* with power-factor $\cos\phi$ = *0.9 lead.* Results are shown in Figure 8-9and in Figure 8-10.

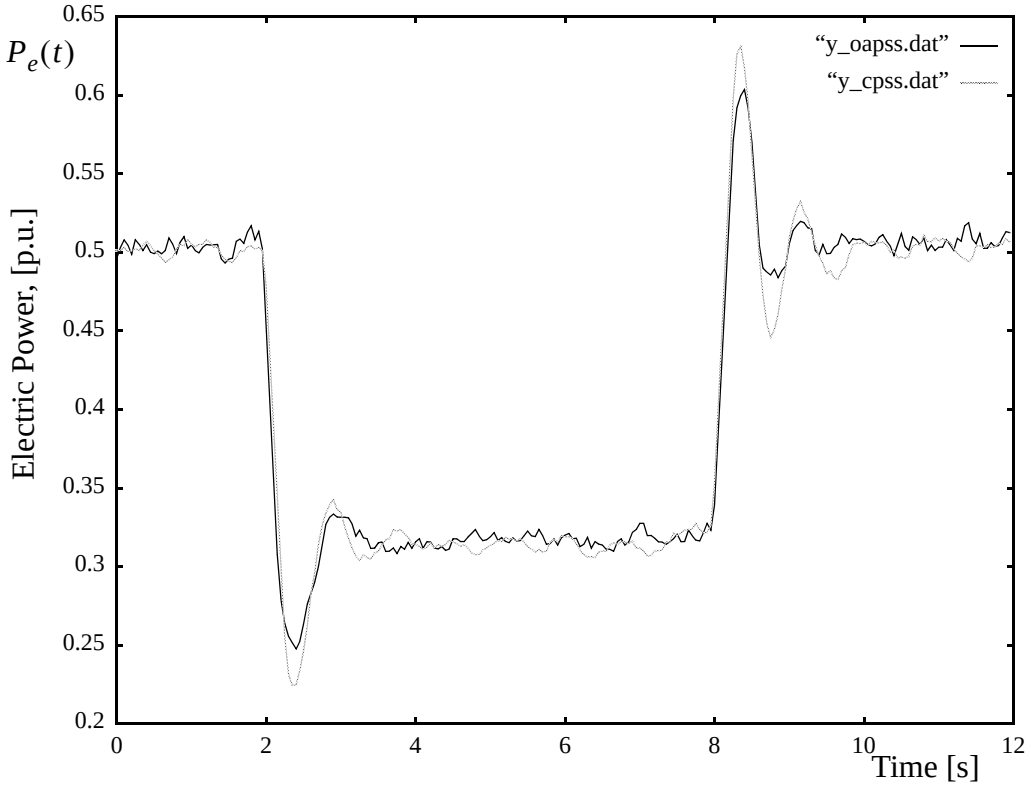

Figure 8-9 Comparison of OAPSS and CPSS responses to a 0.18 p.u. step torque disturbance at Pe = 0.5 p.u., cosϕ=0.9 lead.

The above presented test results verify that both control algorithms perform very well at all power points for this type of disturbance. The difference in performance goes in favor of OAPSS with smaller amplitudes in post-disturbance oscillations.

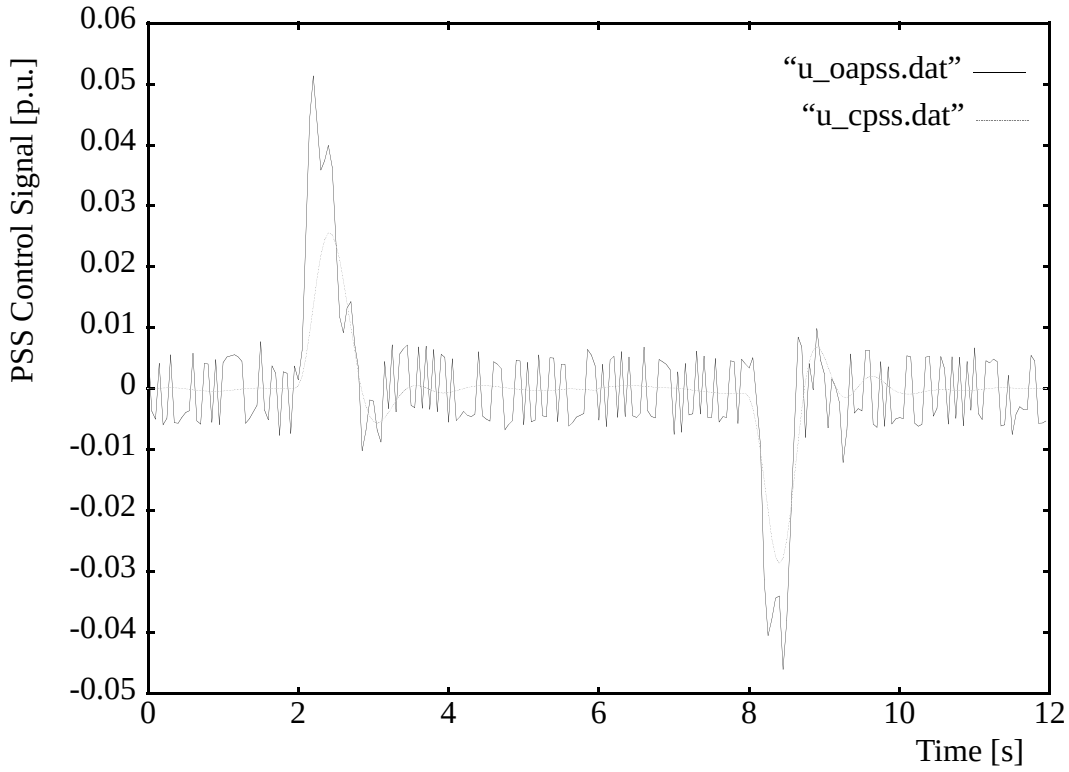

Figure 8-10 Control signal of OAPSS and CPSS for a 0.18 p.u. step torque disturbance at Pe = 0.5 p.u., cosϕ=0.9 lead.

8.3 Three-phase to Ground Fault Test

To investigate the performance of the OAPSS under transient conditions caused by transmission line fault, a three phase to ground fault test has been conducted. In this experiment the micro-synchronous generator was operated at power $P_e = 0.9$ *p.u.* and a power-factor $\cos\phi = 0.85$ *lag.* At this operating condition, with both lines in operation, a three phase to

ground fault was applied at *2 s* in the middle of one transmission line. The faulty transmission line was opened by relay action at both ends *100 ms* later. The first unsuccessful reclosure attempt was made after *600 ms,* and the line was opened again *100 ms* later due to a permanent fault. The second successful reclosure attempt was applied at 8 s and the system returned to the initial operating conditions.

System response with the OAPSS and the CPSS under the above transient conditions is shown in Figure 8-11.

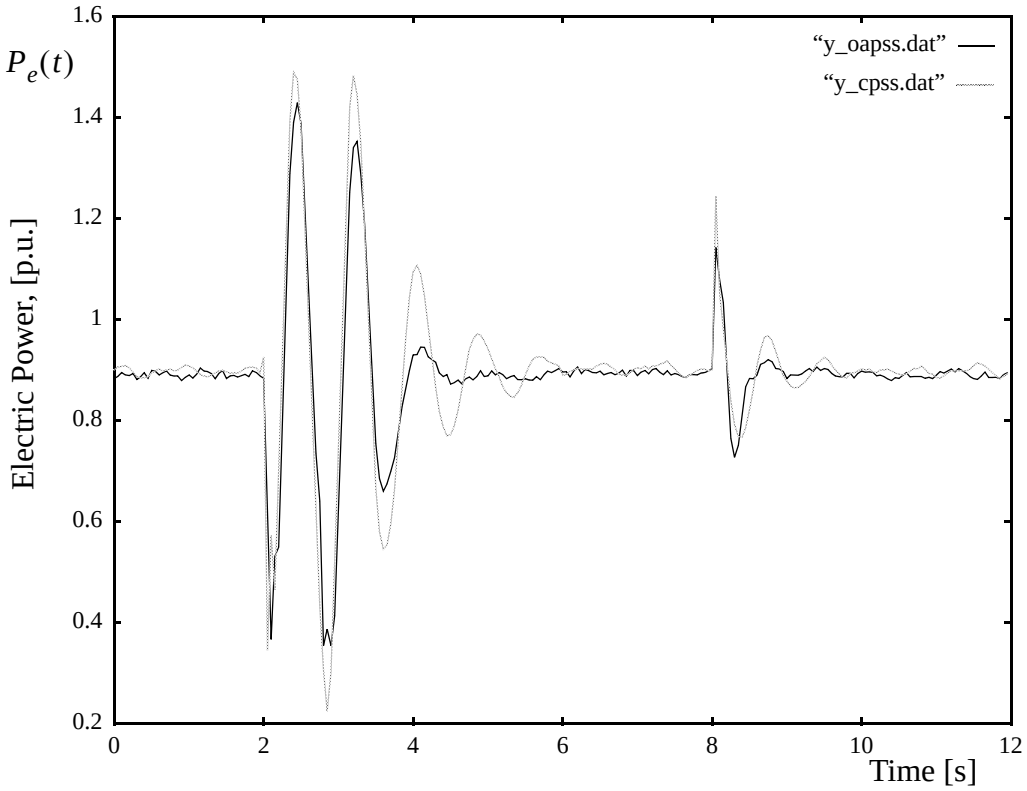

Figure 8-11 Comparison of OAPSS and CPSS responses to a three phase to ground fault at Pe = 0.9 p.u., cosϕ=0.85 lag.

From Figure 8-11 it can be observed that the OAPSS outperforms the CPSS with a smaller overshoot and faster settling time in both cases, at *2 s* and *8 s*.

The comparison of the responses to a three phase to ground fault disturbance when the micro synchronous generator's power $P_e = 0.5$ *p.u.* and power-factor $\cos\phi = 0.8$ *lag* is shown in Figure 8-12 and the control signal generated by these two PSS is given in Figure 8-13.

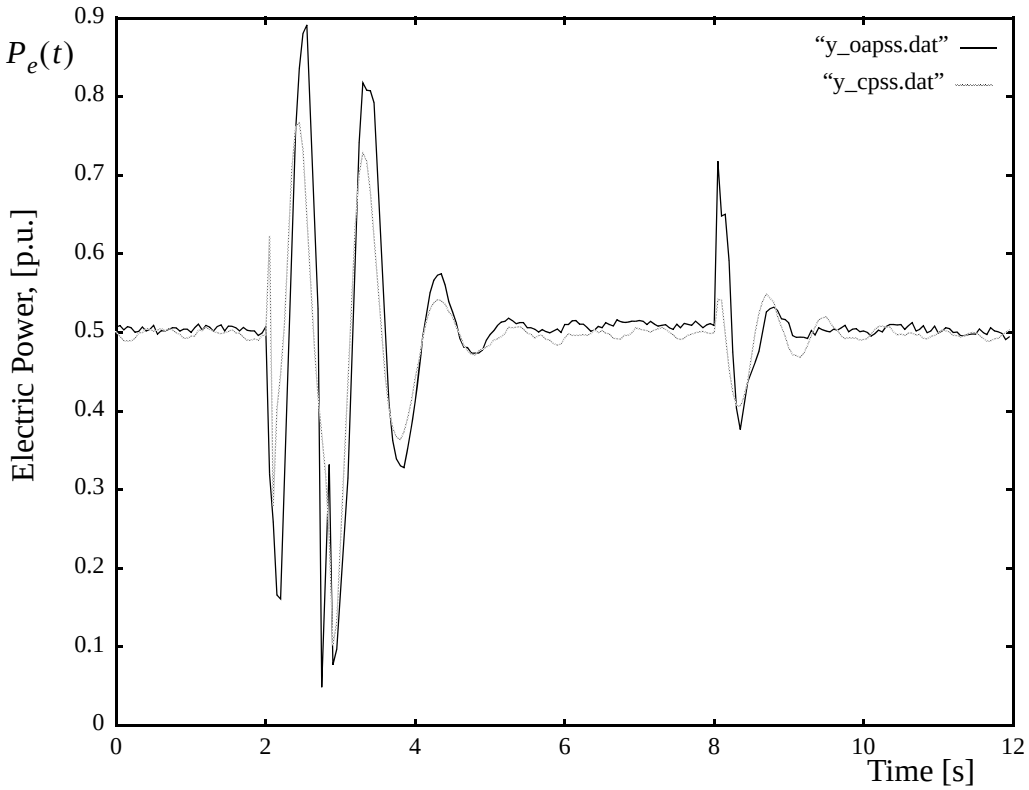

Figure 8-12 Comparison of OAPSS and CPSS responses to a three phase to ground fault disturbance at Pe = 0.5 p.u., cosϕ=0.8 lag.

Figure 8-12 shows a situation where the CPSS outperforms the OAPSS in smaller over-shoots but with both system responses having the same settling time. It is interesting to

mention at this point that the same experiment was conducted earlier with this power system model, which used an Adaptive-Network-based Fuzzy Power System Stabilizer (ANF PSS) [42]. The system response with OAPSS, presented in Figure 8-12, is similar to the response achieved by the ANF PSS, as presented in [42].

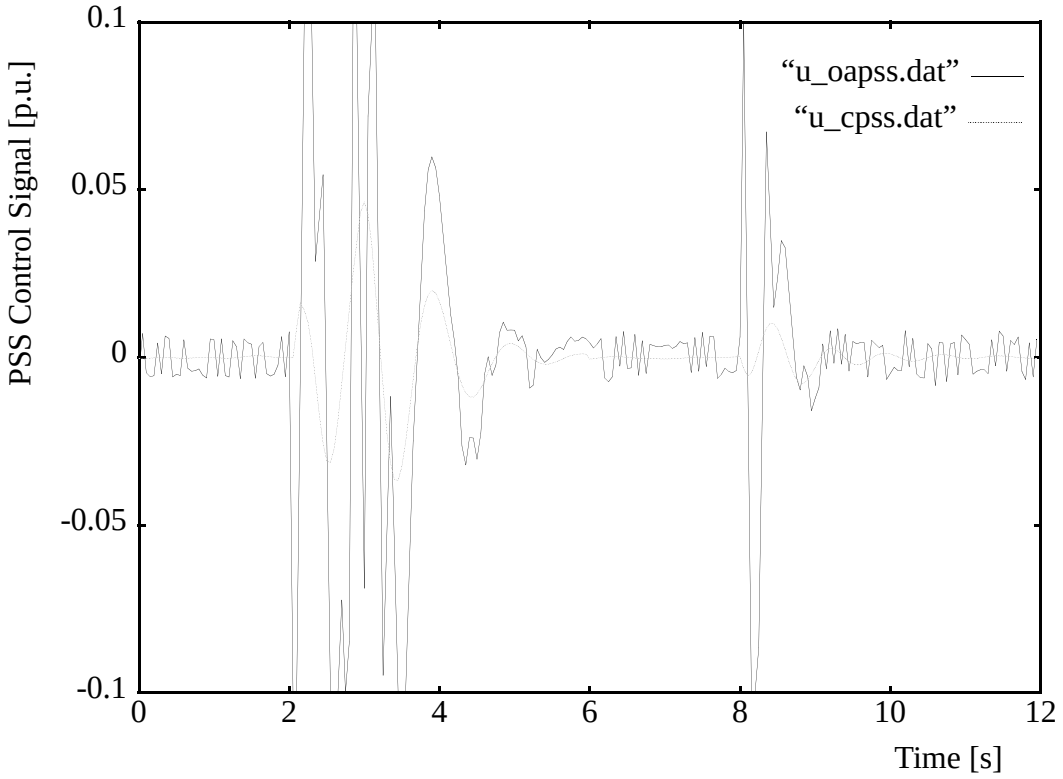

Figure 8-13 Control signal of OAPSS and CPSS for a three phase to ground fault at Pe = 0.5 p.u., cosϕ=0.85 lag.

Figure 8-14 presents the comparison of the performance in response to a three phase fault where the micro synchronous generator's power, P_e, *is 0.5 p.u.* and power-factor $\cos\phi =$ *0.9 lead.*

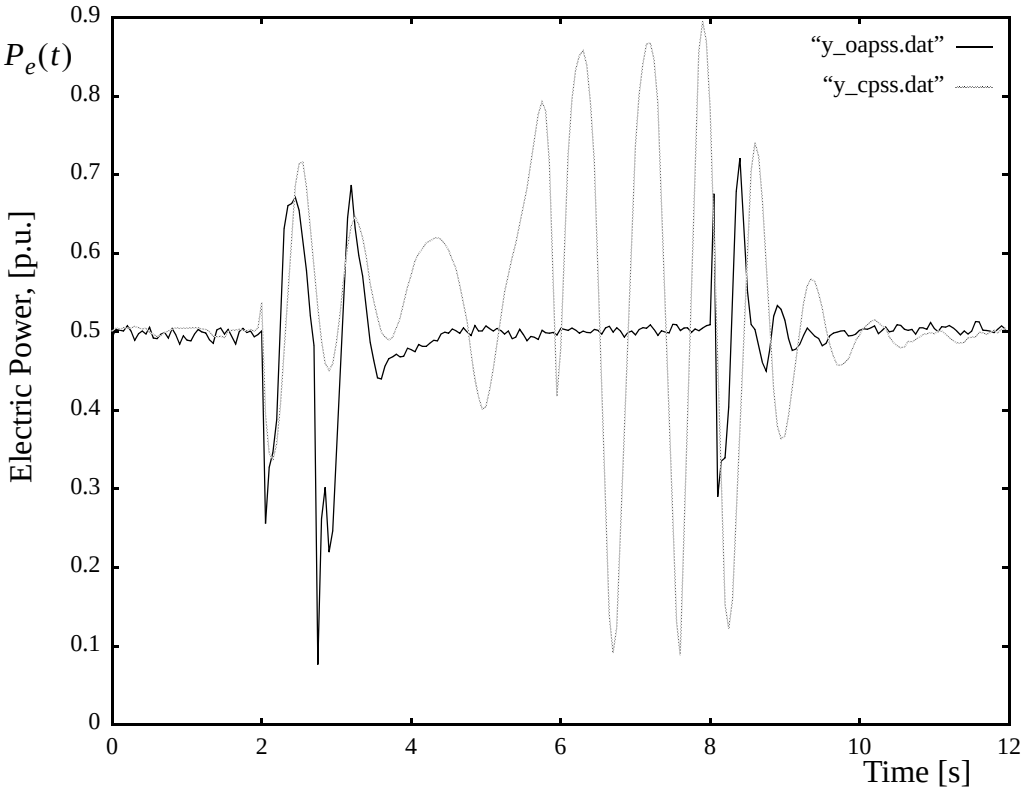

Figure 8-14 Comparison of OAPSS and CPSS responses to a thee phase to ground fault disturbance at Pe = 0.5 p.u., cosϕ=0.9 lead.

System responses to the three phase to ground fault disturbance are shown in Figure 8-14. One can observe that at *2 s* the system response with the CPSS shows smaller oscillations, but these oscillations increase with time and push the system into an unstable oscillatory state up to *8 s,* after which the second transmission line is restored. This test was repeated several times with the same outcome. This test has demonstrated that the system response

with OAPSS is stable but with the CPSS is unstable. Comparison of the control signals for OAPSS and CPSS is given in Figure 8-15.

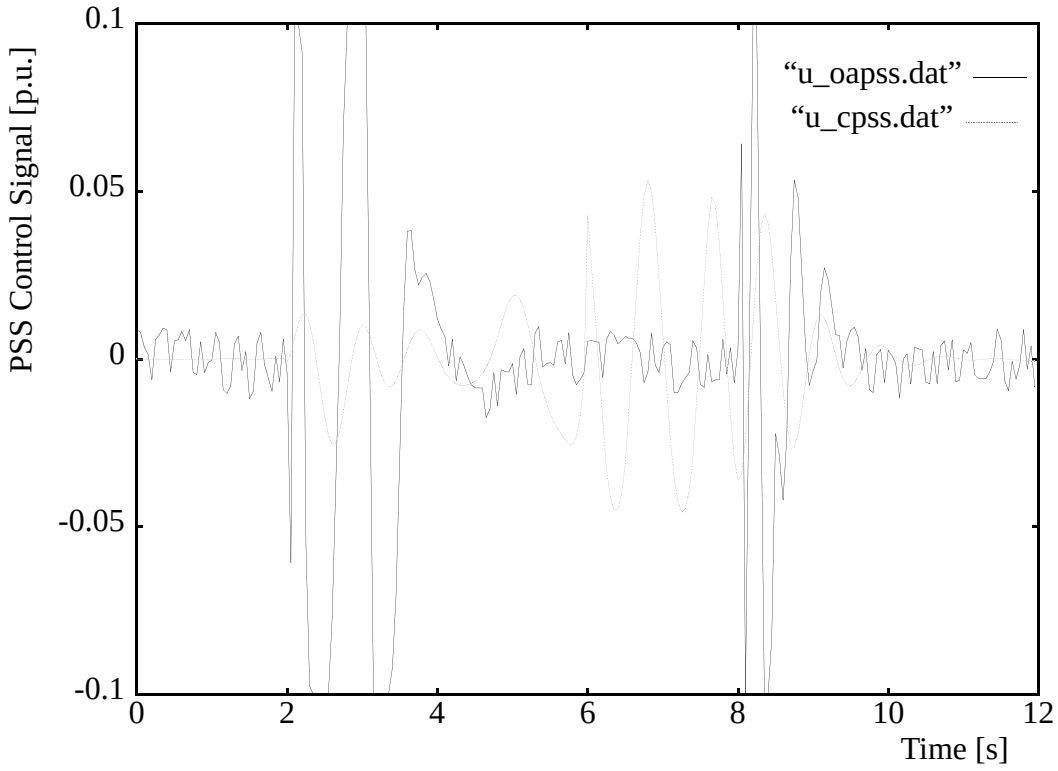

Figure 8-15 Control signal of OAPSS and CPSS for a thee phase to ground fault disturbance at Pe = 0.5 p.u., cosϕ=0.9 lead.

8.4 System Stability Test

A power system stabilizer is used to increase the stability margin of a power system. With extra damping provided by the stabilizer, the generator should be able to operate in syn-

chronous operation at high loads. This test is intended to show the capability of the OAPSS to improve the dynamic stability margin of a power system.

With the micro-synchronous generator operating at P_e=0.3 p.u., the input torque was increased gradually to the maximum level P_e=1.26 p.u. This test was performed with a leading and a lagging power-factor of $\cos\phi = 0.9$. The results, presented in the following, show the generator's electrical power and the power system stabilizers control signal.

Figure 8-16 and Figure 8-17 present the test results for the power-factor of $\cos\phi = 0.9$ lag, using the OAPSS and the CPSS respectively. Both power system stabilizers show acceptable results.

Figure 8-18 and Figure 8-19 present the test results for the power-factor of $\cos\phi = 0.9$ lead, using the OAPSS and the CPSS respectively. Again, both power system stabilizers show acceptable results.

From the above mentioned figures, one can observe that the generator's electric power with the OAPSS contains smaller fluctuations than with the CPSS due to better damping by the OAPSS.

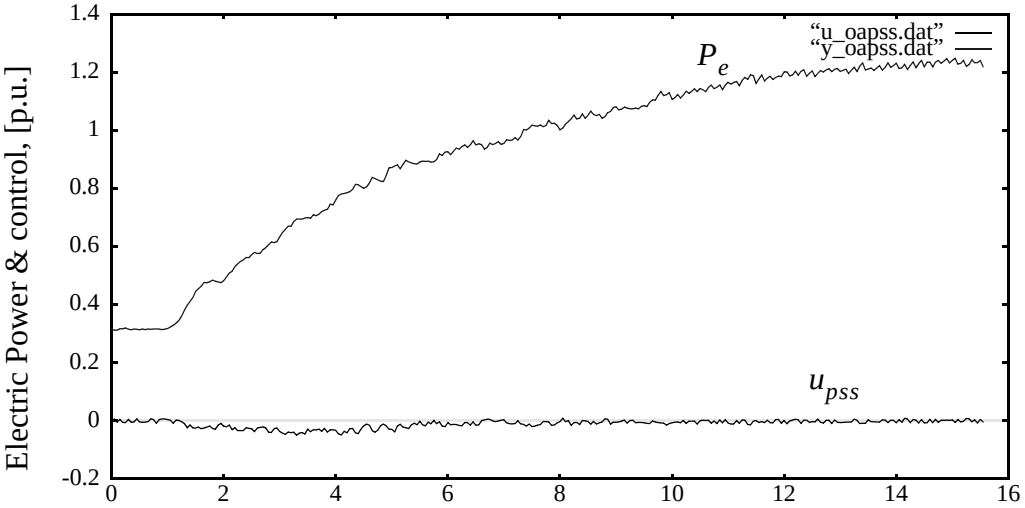

Figure 8-16 OAPSS - Power increase; cosϕ = 0.9, lag

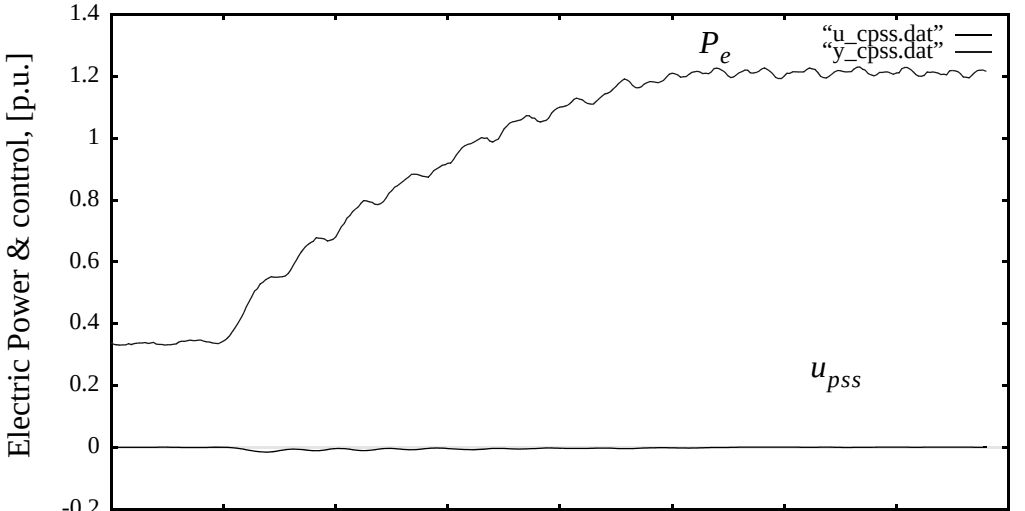

Figure 8-17 CPSS - Power increase; cosϕ = 0.9, lag

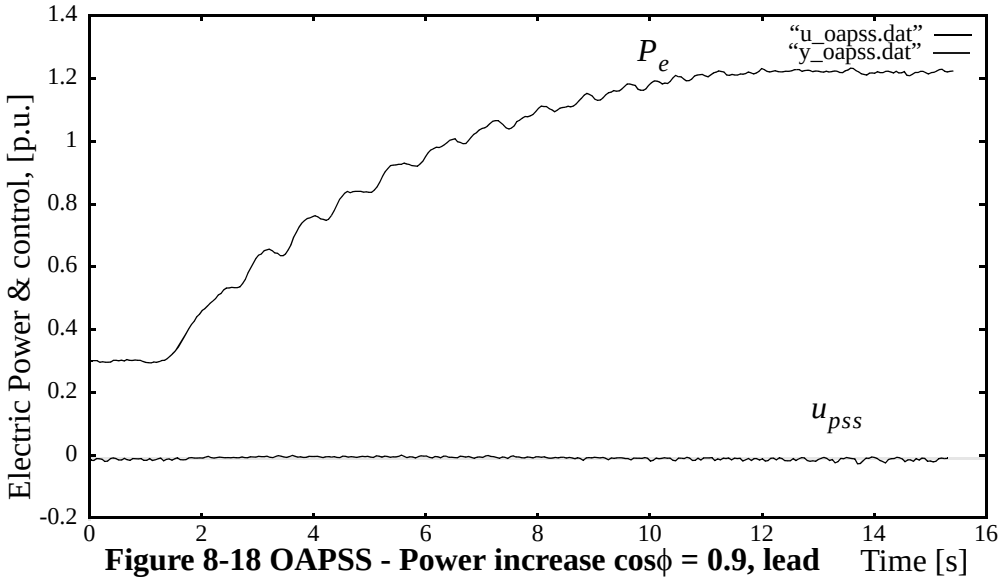

Figure 8-18 OAPSS - Power increase cosϕ = 0.9, lead

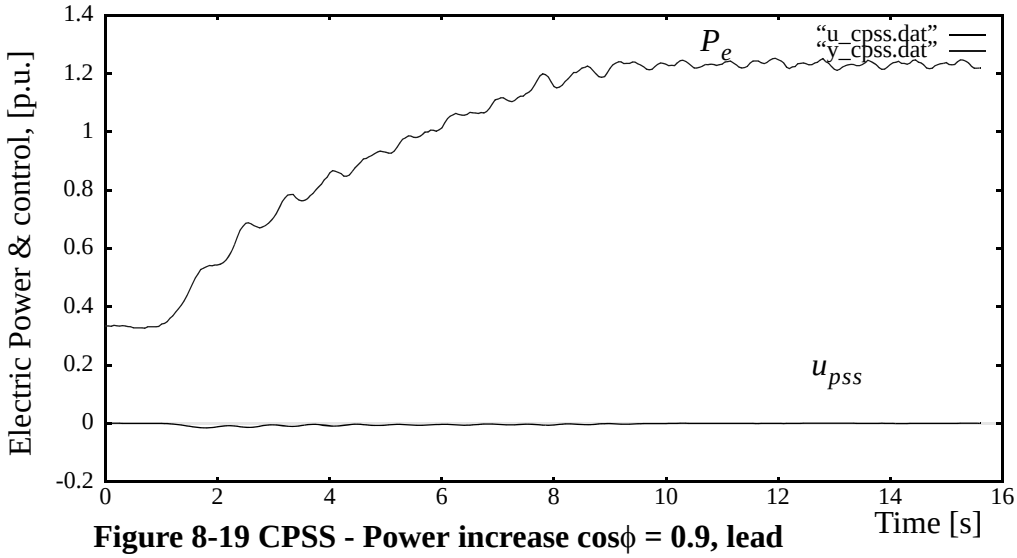

Figure 8-19 CPSS - Power increase cosϕ = 0.9, lead

8.5 Summary

With the real-time digital control environment described in Chapter 7, the optimal adaptive power system stabilizer OAPSS, discussed in Chapters 3 to 6, has been implemented and tested on a physical model power system. The experimental results are discussed and compared with a digitized conventional power system stabilizer CPSS. The test results are presented on graphs which have proved that both the CPSS and the proposed OAPSS are very effective in improving the dynamic performance of the model power system. However, the performance of the CPSS deteriorated when the operating conditions deviated from the design point. An example of this situation is presented in Figure 8-14 where the CPSS could not control unstable operation in the power system model. These experiments have proven that the OAPSS can adapt itself to the new operating conditions and produce consistently good performance.

9 Conclusions and Future Work

It was at the beginning of this century that electrical power engineers first faced the problem of stability. Since that time, power system stability has obtained a broad aspect and has become an independent discipline. It remains in close contact with a number of other disciplines, such as "transient phenomena of electrical machines", "network calculation", "optimal control theory", "digital simulation techniques" [1]. Due to the complex nature of power systems, a lot of work has been published regarding the design of powerful power system controllers. A conventional power system stabilizer (CPSS) has been successfully applied to damp power system oscillations. However, the nonlinear characteristics of power systems are not accounted for by the linear control theory based conventional power system stabilizers. The stabilizer should be able to adapt itself to variations in the system to produce better performance. This motivated the research on other kinds of control techniques such as optimal adaptive control.

9.1 Conclusions

The purpose of this thesis is to design and develop a design technique for optimal adaptive power system stabilizer, which will improve a power system's overall stability in the face of system non-linearity and external disturbances. After extensively studying and comparing the existing adaptive control theories the linear quadratic Gaussian control theory has been selected. The design process is based on such well-formulated procedures as: recursive least square parameter estimation, Kalman filter based state estimation and linear quadratic optimal control design. As well, systematic contributions have been made in all stages of the power system design, development and implementation.

The experimental identification studies, carried out on a micro-synchronous generator, show that an effective linear representation of the power-system dynamics around a particular operating point can be achieved with a reduced-order output-prediction structure. In particular the comparison between the actual system output changes and a one step ahead predicted output from the model is thought to be a particularly efficacious test of model validity. The test results provide considerable confidence in the effectiveness of the identified model.

To achieve a model with the quantities described above, a fifth order infinite impulse response filter structure (IIR) was selected. The recursive least squares adaptive parameter estimation algorithm has been implemented to satisfy the required accuracy and speed of system parameter tracking.

Additional techniques were introduced to increase the algorithm's convergence and robustness. For fast system parameter tracking an adaptive forgetting factor is used. The adaptive algorithm will recognize a sudden operating point change and will put more emphasis on recent measurement data by applying the adaptive forgetting factor. The required robustness is achieved by the implementation of a constraint function in the adaptive algorithm. This constraint is a function of the prediction error and prevents any sudden large changes in the identified system parameters, even if there is a large error in the prediction, caused by exogenous disturbances.

The states of the system are estimated by an adaptive Kalman filter, which is a novel approach, especially in the calculation of the state noise covariance. It is an alternative approach to that of the conventional method of using a predefined measurement noise covariance and state noise covariance. The measurement noise covariance is calculated based on the error in the Kalman filter's prediction and the state noise covariance is calculated based on the error in the estimated system parameters. Employing the adaptive Kalman filter on the micro-synchronous generator has proven to be robust to exogenous disturbances.

The modified adaptive algorithm is suitable, for example, for high performance control applications with noisy feedback signals.

The linear quadratic Gaussian control procedure is a formal one that gives a unique answer to the feedback control problem once the design parameters $Q_C(k)$ and $R_C(k)$ have been selected. In fact, the engineering art in modern design lies in the selection of the

performance index weighting matrices $Q_C(k)$ and $R_C(k)$. Initial values of $Q_C(k)$ and $R_C(k)$ can be obtained by simple “rule of thumb”; but trial and error techniques must be used to achieve high performance. Once $Q_C(k)$ and $R_C(k)$ are defined by the rule of thumb, they are tested and modified to achieve the required system response. The matrix design equations for linear quadratic Gaussian control, calculated on line, guarantee stability and optimal performance in terms of these parameters.

The proposed adaptive optimal power system stabilizer has been implemented in a physical model power system, and tested under various conditions. For comparison a digitized conventional PID power system stabilizer has also been implemented in this environment and tested under the same conditions. The experimental tests have produced results consistent with expectations, proving the correctness and superiority of the proposed optimal adaptive power system stabilizer.

The optimal adaptive controller - synthesized from the identified model - proves to be wide ranging in action and sufficient for all steady-state, dynamic and transient operating conditions tested. It provides good post-fault recovery for the tested disturbances such as: a reference voltage step change, input torque step change and three phase to ground fault.

The application of state space methods to this problem is an original component of the presented work, significant in its ability to achieve stable operation in power systems. Its commercial application is an important field of study.

The idea described in this thesis effectively allows the implementation of optimal-control methods in a power system, while relaxing the requirement for access to the system states

to merely those output variables which need to be directly controlled. The approach described is quite general and is therefore applicable to systems other than that studied here.

9.2 Future Work

To fully maximize the benefits of the proposed optimal adaptive controller as a regulator in a full-scale plant, it may be necessary to carry out further research and modification to the algorithm. It is a long-term research task to develop an optimal adaptive controller. The first step in the research might be focused on developing robust on-line parameter estimation technique, which would produce an accurate model of the plant. The next step is to develop a robust control strategy, by which performance will be selected by defining the desired transient characteristics of the plant, such as overshoot.

To achieve the above described goals, the following are recommended as further research topics:

1. For fast system parameter tracking the calculation method for the adaptive forgetting factor should be improved, by changing the implemented hard-limit into an adaptive soft-limit.

2. The required robustness has been achieved by the implementation of a constraint function in the adaptive algorithm. The calculation of this constraint could be improved by using an expert system such as fuzzy-logic. With this novel approach the adaptive algorithm may perform with the same robustness in all situations without further adjustments.
3. The stability of the identified parameters could be continuously monitored and proper actions taken if stability degradation is detected.
4. The selection of the gain on the Kalman filter's measurement noise covariance matrices, $R_K(nT)$, and state noise covariance matrices, $Q_K(nT)$, as well as the selection of the control algorithm's $Q_C(nT)$ and $R_C(nT)$ matrices should be performed in the sense of "Linear Quadratic Gaussian /Loop-Transfer Recovery Design" theory [6]. The ideal solution would be to implement an expert system which would supervise the plant-output, and if necessary change the $Q_C(nT)$ and $R_C(nT)$ parameters according to the desired control performance.

References

[1] László Z. Rác and Béla Bókay, “Power System Stability”, Akadémiai Kiadó, Budapest, 1988

[2] Grahan Rogers “Demystifying power system oscillations”, IEEE Computer Application in Power, Vol. 9, No. 3, pp 30-35, July 1996

[3] John E. Gibson, Ph.D. “Nonlinear Automatic Control” McGraw-Hill Book Company, New York, 1963

[4] Michael Athans, Peter L. Falb, “Optimal Control - An Introduction to the Theory and Its Applications”, McGraw-Hill Book Company, New York, 1966

[5] E. I. Verriest and K. L. Lewis, “On the linear Quadratic minimum-time problem”, IEEE Transaction on Automatic Control, Vol. 36, No. 7, July 1991

[6] Frank L. Lewis, “Applied Optimal Control & Estimation - Digital Design & Implementation”,Prentice-Hall, Inc. Englewood Cliffs, New Jersey, 1992

[7] Ricardo Mariano, Patrizio Tomei, “Nonlinear Control Design” Prentice Hall, UK, 1995

[8] C. F. Beards, “Vibrations and Control Systems”, John Wiley & Sons - Ellia Horwood Limited, Chichester - England, 1988

[9] John E. Gibson, Ph.D. “Nonlinear Automatic Control” McGraw-Hill Book Company, New York, 1963

[10] Francesco Castella, Arturo Locatelli, Nicola Schiavony, “Nonlinear controllers for vibration suppression in a large flexible structure”, Dipartmento di Electtronica e Informazione - Politecnico di Milano, Milano, Italy, 1995

[11] J.R. Mortlock and M.W. Humphrey Davies, “Power System Analysis”, Chapman and Hall, London, England, 1952

[12] Karl J. Åström, Björn Wittenmark, “Computer Controlled Systems”, Prentice Hall, Englewood Cliffs, 1984

[13] Rolf Iserman, “Digital Control Systems” 2nd. ed., Springer-Verlage, Berlin, Heidelberg, 1991

[14] Simon Haykin, “Introduction to Adaptive Filters”, Macmillan Publication Company, New York, 1984

[15] Karl J.Åström, Björn Wittenmark, “Adaptive Control” 2nd. ed., Addison-Wesley Publishing Company, Reading, Massachusetts, 1995

[16] Bernard Widrow, Eugene Walch, “Adaptive Inverse Control”, Prentice Hall, Upper Saddle River, 1996

[17] Mohinder S. Grewal, Angus P. Andrews, “Kalman Filtering Theory and Practice”,,Prentice Hall, Englewood Cliffs, 1993

[18] Robert Grover Brown, Patrick Y. C. Hwamg, “Introduction to Random Signals and Applied Kalman Filtering”, John Wiley & Sons, Inc., New York, 1983

[19] Qijun Xia, Ming Rao, Yiqun Ying, Xuemin Shen, “Adaptive fading Kalman Filter with an Application”, Automatica, Vol. 30, No. 8, pp. 1333-1339, Great Britannia 1994

[20] Alirez Moghaddamjoo, R. Lynn Kirlin, “Robust adaptive Kalman filtering with unknown inputs”, IEEE Transaction on Acustics, Speech and Signal Processing, Vol. 37, No. 8, pp. 1166-1175, USA, 1989

[21] Guanrong Chen, “Approximate Kalman Filtering”, Word Sientific Publishing Co, Pte. Ltd., River Edge, NJ, 1994

[22] Simon Haykin, “Adaptive Filter Theory”, 2nd. ed., Prentice-Hall, Inc. Englewood Cliffs, New Jersey, 1991

[23] Petros A. Ioannous, Jin Sun, “Robust Adaptive Control”, Prentice-Hall, Inc. Upper Saddle River, New Jersey, 1996

[24] Bernard Widrow, Eugene Walach, “Adaptive Inverse Control”, Prentice Hall, Inc., Upper Saiddle River, New Jersey, 1996

[25] Charles L. Phillips, H. Troy Nagle, Jr., “Digital Control System Analysis and Design”, Prentice-Hall, Inc. Englewood Cliffs, New Jersey, 1991

[26] Ching-Fang Lin “Advanced Control System Design”, Prentice-Hall, Inc. Englewood Cliffs, New Jersey, 1991

[27] Arthur E. Bryson, Jr., Yu-Chi Ho, “Applied Optimal Control - Optimization, Estimation and Control”, Hemisphere Publishing Corporation, Washington, D.C., 1975

[28] George J. Thaler, Marvin P. Pastel, “Analysis and Design of Nonlinear Feedback Control Systems” McGraw-Hill Book Company, New York, 1962

[29] A. A. Fel’Dbaum, “Optimal Control Systems”, Academic Press New York, 1965

[30] E. F. Camacho, C. Bordons, “Model Predictive Control in the Process Industry” Springer-Verlag, London, 1995

[31] Arthur E. Bryshon, Jr., Yu-Chi Ho, “Applied Optimal Control”, Hemisphere Publishing Corporation, Washington, D.C., 1975

[32] Claude M. Summers, “The Faraday electrical machines laboratory”, Proceedings of the IEEE, Vol. 64, No. 11, pp. 1556-1582, November 1976

[33] F. P. deMello and C. Concordia, “Concepts of synchronous machine stability as affected by excitation control”, IEEE Transaction on Power Apparatus and Systems, PAS-88, pp. 316-329, April 1969

[34] C. Concordia,”Synchronous Machines”, John Wiley & Sons Ltd., New York, NY, 1951

[35] P. M. Anderson and A. A. Found, “Power System Control and Stability”, Iowa State University Press, Iowa, USA, 1977

[36] Shen Chen, “Power System Uncertainty Analysis And Robust Stabilizer Design”, A Dissertation University of Calgary, 1995

[37] C. Richard Johnson, Jr., “On the interaction of adaptive filtering, identification, and control”, IEEE Signal Processing Magazine, Vol. 12, No. 2, pp 22-37, March 1995

[38] D.W. Huber, G.S. Hope and O.P. Malik, “Synchronous machine field time constant regulator”, Manual in Department of Electrical Engineering, The University of Calgary, Calgary, Canada

[39] Bernard Adkins, Ronald G. Harley, “The General Theory of Alternating Current Machines”, Chapman and Hall, London, England, 1975

[40] Narain G. Hingorani, “Power electronics in electric utilities: role of power electronics in future power systems”, Proceedings of the IEEE, Vol. 76, No. 4, pp. 481-482, April 1988

[41] Ali Hariri, “An Adaptive Fuzzy Logic Power System Stabilizer”, A Dissertation, University of Calgary, 1996

[42] Ali Hariri, Presentation at the research seminar, University of Calgary, 1997

[43] Mahmud Gilany, “A Microprocessor Based Relay for parallel Transmission Line”, A Thesis, University of Calgary, 1992

Appendix A Park's Equations

Mathematically, the *d-q* decomposition method transforms the basic electrical quantities of synchronous machines (voltages, currents, flux-linkages) from the stator three-phase reference frame into another one represented by the direct and quadrature axis of the rotor and a zero-sequence system (this latter usually does not exist at all). Park's equations are related to a "model-machine", characterized by two rotor circuits (the field circuit and a fictitious one) in the *d*-, and two (both fictitious circuits) in the *q*- direction. The fictitious circuits serve for simulation of the solid rotor current effects in case of cylindrical-rotor machines. The same equations are also valid for salient pole machines, and in this case they correspond to the damping circuits. It is assumed further that the stator coils are star-connected, but not effectively grounded. Consequently, zero sequence currents cannot flow. With this assumptions, the voltage and flux-linkage equations of synchronous machines using Park's reference frame are [1]:

A.1 Voltage Equations

$$u_d = -\omega\psi_q + \frac{d}{dt}\psi_d - ri_d \tag{A.1}$$

$$u_q = \omega\psi_d + \frac{d}{dt}\psi_q - ri_q \tag{A.2}$$

$$u_f = \frac{d}{dt}\psi_f + r_f i_f \tag{A.3}$$

$$0 = \frac{d}{dt}\psi_{1d} + r_{1d}i_{1d} \tag{A.4}$$

$$0 = \frac{d}{dt}\psi_{fq} + r_{fq}i_{fq} \tag{A.5}$$

$$0 = \frac{d}{dt}\psi_{1q} + r_{1q}i_{1q} \tag{A.6}$$

A.2 Flux-Linkage Equations

$$\psi_d = L_{ad}(i_f + i_{1d}) - L_d i_d \tag{A.7}$$

$$\psi_q = L_{aq}(i_{fq} + i_{1q}) - L_q i_q \tag{A.8}$$

$$\psi_f = L_f i_f + L_{ad}(i_{1d} - i_d) \tag{A.9}$$

$$\psi_{1d} = L_{1d}i_{1d} + L_{ad}(i_f - i_d) \tag{A.10}$$

$$\psi_{fq} = L_{fq}i_{fq} + L_{ad}(i_{1q} - i_q) \tag{A.11}$$

$$\psi_{1q} = L_{1q}i_{1q} + L_{aq}(i_{fq} - i_q) \tag{A.12}$$

A.3 Torque Equation

$$T_e = \frac{\omega_0}{2}(\psi_d i_q - \psi_q i_d) \tag{A.13}$$

All the above variables are per unit quantities, where: u, i and ψ are voltage, current and flux-linkage, respectively, in the circuits marked by the subscript; L and r are self-induc-

tion coefficient and ohmic resistance, respectively, L_{ad} and L_{aq} are mutual induction in the direct and quadrature axes, respectively, *d, f, 1d* subscripts denote direct axis circuits: stator Park component, field circuits and damping circuit respectively; *q, fq, 1q* subscripts denote quadrature axis circuits: stator Park component (fictitious) field circuits and damping circuit respectively.

Voltages and currents in the stator circuits are per unit quantities referred to machine-rated values; all per unit flux linkages are related to that base value which, multiplied by ω_0, gives the related stator voltage. All rotor circuit currents are related to the field current, which produces 1 p.u. field flux linkage. On this basis the per unit values of all inductances and resistances can be determine[1].

A.4 The general torque equation

At any instant the torque developed by the machine depends on the currents following in the windings. The torque developed by the interaction between the flux and the currents is called the electrical torque T_e, and differs from the externally applied torque T_m, if the speed ω varies, because of the inertia of the machine [39].

$$T_m = T_e + J\frac{d\omega}{dt} \tag{A.14}$$

where J is the moment of inertia.

Appendix B Continuous Nonlinear Optimal Controller

These equations must be solved to yield the optimal control $u(t)$ that minimizes the Performance Index.

System model:

$$\frac{dx}{dt} = f(x, u, t) \qquad t \geq t_0 \qquad t_o \text{ fixed} \tag{B.1}$$

Performance index:

$$J(t_0) = \phi(x(T), T) + \int_{t_0}^{T} L(x, u, t)dt \tag{B.2}$$

Final state constraint:

$$\psi(x(T), T) = 0 \tag{B.3}$$

Hamiltonian:

$$H(x, u, t) = L(x, u, t) + \lambda^T f(x, u, t) \tag{B.4}$$

State equation:

$$\frac{dx}{dt} = \frac{\partial H}{\partial \lambda} = f \qquad t \geq t_0 \tag{B.5}$$

Costate equation:

$$-\frac{d\lambda}{dt} = \frac{\partial H}{\partial x} = \frac{\partial f}{\partial x}^T \lambda + \frac{\partial L}{\partial x} \qquad t \leq T \tag{B.6}$$

Stationary condition:

$$0 = \frac{\partial H}{\partial u} = \frac{\partial}{\partial x} L + \frac{\partial f}{\partial u}^T \lambda \tag{B.7}$$

Boundary conditions:

$$x(t_0) \text{ given}$$
$$\left(\frac{\partial \phi}{\partial x} + \left(\frac{\partial \Psi}{\partial x}\right)^T \nu - \lambda\right)\Big|_T dx(T) + \left(\frac{\partial \phi}{\partial t} + \left(\frac{\partial \Psi}{\partial t}\right)^T \nu + H\right)\Big|_T dT + 0 \tag{B.8}$$

Appendix C Single-Machine Power System Simulation

The synchronous generator equations, in the form of Park's two-axis machine representation, are achieved with the transients in the stator circuits neglected and the effect of rotor amortisseur neglected [36]

C.1 Generator Model

$$\dot{\delta} = \omega\omega_0 \tag{C.1}$$

$$\dot{\omega} = \frac{1}{H}(T_m + g + K_d\omega - T_e) \tag{C.2}$$

$$\dot{\lambda}_d = e_d + r_a i_q + (1+\omega)\lambda_q \tag{C.3}$$

$$\dot{\lambda}_q = e_q + r_a i_q + (1+\omega)\lambda_d \tag{C.4}$$

$$\dot{\lambda}_f = e_f - r_f i_f \tag{C.5}$$

$$\dot{\lambda}_{kd} = -r_{kd} i_{kd} \tag{C.6}$$

$$\dot{\lambda}_{kq} = -r_{kq} i_{kq} \tag{C.7}$$

C.2 Transmission network equations

$$v_d = v_b \sin(\delta) + r_e i_d + x_e i_q \quad \text{(C.8)}$$

$$v_q = v_b \cos(\delta) + r_e i_q + x_e i_d \quad \text{(C.9)}$$

C.3 IEEE Standard type ST1A AVR and exciter model

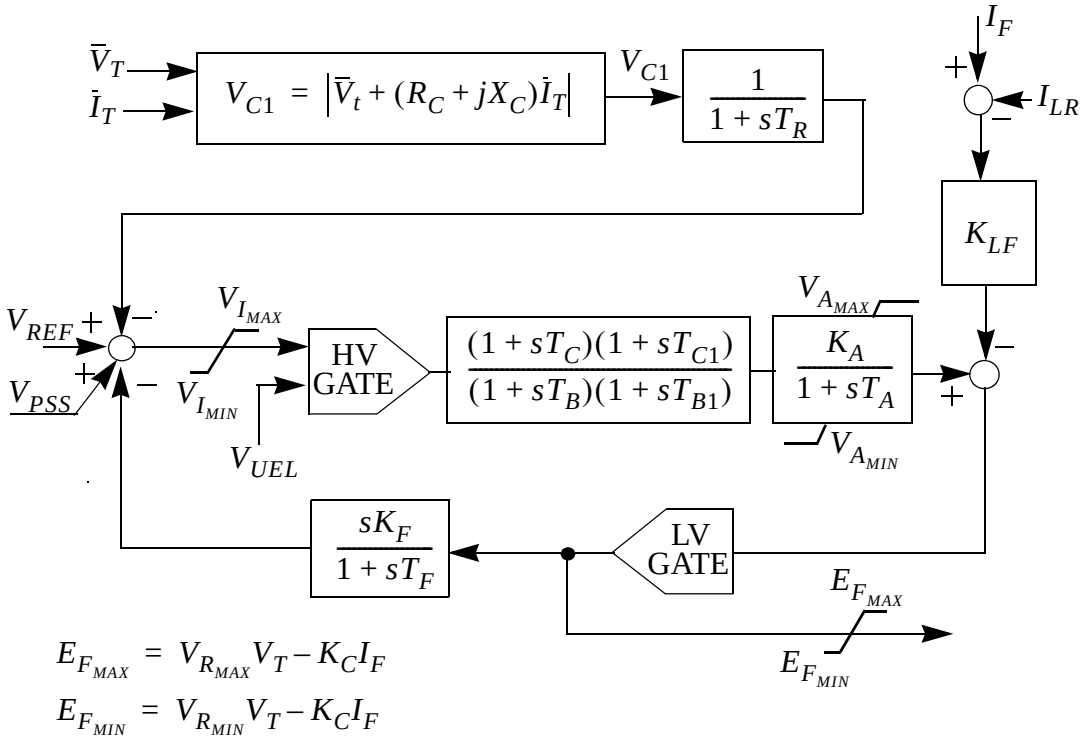

Figure C-1 AVR and Exciter Model

C.4 Governor transfer function

$$g(s) = \left[a + \frac{b}{1 + sT_g}\right]\dot{\delta} \qquad \text{(C.10)}$$

C.5 IEEE Standard PSS1A Type Conventional PSS

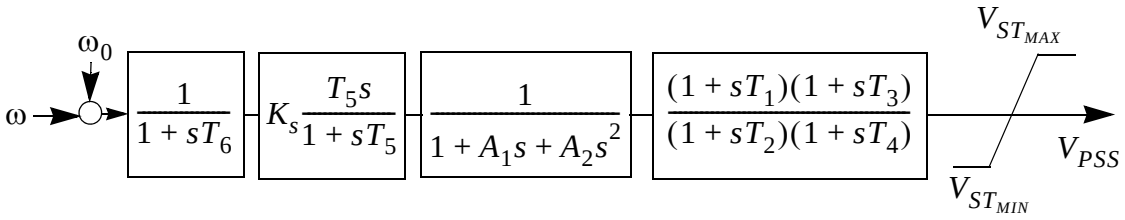

Figure C-2 IEEE Standard Power System Stabilizer

C.6 Parameters

Table 9-1 Parameters used in simulation study

$r_a = 0.007$	$r_f = 0.00089$	$x_f = 1.33$	
$x_d = 1.24$	$x_q = 0.743$	$x_{md} = 1.126$	$x_{mq} = 0.626$
$r_{kd} = 0.023$	$r_{kq} = 0.023$	$x_{kd} = 1.15$	$x_{kq} = 0.625$
$r_e = 0.05$	$x_e = 0.3$	$K_d = 0.0$	$H = 4.0$
$R_C = 0.0$	$X_C = 0.0$	$K_C = 0.08$	$T_R = 0.0$
$T_C = 1.0$	$T_B = 10.0$	$T_{C1} = 0.0$	$T_{B1} = 0.0$
$T_F = 1.0$	$K_F = 0.05$	$T_A = 0.01$	$K_A = 200.0$

Table 9-1 Parameters used in simulation study

$V_{I_{MIN}} = -999$	$V_{I_{MAX}} = 999$	$V_{A_{MIN}} = -999$	$V_{A_{MAX}} = 999$
$V_{R_{MIN}} = -6.7$	$V_{R_{MAX}} = 7.8$	$V_{UEL} = -999$	$V_{OEL} = 999$
$a = -0.001328$	$b = -0.17$		
$T_1 = 0.15$	$T_2 = 0.03$	$T_3 = 0.15$	$T_4 = 0.03$
$T_5 = 2.5$	$T_6 = 0.005$	$A_1 = 0.0$	$A_2 = 0.0$
$V_{ST_{MIN}} = -0.1$	$V_{ST_{MAX}} = 0.1$	$K_S = 5.0$	

All resistances and reactances are in PER UNIT and time constants in seconds [36].

Appendix D Physical Model Power System

D.1 The micro-synchronous generator

Table 9-2 The micro-synchronous generator parameters

$r_a = 0.026$	$r_{kd = 0.083}$	$r_{kq} = 0.0083$
$r_f = 0.000747$	$x_f = 1.27$	$H = 4.75$
$x_d = 1.2$	$x_{kd} = 1.25$	$x_{md} = 1.129$
$x_q = 1.2$	$x_{kq} = 1.25$	$x_{mq} = 1.129$

D.2 The transmission line

Both transmission lines consist of six 50 km equivalent π-sections. For each π-section, the parameters are:

Table 9-3 *pi*-section parameters

$R = 0.1\Omega$	$L = 1.7mH$	$C = 0.83\mu F$

D.3 Conventional Power System Stabilizer

The parameters of the conventional power system stabilizer are

Table 9-4 Conventional power system stabilizer parameters

$K_s = -8.0$	$T_1 = 0.06$	$T_2 = 0.1$	$T_3 = 0.1$	$T_4 = 0.08$

All resistances and reactances are in per unit and time constants in seconds [41].

Index

A

B

C

D

E

F

G

H

I

K

L

M

N

O

P

Q

R

S

T

U

V

W

Z